# WELL PRODUCTIVITY ENHANCEMENT OF HIGH TEMPERATURE HETEROGENEOUS CARBONATE RESERVOIRS

A Dissertation

by

GUANQUN WANG

Submitted to the Office of Graduate and Professional Studies of
Texas A&M University
in partial fulfillment of the requirements for the degree of

DOCTOR OF PHILOSOPHY

| | |
|---|---|
| Chair of Committee, | Hisham A. Nasr-El-Din |
| Committee Members, | Robert H. Lane |
| | Stephen A. Holditch |
| | Mahmoud El-Halwagi |
| Head of Department, | A. Daniel Hill |

May 2014

Major Subject: Petroleum Engineering

## ABSTRACT

Acidizing is one of the most popular techniques for well productivity enhancement during oil and gas production. However, the treatment method is not very effective when the wellbore penetrates through multiple layers of heterogeneous reservoirs. Uneven acid distribution always results in productivity enhancement under expectation. When such a well is drilled, the temperature of the well could be too high to keep the acid reaction under control. The acid used in the treatment fluid, most commonly HCl, would react with the tubular and the formation at a very high rate. Rather than creating long wormholes to bypass the damaged area, face dissolution, loss of pipelines, and potential damage are the outcomes after the treatment. Thus, several new techniques were proposed in this study to solve the issues discussed above.

To address the heterogeneity of the reservoir, viscoelastic surfactants (VES) were used as diverting agents during acidizing treatments. A recently developed chelating agent, L-glutamic acid-N,N-diacetic acid (GLDA), was evaluated as a possible alternative for the traditional HCl. Coreflood tests and measurements of rheology properties of the treatment fluids were used to investigate the performance of the treatment fluids based on the two new systems.

In total, two VES were evaluated for their diverting abilities. The first VES was based on amine oxide. It was found that the live VES-based acids had the highest apparent viscosity when the concentration of HCl was 5 wt%. During the coreflood tests, the VES-based acid was only able to build up pressure drop across the core at injection

rates less than 1 $cm^3$/min. A significant amount of the VES was left inside the core after the treatment, which reduced the efficiency of production enhancement.

The other VES, based on carboxysulfobetaine, can tolerate high temperatures up to 325°F. According to the viscosity measurements of the spent VES-based acid, the addition of various corrosion inhibitors lowered the fluid viscosity at temperatures above 150°F. Mutual solvent was able to break the wormlike micelles formed by the VES in the presence of calcium chloride. The diverting ability of the VES was proved through coreflood tests.

For the GLDA-based treatment fluids, two additives were added into the system in effort to improve the efficiency of the treatments. Polymers and VES were added into the GLDA to achieve even fluid distribution during treatment. A significant viscosity increment was observed with the help of the viscosifier, which could expand the application of the GLDA.

## DEDICATION

To my wife and parents

## ACKNOWLEDGEMENTS

I would like to thank my committee chair, Dr. Nasr-El-Din, for his support and guidance throughout my PhD in the department of petroleum engineering. His patience, encouragement, and dedication to his work provided the energy for me to work hard on several projects during the last four years. In addition, I would like to thank my committee members, Dr. Lane, Dr. Holditch, and Dr. El-Halwagi, for their patience and support throughout the course of this research.

Thanks also go to my friends and colleagues and the department faculty and staff for making my time at Texas A&M University a great experience. I also want to extend my gratitude to AkzoNobel, which provided the funding, chemicals, and technical support.

Finally, I would like to give thanks to my mother and father for their encouragement and support and to my wife for her patience and love.

## TABLE OF CONTENTS

Page

ABSTRACT ..... ii

DEDICATION ..... iv

ACKNOWLEDGEMENTS ..... v

TABLE OF CONTENTS ..... vi

LIST OF FIGURES ..... viii

LIST OF TABLES ..... xv

1. INTRODUCTION ..... 1

1.1 Techniques Used in Well Productivity Enhancement ..... 1
1.2 History of the Development of Acidizing Formula ..... 2
1.3 Application of Viscoelastic Surfactant before Used in Acidizing ..... 4
1.4 Application of Viscoelastic Surfactant as Diverting Agent in Acidizing ..... 5
1.5 General Information of Viscoelastic Surfactant ..... 8
1.6 Application of Chelating Agents in Well Stimulation ..... 50

2. PERFORMANCE OF AMINE-OXIDE VES-BASED ACID IN STIMULATION ..... 54

2.1 Background ..... 54
2.2 Materials ..... 54
2.3 Acid Preparation ..... 55
2.4 Equipment ..... 55
2.5 Core Preparation ..... 58
2.6 Experimental Procedures ..... 59
2.7 Results and Discussion ..... 60
2.8 Conclusions ..... 80

3. FORMATION DAMAGE CAUSED BY THE RETENTION OF VES ..... 82

3.1 Background ..... 82
3.2 Materials and Equipment ..... 82
3.3 Experimental Procedure ..... 83
3.4 Results and Discussion ..... 83
3.5 Conclusions ..... 96

Page

4. EFFECTS OF ADDITIVES ON THE PERFORMANCE OF GLDA.....98

4.1 Background .....98
4.2 Materials and Equipment .....98
4.3 Preparation of Treatment Fluids and Experimental Procedure .....99
4.4 Results and Discussion.....99
4.5 Conclusions .....105

5. EVALUATION OF THE VES AIMING FOR HIGH TEMPERATURE APPLICATIONS .....107

5.1 Background .....107
5.2 Materials and Equipment .....107
5.3 Acid Preparation.....109
5.4 Experimental Procedure .....111
5.5 Results and Discussion.....111
5.6 Conclusions .....141

6. VISCOSIFIED GLDA WITH VES AND POLYMER.....143

6.1 Background .....143
6.2 Materials and Equipment .....143
6.3 Fluid Preparation and Experimental Procedure .....143
6.4 Results and Discussion.....144
6.5 Conclusions .....154

7. CONCLUSIONS.....156

REFERENCES.....161

## LIST OF FIGURES

FIGURE Page


1.1 Different types of surfactant divided based on the charge carried. Top to bottom: nonionic, anionic, cationic, and zwitterionic.....10

1.2 Addition of surfactants reduces the surface tension of water until the surfactant concentration reaches the CMC.....11

1.3 Various structure formed by surfactants under various packing parameter.....12

1.4 Adsorption of zwitterionic surfactant on the surface at various concentrations...13

1.5 Friction factor of solvent at various temperatures.....14

1.6 Viscosity and absolute value of viscosity at various shear rates.....15

1.7 Storage modulus and viscous modulus as a function of shear rates.....16

1.8 Effect of temperature on fluid viscosity behavior.....17

1.9 Effects of NaCl on the apparent viscosity of EHAC based fluid.....18

1.10 Temperature sensitive VES system.....19

1.11 Transition from short micelles to long entangled wormlike micelles at different VES fraction.....20

1.12 Length of micelles increases with increasing surfactant fraction in solution…...21

1.13 Different viscosity behavior of three amine oxide VES as a function of temperature.....22

1.14 EDAB solutions at different VES concentrations and under the crossed polarizers.....23

1.15 CMC value as a function of zwitterionic surfactant fraction in an anionic and zwitterionic surfactant mixing solution.....24

1.16 Surface tension as a function of VES concentration and zwitterionic VES fraction.....25

1.17 Viscosity as a function of VES concentration and zwitterionic VES fraction.....26

FIGURE Page

1.18 Absolute value of viscosity, storage modulus and viscous modulus as a function of rotating speed.....27

1.19 Effects of anionic surfactant and cationic surfactant on the viscosity of zwitterionic surfactant solutions.....28

1.20 TEM images of VES vesicles with the presence of hydrocarbon and hexanol…….....29

1.21 Transition from vesicles to wormlike micelles.....30

1.22 Viscosity of solutions with constant overall cationic and anionic mixing surfactants concentration and various ratio of cationic surfactant.....32

1.23 Viscosity of solutions with constant cationic and anionic surfactants mixing ratio and various overall surfactant concentrations.....33

1.24 Shear thickening of diluted VES-based solutions as the increase of shear rate and fixed shear rate mixing for a long time.....35

1.25 Shear thickening and phase behavior change of diluted VES-based solutions as the increase of shear stress.....35

1.26 Effects of temperature on the viscosity of VES-based fluids for solid suspension application.....36

1.27 Effects of VES concentration on the viscosity of VES-based fluids for solid suspension application.....37

1.28 Effects of size of counterion species on the micelles formed by VES.....38

1.29 Effects of cis and trans structure in the alkyl group on the micelles formed by VES.....39

1.30 Effects of temperature on the viscosity of high salinity VES-based fluids.....40

1.31 Breaking down of wormlike micelles formed by VES via addition of hydrocarbon.....41

1.32 Phase separation of VES-based wormlike micelles solutions with the addition of excess amount of hydrocarbon.....41

FIGURE Page

1.33 Effect of alcohol on the viscosity of VES-based fluid.....42

1.34 Parameters to describe the wormlike micelle structure.....43

1.35 Synthesis route of amidosulfobetaine surfactants.....45

1.36 Synthesis route of erucyl amidobetaines.....46

1.37 Surface tension plotted as a function of EDAS concentration at various temperatures.....47

1.38 Apparent viscosity as a function of shear rate for various EDAS concentrations at 25 ℃.....48

1.39 Viscosity as a function of NaCl concentration for EDAS solutions at their natural pH values at 25 ℃.....48

1.40 Viscosity as a function of pH for EDAS fluids at 25 ℃.....49

1.41 Schematic illustration of the solubility increase of long-chain amidosulfobetaines by adding salt.....49

2.1 Chemical structure of the amine oxide viscoelastic surfactant.....54

2.2 High pressure high temperature rheometer.....56

2.3 Coreflood setup.....57

2.4 pH meter.....57

2.5 Atomic absorption spectroscopy.....58

2.6 Apparent viscosities of live VES-based acid were measured at various HCl concentrations.....61

2.7 Apparent viscosities of live and spent acid at 25 ℃ and various shear rates. The initial HCl concentration was 5 wt%.....62

2.8 Apparent viscosities of live and spent acid at 100 $s^{-1}$ and under various temperatures.....63

2.9 G’ and G” of live VES acid system as a function of frequency at 28°C.....64

FIGURE Page

2.10 G' and G" of live VES acid system as a function of temperature at 1 Hz.....65

2.11 Normalized pressure drop across the core during the VES-based acid injection at 0.5 and 1 $cm^3$/min, respectively.....68

2.12 Normalized pressure drop across the core when the VES-based acid system was injected at 2.5 and 10 $cm^3$/min, respectively.....69

2.13 Normalized pressure drop across the core when the VES-based acid was injected into cores with lower initial permeability at 1, 5, and 10 $cm^3$/min, respectively……...70

2.14 Volume of the VES-based acid required to achieve breakthrough as a function of the injection rate.....72

2.15 pH value and density of the core effluent samples when the coreflood test was conducted at 5 $cm^3$/min.....74

2.16 Calcium ions, surfactant, and acid concentrations in the core effluent samples when the coreflood tests were conducted at 5 $cm^3$/min.....75

2.17 Volume of VES-based acid needed to achieve breakthrough and maximum.....76

2.18 CT scan images of the Pink Dessert limestone cores after acid treatment.....79

3.1 Normalized pressure drop across the core when 0.25 PV of VES-based 20 wt% acid was injected into the carbonate cores at various rates.....86

3.2 Normalized pressure drop across the core when 0.25 PV of VES-based 15 wt% HCl acid was injected into the carbonate cores at various rates.....87

3.3 Normalized pressure drop across the core when 0.25 PV of VES-based 10 wt% HCl acid was injected into the carbonate cores at various rates.....88

3.4 Analysis of the pH and density of the core effluent when the core was treated with 20 wt% HCl at 5 $cm^3$/min.....89

3.5 Analysis of the concentration of calcium ions and VES of the core effluent when the core was treated with 20 wt% HCl at 5 $cm^3$/min.....90

3.6 CT scan images of the cores after treatment of VES-based acids.....93

FIGURE Page

4.1 Pressure drop across the core during GLDA treatment injection with the additives of cationic surfactant and corrosion inhibitor.....101

4.2 Pressure drop across the core during GLDA treatment injection.....102

4.3 Pressure drop across the core during GLDA treatment injection with the additives of cationic surfactant.....103

4.4 Pressure drop across the core during GLDA treatment injection with the additives of corrosion inhibitor.....104

4.5 CT scan images of the Indiana limestone cores after treatment of GLDA-based fluids.....105

5.1 Effect of 0.5 vol% CI on the viscosity of 4 vol% VES-based fluid at 75 ℉.....112

5.2 Effect of 1 vol% CI on the viscosity of 4 vol% VES-based fluid at 75 ℉.....113

5.3 Effect of 0.5 vol% CI on the viscosity of 4 vol% VES-based fluid at 150 ℉.....114

5.4 Effect of 1 vol% CI on the viscosity of 4 vol% VES-based fluid at 150 ℉.....115

5.5 Effect of 0.5 vol% CI on the viscosity of 4 vol% VES-based fluid at 250 ℉.....116

5.6 Effect of 1 vol% CI on the viscosity of 4 vol% VES-based fluid at 250 ℉.....117

5.7 Effect of 0.5 vol% CI on the viscosity of 4 vol% VES-based fluid at 325 ℉.....118

5.8 Effect of 1 vol% CI on the viscosity of 4 vol% VES-based fluid at 325 ℉.....119

5.9 Effect of 0.5 vol% CI on the viscosity of 4 vol% VES-based fluid at 10 $s^{-1}$.....120

5.10 Effect of 1 vol% CI on the viscosity of 4 vol% VES-based fluid at 10 $s^{-1}$.....121

5.11 Viscosity of spent acids of the current VES and the new VES at 10 $s^{-1}$.....123

5.12 Effect of different concentrations of mutual solvent on the viscosity of 4 vol% VES-based fluid at 75 ℉.....125

5.13 Effect of different concentrations of mutual solvent on the viscosity of 4 vol% VES-based fluid at 150 ℉.....126

FIGURE Page

5.14 Effect of different concentrations of mutual solvent on the viscosity of 4 vol% VES-based fluid at 250 ℉....127

5.15 Effect of different concentrations of mutual solvent on the viscosity of 4 vol% VES-based fluid at 325 ℉....128

5.16 Pressure drop across the core during injection of 4 vol% VES-based 20 wt% HCl during single coreflood test....130

5.17 Inlet (left) and outlet (right) faces of the 20 in. Indiana limestone core after test with 4 vol% VES-based 20 wt% HCl....131

5.18 CAT scan images of the 20-inch Indiana limestone core after treatment with 4 vol% VES-based 20 wt% HCl in the single coreflood test....132

5.19 Pressure drop across the core during injection of 4 vol% VES-based 20 wt% HCl during the first set of parallel coreflood test....134

5.20 CAT scan images of the 6-inch Indiana limestone core ($k_{initial}$ = 128 md) after treatment with 4 vol% VES-based 20 wt% HCl in the first set of parallel coreflood tests....135

5.21 CAT scan images of the 6-inch Indiana limestone core ($k_{initial}$ = 1.66 md) after treatment with 4 vol% VES-based 20 wt% HCl in the first set of parallel coreflood tests....136

5.22 Pressure drop across the core during injection of 4 vol% VES-based 20 wt% HCl during the second set of parallel coreflood tests....138

5.23 CAT scan images of the 6-inch Indiana limestone core ($k_{initial}$ = 7 md) after treatment with 4 vol% VES-based 20 wt% HCl in the second set of parallel coreflood tests....139

5.24 CAT scan images of the 6-inch Indiana Limestone core ($k_{initial}$ = 2.5 md) after treatment with 4 vol% VES-based 20 wt% HCl in the second set of parallel coreflood tests....140

5.25 Volume of core effluent sample collected during the second set of parallel coreflood tests....141

6.1 Flakes and phase separation when preparing HT VES-based GLDA....145

FIGURE Page

6.2 Viscosity of 20 wt% GLDA at various shear rates at 200 ℉.....146

6.3 Viscosity of GLDA solutions at various VES-A concentrations at 200 ℉.....147

6.4 Viscosity of GLDA solutions at various VES-B concentrations at 200 ℉.....148

6.5 Viscosity of 0.2 wt% xanthan gum-based GLDA solutions at various temperatures.....149

6.6 Viscosity of 0.2 wt% guar-based GLDA solutions at various temperatures.....150

6.7 Viscosity of 5 vol% VES-A based GLDA and EDTA solutions at 200 ℉.....151

6.8 Viscosity of 5 vol% VES-B based GLDA and EDTA solutions at 200 ℉.....152

6.9 Viscosity of 0.2 wt% guar-based GLDA and EDTA solutions at 200 ℉.....153

6.10 Viscosity of 0.2 wt% xanthan gum-based GLDA and EDTA solutions at 200 ℉.....154

## LIST OF TABLES

TABLE Page


1–1 Examples of Surfactants in Each Category ..... 10

2-1 Formula of the VES-based Acid with 5 wt% HCl ..... 61

2-2 Power-Law Parameters for VES-based 5 wt% HCl Solution at 25 ℃ ..... 62

2-3 Summary of Coreflood Experiments ..... 67

2-4 Summary of VES Material Balance ..... 78

3-1 Summary of the Coreflood Tests ..... 84

3-2 Summary of the Core Properties ..... 84

3-3 Formula of the VES-based Acid Examined ..... 85

3-4 Time of Occurrence of Calcium Ions and VES ..... 91

3-5 Material Balance of VES after Treatment ..... 92

4-1 Summary of the Coreflood Tests ..... 101

5-1 Main Components of the Three Corrosion Inhibitors ..... 108

5-2 Composition of Live VES-Based 20 wt% HCl ..... 109

5-3 Compositions of Various Spent VES-Based Acid Solutions ..... 110

# 1. INTRODUCTION

During the production of the oil and/or gas from various reservoirs, the productivity of the well tends to decrease with time due to loss of driving force, formation damage, water production, and other possible reasons. Under certain conditions, the wells are originally low in productivity due to the low permeability of the reservoir and the high viscosity of the crude oil. Thus, achieving the desired production rate for a certain well is a great challenge to the oil and gas industry.

## 1.1 Techniques Used in Well Productivity Enhancement

To enhance the productivity of the well, several techniques have been widely used for decades to achieve the goal. For wells that lose their driving forces, gas injection, and water injection, water/chemical flooding are the main methods to push the residue oil out from the reservoir. For cases with unexpected water production, blockage of the water production zone with mechanical and chemical techniques is applied. For the wells and reservoirs with formation damage and low initial permeability, acidizing and fracturing are the main forces to solve the problems. Fracturing includes two main types: hydraulic fracturing and acid fracturing. In both cases, fracturing fluids are injected into the formation beyond the fracture pressure, and cracks are created to provide flow channels for the trapped oil and gas. Proppants are carried in together with treatment fluid to support the cracks from closing in the sandstone and the shale formations. Acids are part of the formula of the fracturing fluid to create mismatching

teeth in the carbonate formation to maintain open channels. The technique is a good choice for conditions under which the permeability of the formation is less than 0.1 md. More commonly, acidizing is used to improve the permeability of the wells that cannot produce efficiently. The basic mechanism of acidizing is to dissolve the minerals present in the formation and create channels for the liquid to flow through. For sandstone formations, the main composition of the rock is silica, which can only be dissolved by hydrofluoric acid (HF). However, some of the sandstone formations could contain up to 10% carbonate, which could adversely cause damage when interacting with HF and soluble in hydrochloric acid (HCl). Thus, one of the most popular formulas was to mix HF and HCl to create channels for the oil and/or gas to flow. For carbonate formations, the main composition, carbonate, could be up to 99% present in the mineral. Thus, most of the acid formulas are based on HCl at various concentrations. Channels with much larger diameters and lengths could be created after the treatment. As the shape of the channel looks like the propagations of worms, they are named as wormholes. The formula was not straightforward, which is composed of only HCl and water. Many scientists and experts have worked hard to provide a formula that could be used under various conditions. Thus, the history of the development of the acid formula for carbonate formations needs to be discussed.

## 1.2 History of the Development of the Acidizing Formula

The first acidizing treatment was conducted by Ohio Oil Company in 1895 using HCl, and such methods were first recorded in 1896 (Williams et al. 1979). However, the

high corrosivity of HCl could cause adverse effects, and corrosion inhibitor was introduced to overcome the shortage. Since then, a wide range of additives with various functions was developed, such as viscosifiers, friction reducers, pH buffers, etc. With the increasing number of wells, numerous challenges were encountered by the industry. One of them is that the wells penetrate through various layers of heterogeneous reservoirs, which results in uneven acid displacement. To distribute the acid treatment fluid homogeneously, two main branches of methods were introduced (Hill and Rossen 1994): mechanical and chemical. The mechanical methods include zone isolators, packers, ball sealers, coiled tubing methods, etc. The chemical methods include foam acids, particulate diverting agents, gelled acids, emulsified acids, etc. The mechanical methods were proven to be more expensive and time consuming than the chemical methods (Chang et al. 2007) and were neither applicable nor effective in open holes. Chemical methods were more effective and the treatment could still be under control even deep inside the formation. One method is to use gelled acids to achieve deep acid penetration to obtain maximum stimulation benefits (Deysarkar et al. 1984). Polymers were first introduced as a viscosifier in the acid system. Polymers that are not crosslinked are not as effective as the acid soluble polymers, or crosslinked polymers, introduced in mid 1970s. These polymers can increase the viscosity of the injection fluid to improve the performance of HCl (Pablet et al. 1982; Yeager et al. 1997; Metcalf et al. 2000). To apply crosslinked polymers in in-situ gelled acids, it usually contains acid, polymer, crosslinker, breaker, buffer, and some other possible additives. Generally, in-situ gelled acids are good to use. However, retention of polymer inside the formation can cause

severe damage and significantly reduce the permeability of the reservoir. Thus, viscoelastic surfactants were applied instead, in the in-situ gelled acid treatment fluids.

### 1.3 Application of Viscoelastic Surfactant before Used in Acidizing

Before the widespread application of viscoelastic surfactant (VES), polymers were the only choice of the oil and gas industry to form gelled acid. The first ever application of VES to increase fluid viscosity through gelation was introduced in 1986 (Kubala 1986). The primary characteristic of the surfactant was retained, as the VES also functionalized to create foams. The main disadvantages of polymer-based gelled acids include “fish-eye” and/or microgel presentation, polymer degradation after extensive shear, and filtration problems without sufficient shear. Thus, VES was introduced to replace polymers to aid in the suspension of the gravel carrier fluid (Nehmer 1988). Because VES is easy to mix, it causes no formation damage, improves leakoff characteristics, and provides better suspension properties. An increase in work had involved the use of VES. Then, fracturing fluids based on VES without solids were used in the field (Stewart et al. 1995). The VES-based fracturing fluid was extensively compared with the conventional polymer-based fluids (Parlar 1995). Many advantages were noticed during the following field applications (Brown et al. 1996). Then this special VES, a quaternary ammonium salt derived from long-chain fatty acids, was widely used and systematically studied in the laboratory (Samuel et al. 1999). The concentration of VES, temperature, type of salts, and fluid salinity were well investigated. The mechanism of the transition from spherical to wormlike micelle was

proposed (Lin et al. 1994). Later, VES was used as diverting agent during matrix acidizing to evenly distribute the treatment fluid (Chang et al. 2000).

## 1.4 Application of Viscoelastic Surfactant as Diverting Agent in Acidizing

A VES-based in-situ gelled acid system can be prepared by adding surfactant into the acid. VES forms spherical micelles, initially, inside the fluid when its concentration is above the critical micelle concentration, which has negligible effect on the fluid viscosity. During the reaction between the acid and the carbonate formation, the pH of the fluid will increase to nearly 4.5 with the generation of multivalent cations, which are mainly $Ca^{2+}$ and $Mg^{2+}$. These cations will assist the VES in forming wormlike micelles that are much longer than the spherical micelles. Furthermore, the micelles could become entangled with each other through the branches on the micelles, which would result in a significant increase in fluid viscosity. Therefore, VES fluids can be used to improve the fluid diverting ability in acidizing treatments. VES acid systems have been successfully applied in the oilfield industry as fracturing fluids and matrix acidizing fluids (Chase et al. 1997; Chang et al. 2001; Nasr-El-Din et al. 2003). Unlike polymer-based in-situ gelled acid, with huge amounts of residues left in the formation, wormlike micelles formed by VES can be easily broken by the hydrocarbons produced during flowback. When reservoir fluid does not naturally break the VES based in-situ gel, a post flush of mutual solvent is recommended to ensure the breaking of the gel (Samuel et al. 1997; Yang 2002; Nasr-El-Din et al. 2006a). When applying the VES in the acid, rather than the creation of foam during the treatment with the assistance of

nitrogen gas, single liquid phase treatments were designed. Diversion from high permeability zones to low permeability zones, as well as from a water-rich zone to an oil-rich zone was achieved. The new self-diverting acidizing treatment was further studied in the laboratory. Effects of temperature, influence of fluid pH, and the comparison with conventional treatment methods were shown (Chang et al. 2001a). Then, the treatment carried out with VES-based acid in a deep-water high permeability formation was a great success (Chang et al. 2001b). Internal breaker was evaluated. It did help to break down wormlike VES micelles during the flowback process, and no adverse effect was noticed (McCarthy et al. 2002). The first generation of VES was mainly quaternary amines (cationic surfactants) or fatty acids (anionic surfactants). Their intolerance of the high salinity of treatment fluids and low thermal stability limited their applications. Thus, the new generation of VES, zwitterionic surfactant, was developed (Daniel et al. 2002). The zwitterionic surfactant was widely used in all aspects during oil and gas production: diversion of acid from high permeability zones, matrix stimulation, acid fracturing, and fluid loss control (Nasr-El-Din et al. 2003). The maximum pressure ratio, defined as $dP_{max}/dP_0$, was introduced to characterize the diverting ability of various acid systems (Lungwitz et al. 2006). In addition, this new VES-based acid system was proven very effective even facing the challenge of high heterogeneity in long horizontal wells with open-hole completion (Nasr-El-Din et al. 2006c). During the treatment process, a combination of chemicals will be used to achieve various purposes. Thus, effects of other commonly used additives in acidizing on VES were evaluated (Nasr-El-Din et al. 2008). The mutual solvent, citric acid, methanol, and emulsifiers all

exhibited the characteristics that led to the reduction of the viscosity of the VES-based acid. All VES-based acids reached the maximum viscosity point at a certain temperature and decreased after that with continuous heating. More than 200 wells were treated with VES-based acids. No operational problems were encountered. The quick cleanup process and long-term sustainability of the stimulation outcome both benefit the production of the treated wells (Nasr-El-Din and Samuel 2007). Successful treatments with VES-based acid were observed. Acid diversion was confirmed with parallel coreflood tests in the laboratory (Nasr-El-Din et al. 2006b). To stabilize VES gels, a special stabilizer was used to enhance its tolerance to high temperatures (Crews et al. 2008). Meanwhile, to assure the flow of the VES after treatment, internal breaker was added to the formula to achieve a high production rate. Another series of internal breakers for VES gels were developed and evaluated. They could benefit the system, especially when the gel was under low shear rates (Crews and Huang 2007). The reaction kinetics between the VES-based acid and the carbonate formation was studied (Nasr-El-Din et al. 2009). VES reduced the dissolution rate of calcite in two ways: by reducing the diffusion of key ions and forming barriers on the interface. A model to predict the performance of the VES was proposed based on a series of lab work (Al-Ghamdi et al. 2009). The injection rate of the acid was the key parameter in this model. The calcium ion concentration in the core effluent was the indicator of the propagation for the spent acid front. Long cores are preferred during the tests to have a better observation of the wormhole creation. Then, a series of parallel coreflood tests were conducted to improve the model and predict the performance of potential acidizing

treatments (Al-Ghamdi et al. 2010). Another key parameter is the propagation front of the VES. However, the concentration of VES in the core effluent was not able to be determined until a titration method was proposed (Yu and Nasr-El-Din 2009). The two-phase titration was dependent on the competition between the titrant and the color indicator. Following that, the retention of VES in the treated core was analyzed. Even with the help of 10 vol% mutual solvent, only 20 wt% of the original VES could be washed out (Yu et al. 2011). The zwitterionic surfactants used in the previous tests are mostly carboxybetaine. A new amphoteric surfactant based on amidoamine-oxide was developed. A series of evaluations was conducted to understand the performance and properties of the new VES (Li et al. 2010). Temperature, salinity, corrosion inhibitor, shear history, and many other factors were well studied with the new VES system on both live and spent acid. Combinations of weak organic acids and HCl with the presence of VES were examined for potential high temperature applications (Li et al. 2011). All organic acids tend to decrease the viscosity of the VES-based acids. Additional VES is recommended to maintain the same level of viscosity if applied in the mixing system. As VES is very helpful in the oil and gas industry, more background knowledge about VES will be addressed.

## 1.5 General Information of Viscoelastic Surfactant

Surfactants, a blend of surface-active agents, are organic compounds that contain both hydrophobic groups (tail) and hydrophilic groups (head). As they have this special amphiphilic characteristic, they tend to get involved in changing the physical properties

near the interfaces or in forming micelles. Generally, surfactants are used in detergents, paints, inks, shampoos, toothpastes, etc. As in the petroleum industry, surfactants are widely used in emulsion, foam, anti-emulsion, changing of wettability, reduction of interfacial/surface tension, increment of viscosity of drilling fluids, etc. The main application that will be discussed in detail is its diverting ability by the formation of micelles in acid stimulation.

Surfactant can be divided into four different categories based on the charge of the molecule: nonionic, cationic, anionic, and zwitterionic (**Figure 1.1**). Several samples in each classification are given in **Table 1–1**. Micelles can be formed by various kinds of surfactants with or without the assistance of corresponding counterparts. However, the concentration of the surfactant should be above the critical micelle concentration (CMC). The CMC is determined by measuring the surface tension of a certain fluid at various concentrations of the surfactant. The surface tension tends to decrease with the increase of the surfactant concentration in the first region. When the concentration of the surfactant reaches CMC, the surface tension remains almost constant and even the concentration of the surfactant keeps increasing, as shown in **Figure 1.2**. Originally, the surfactant molecules form spherical micelles. With the introduction of other components, the spherical micelle will shift to wormlike or rod-like micelles. The wormlike micelles tend to entangle with each other through the branches and a pseudo-polymer network is established. Thus, the VES-based solution exhibits a much higher viscosity and viscoelasticity.

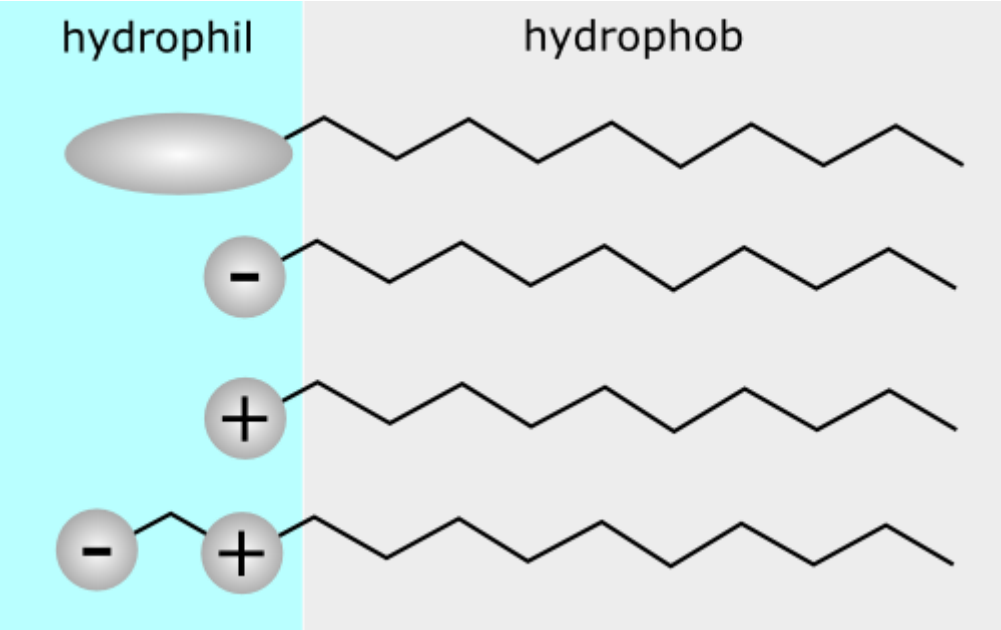


**Figure 1.1:** Different types of surfactant divided based on the charge carried. Top to bottom: nonionic, anionic, cationic, and zwitterionic (http://en.wikipedia.org/wiki/File:TensideHyrophilHydrophob.png).

**Table 1–1:** Examples of Surfactants in Each Category

| Class | Example |
|---|---|
| Anionic | Na stearate |
| | Na dodecyl sulfate |
| | Na dodecyl benzene sulfate |
| Cationic | Laurylamine hydrochloride |
| | Trimethyl dodecylammonium chloride |
| | Cetyl trimethylammonium bromide |
| Nonionic | Polyoxyethylene alcohol |
| | Alkylphenol ethoxylate |
| | Propylene oxide-modified polymethylsiloxane |
| Zwitterionic | Dodecyl betaine |
| | Lauramidopropyl betaine |
| | Cocoamido-2-hydroxy-propyl sulfobetaine |

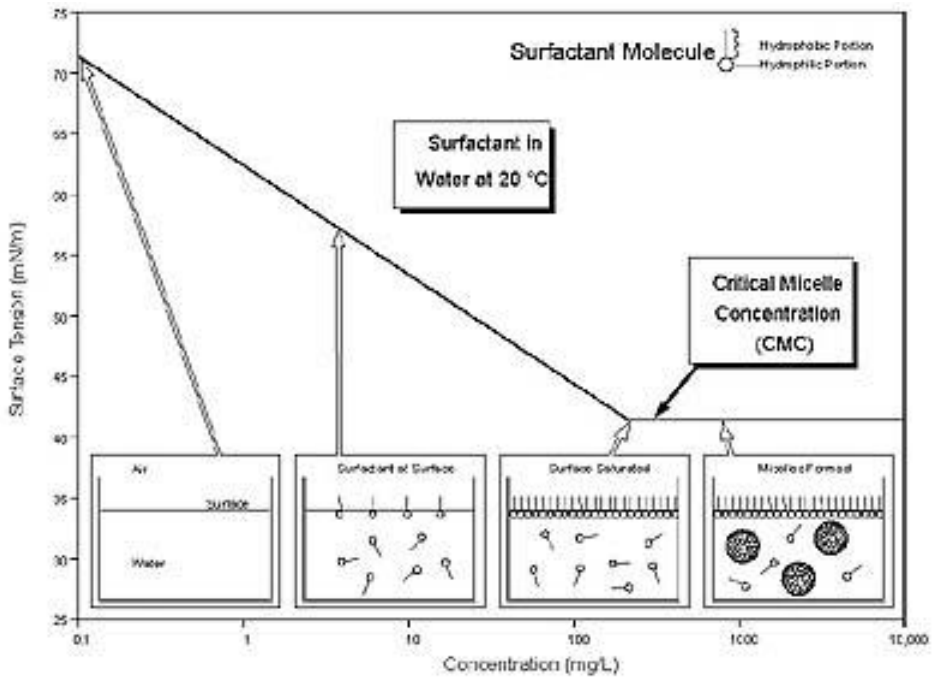


**Figure 1.2:** Addition of surfactants reduces the surface tension of water until the surfactant concentration reaches the CMC (http://www.kruss.de/uploads/pics/4-en.jpg).

The theory for the VES to form micelles was first proposed in 1976 (Israelachvili et al. 1976). The analysis was based on thermodynamic considerations of the surfactants when they were present in the solution. Free energy from the surfactants is the key factor that affects the formation of micelles. The paper implied a specific parameter to determine the possible formation of the surfactants. It is the ratio between the volume taken by one surfactant molecule in the solution to the product of the effective length of the surfactant molecule and the cross-section area of its hydrophilic head. When this number is less than 1/3, the VES forms spherical micelles. When the number is between

1/3 and 1/2, the wormlike micelles could be formed. If the value is over 1/2, a planar bilayer will be formed. Different structures of the micelles are shown in **Figure 1.3**.

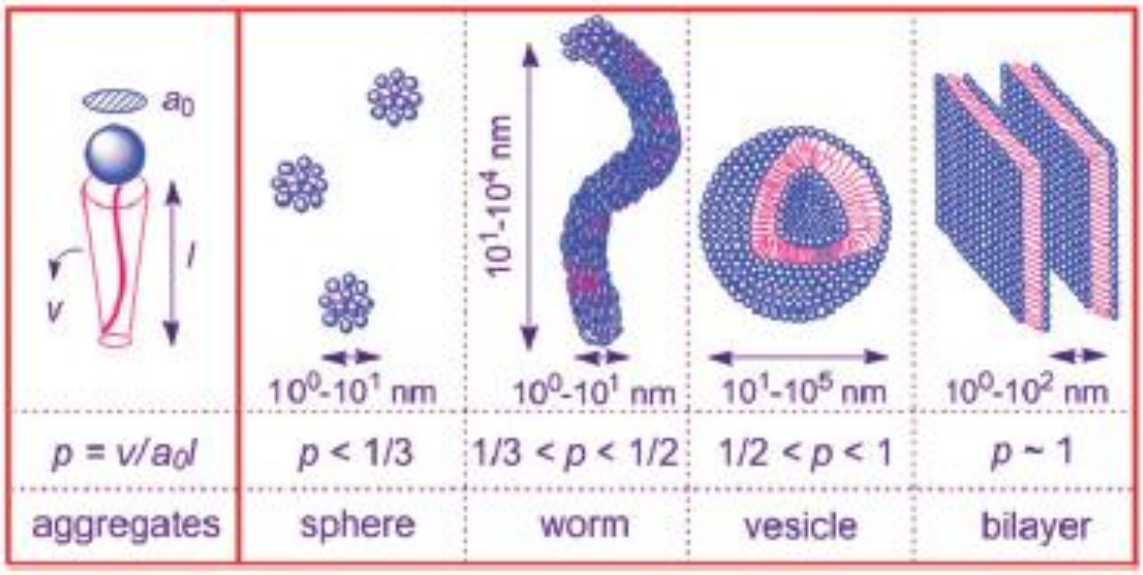


**Figure 1.3:** Various structures formed by surfactants under various packing parameters (Chu et al. 2013).

Just like the other surfactants, VES also tends to attach to certain polar surfaces based on the net charge carried by the molecule. This is an important characteristic to consider when it is necessary to use them to change the rheological properties of the fluid. The adsorption of the VES could cause a reduction of the amount presented to change the fluid property and rewet the surface of the rock. Thus, the concentration of the VES needs to reach a certain level such that the material can really achieve the goals that were set at the beginning of the treatment. The problem of the adsorption of ultra-

long-chain zwitterionic surfactants was addressed and it was distinguished into three main divisions based on the concentration of the VES, as shown in **Figure 1.4**.

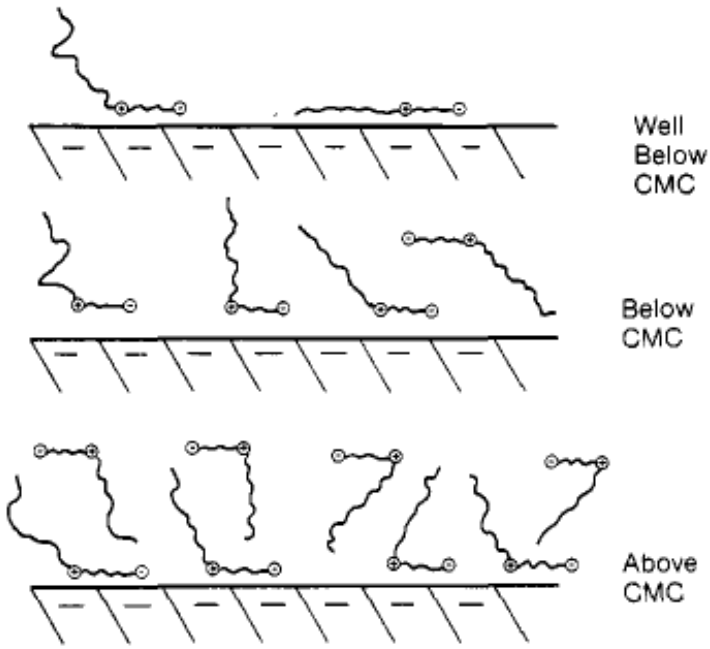


**Figure 1.4**: Adsorption of zwitterionic surfactant on the surface at various concentrations (Brode 1988).

With the name of surfactant, the VES can also assist in the drag reduction during the injection of the treatment fluid. The most popular used VES in the oil and gas industry are mainly amine-based molecules with unsaturated long chain alkyl groups or short hydroxyethyl groups. The special structures assist the VES in becoming more soluble at low temperatures while maintaining the high critical temperatures. The most significant factor of the function of the VES at constant concentration is temperature.

The drag reduction caused by the VES significantly increases with the increase of temperature. Details of the friction factor change with temperature was provided in **Figure 1.5**.

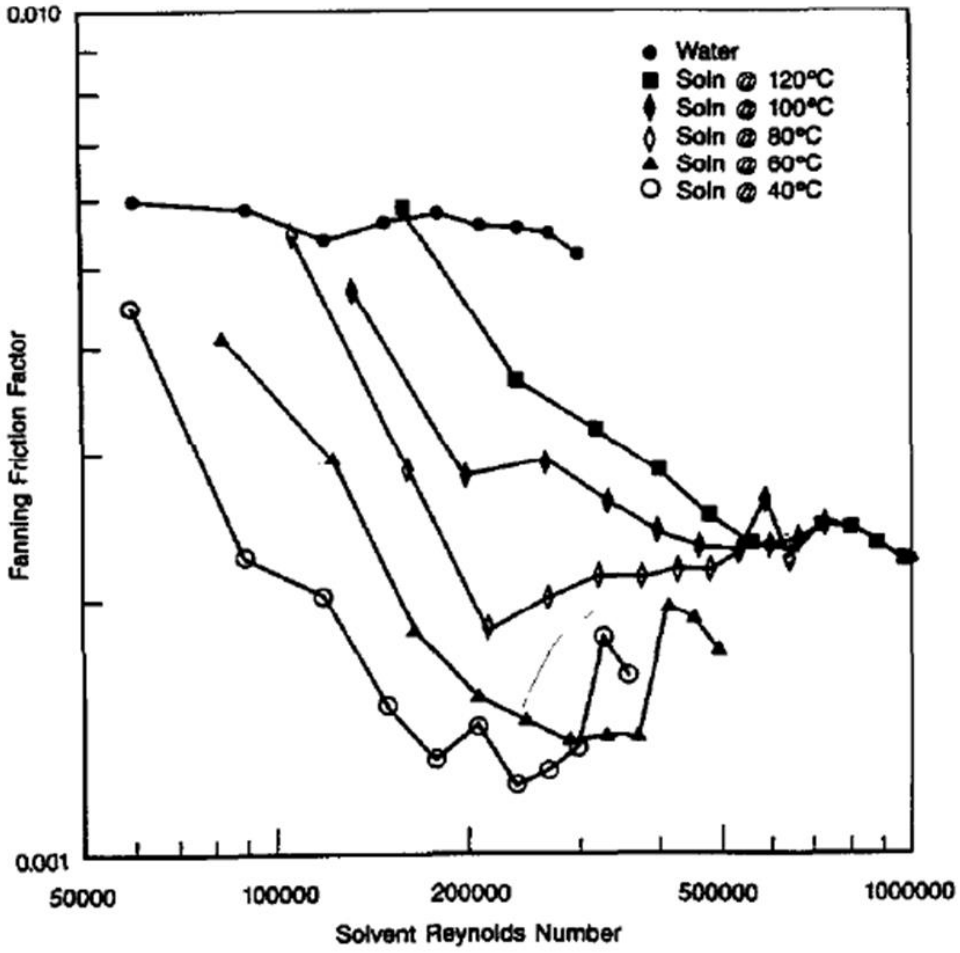


**Figure 1.5**: Friction factor of solvent at various temperatures (Rose and Foster 1988).

As in the oil and gas industry, another function of the VES that has been widely used during matrix acidizing and fracturing treatment is the non-Newtonian fluid

behavior. At very low concentrations of the VES, the fluids behave as the Newtonian fluid with a slightly higher viscosity than water. However, when the concentration of the VES is significantly above the CMC, wormlike micelles could be formed with the assistance of the counter ion species and the fluids behave as non-Newtonian fluids. The viscosity of the fluid decreases with the increase in shear rate, as shown in **Figure 1.6**. In addition, the storage modulus and loss modulus of the fluid significantly depend on the rotating frequency, **Figure 1.7**.

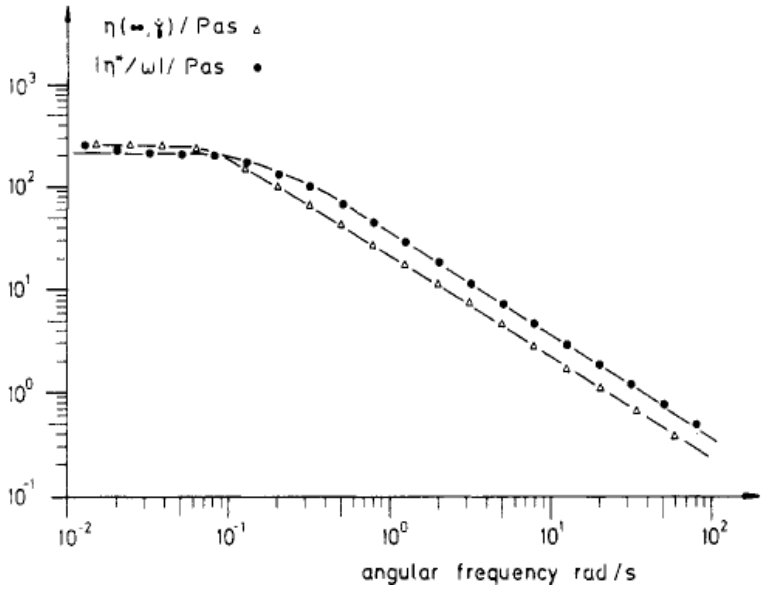


**Figure 1.6**: Viscosity and absolute value of viscosity at various shear rates (Rehage and Hoffmann 1988).

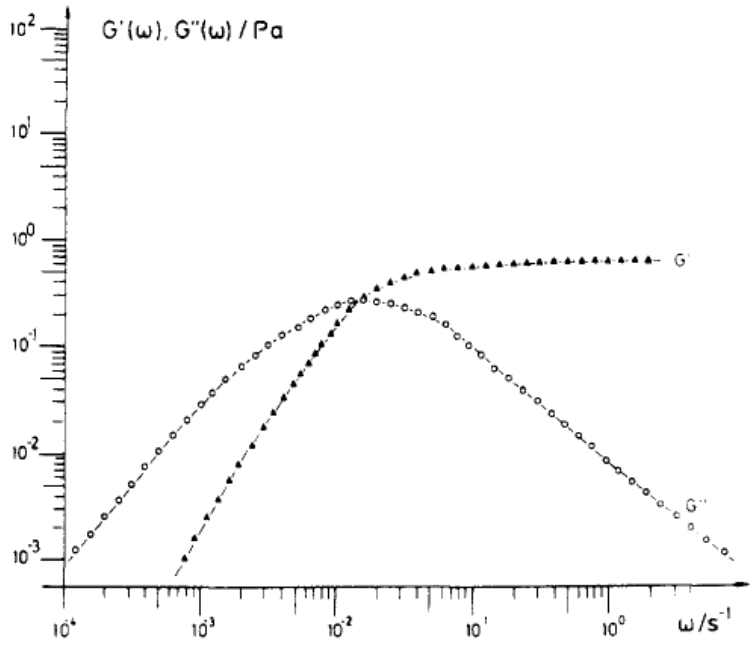


**Figure 1.7**: Storage modulus and viscous modulus as a function of shear rates (Rehage and Hoffmann 1988).

Generally, the aggregation behavior of the VES molecules is induced by the increment of the surfactant concentration. However, temperature also plays an important role during the formation and deconstruction of the micelles. The effect was investigated through the measurement of the fluid viscosity, as shown in **Figure 1.8**. At a constant surfactant concentration, there are three regions based on the fluid temperature. In region I, at low temperatures, the solutions are clear and have been shown to contain spherical or wormlike micelles. With increasing temperature to region II, a reduction in the head group area requirement promotes an increase in micelle lengths. The overlapping micelles form a gel network structure in solution via hydrogen bridge-bonds. Thus, a

shear-thinning behavior is observed. At higher temperatures, the gel structure is destroyed when the cloud point is reached in the region III.

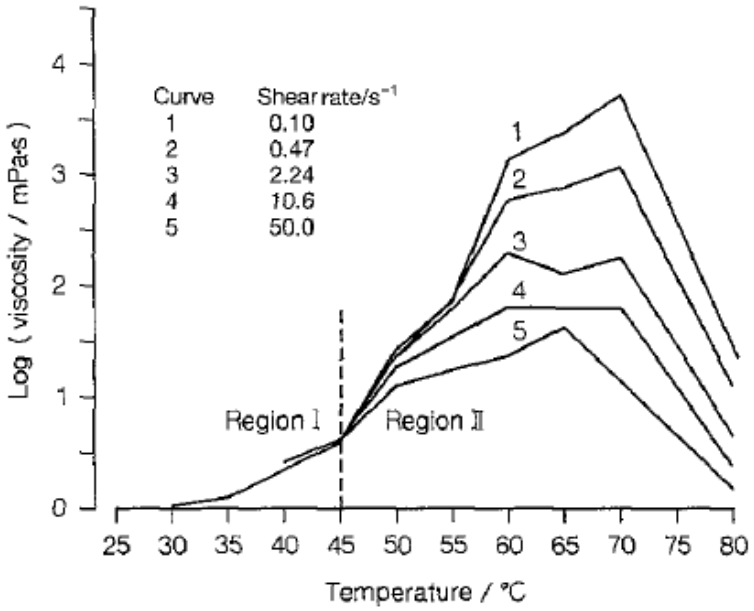


**Figure 1.8:** Effect of temperature on fluid viscosity behavior (Greenhill-Hopper et al. 1988).

Salt concentration also affects the viscosity of the VES-based fluid, as suggested in **Figure 1.9**. The addition of salt at lower concentrations usually assists the formation of the wormlike micelle and the entanglement between the micelles. However, when the salt concentration was above the critical point, the viscosity of the fluid tended to decrease.

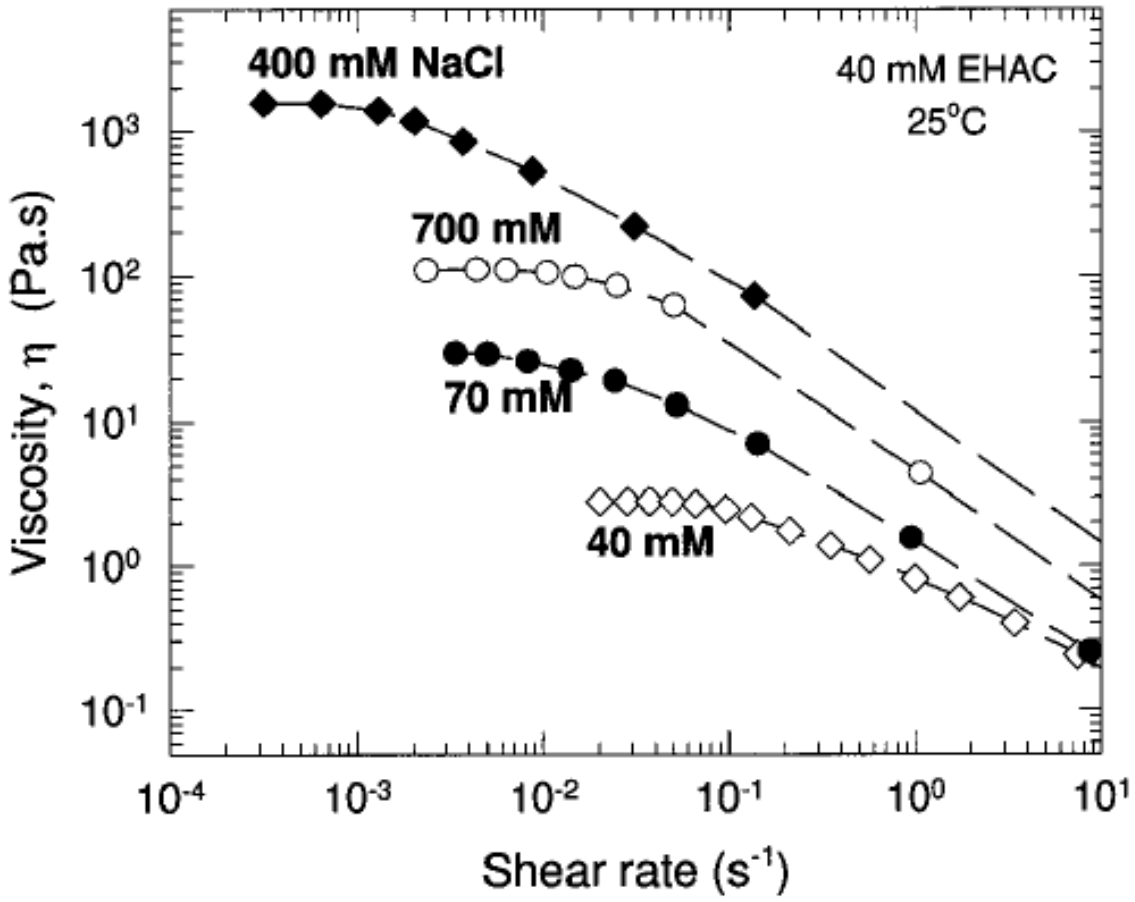


**Figure 1.9**: Effects of NaCl on the apparent viscosity of EHAC based fluid (Raghavan and Kaler 2001).

The excess amount of salt made the micelles formed at the first place transfer into vesicles. The transformation can be reversed by heating up the fluid. The mechanism is that excess salt was weakly bonded between VES molecules. Heating helps desorption of the excess amount of salt and wormlike micelles will be formed. Schematic description is provided in **Figure 1.10**.

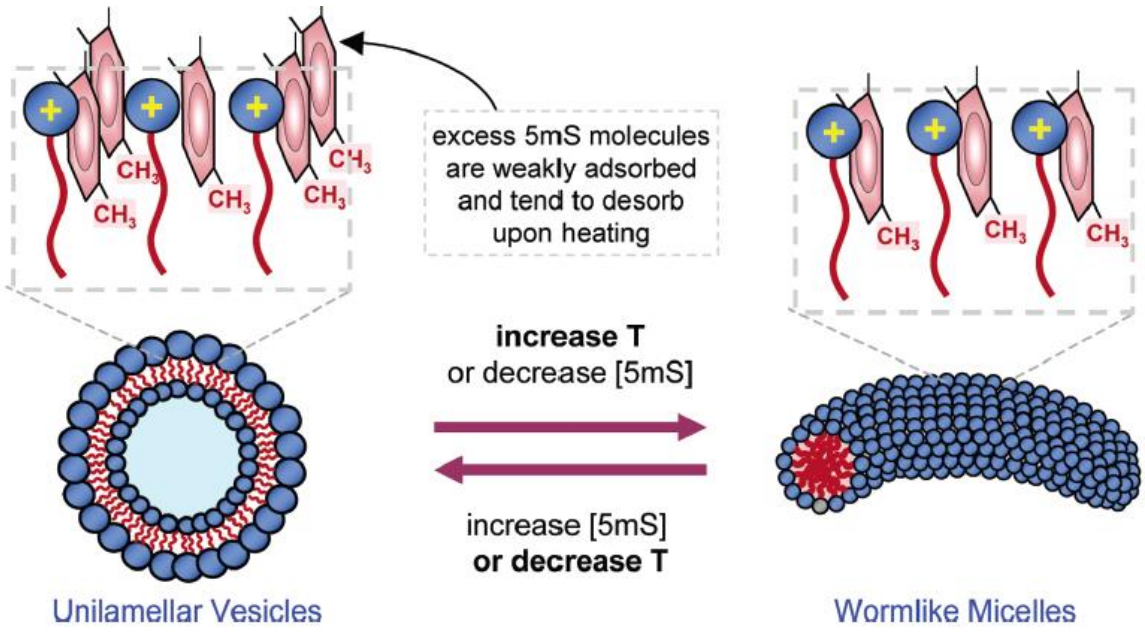


**Figure 1.10**: Temperature sensitive VES system (Davies et al. 2006).

Thus, with the very impressive research and development of the VES, the application of a specially designed VES was patented in 1988. Instead of using polymer as the thickener in the oil and industry, VES was introduced with various advantages over the conventional method. The whole thickening process is easily reversible. The VES was added to the target solution and the fluid was very good at carrying solids. When the mission was accomplished, there were several ways to reduce the fluid viscosity, including change of pH, introduction of hydrocarbon, change of temperature, etc. (Rose et al. 1988).

The statics and dynamics of the wormlike micelles were very well investigated. With the increment of surfactant volume fraction, the state of the fluid will change. The wormlike micelles become flexible when they reach a certain length. Then the micelles

continue to grow and start to entangle with one another as the energy required to form the structure is met. The phase change from shorter micelles to longer micelles was illustrated in **Figure 1.11**.

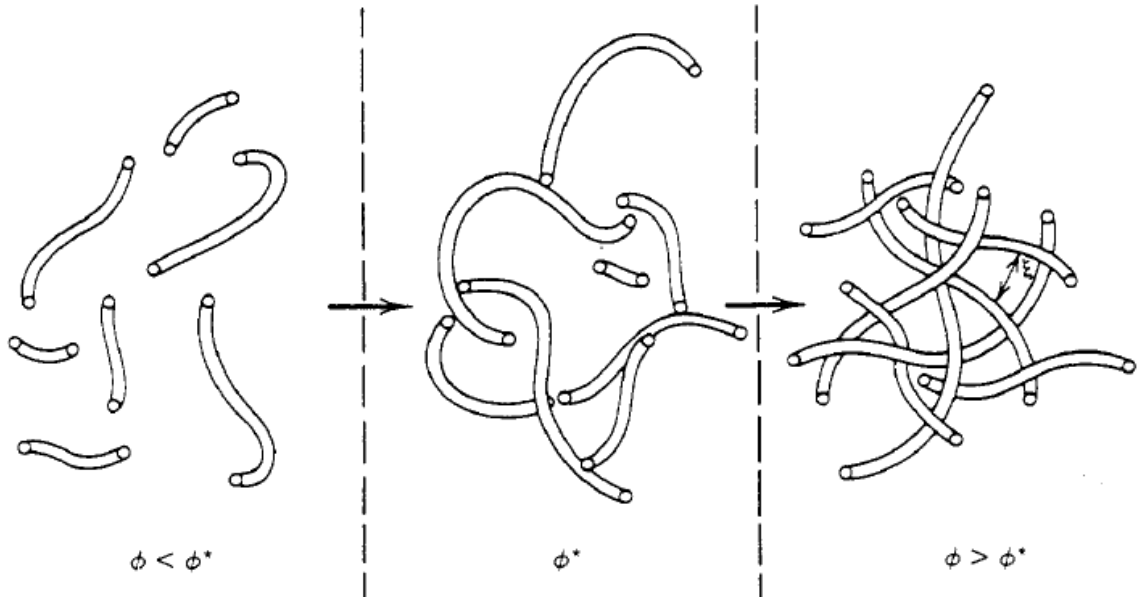


**Figure 1.11**: Transition from short micelles to long entangled wormlike micelles at different VES fraction (Cates and Candau 1990).

The concentration of the zwitterionic surfactant itself also significantly affects the viscosity of the fluid. As suggested in **Figure 1.12**, when the solution is diluted, the fluid viscosity increases linearly with surfactant concentration. However, as the formation of the wormlike micelles and the entanglement between the micelles start, the fluid viscosity increases in a power-law behavior with the surfactant concentration.

Various regions based on the surfactant concentration were identified and proper mechanisms of the change of the power-law order were proposed, as shown in **Figure 1.13**.

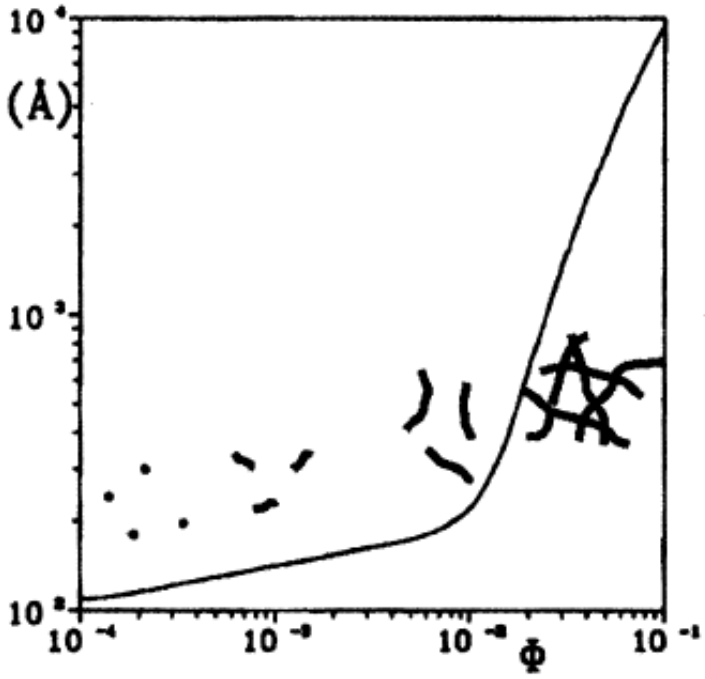


**Figure 1.12**: Length of micelles increase with increasing surfactant fraction in solution (Candau and Oda 2001).

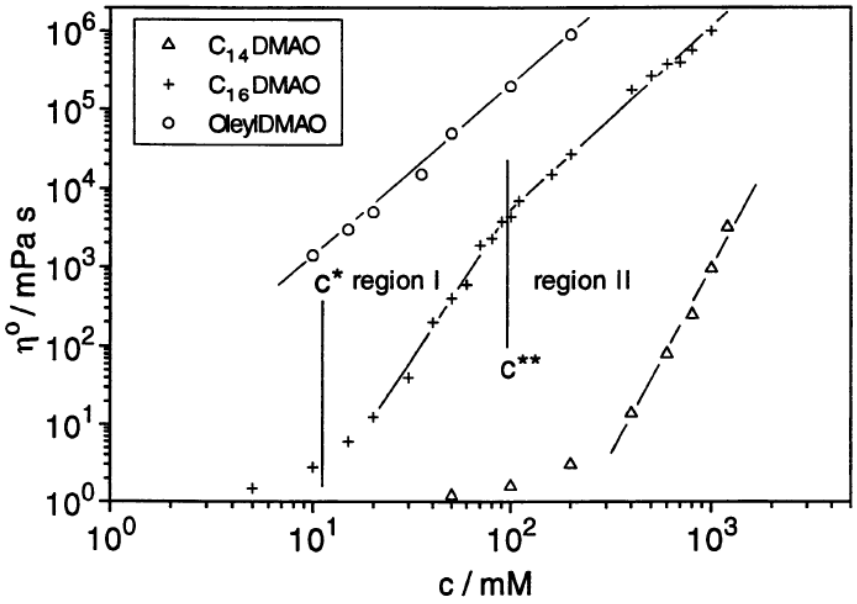


**Figure 1.13**: Different viscosity behaviors of the three amine oxide VES as a function of temperature (Hoffmann 1994).

The appearance of the VES-based solutions can be quite different from each other at various concentrations, **Figure 1.14**. The fluid is only slightly viscous at low VES concentrations. As the VES concentration increases, formation of wormlike micelles turns the fluid highly viscoelastic. With more VES added into the solution, the solution is no longer viscoelastic but only elastic. The higher VES concentration fluids are flow-birefringent, as they exhibit bright streaks under crossed polarizers when the vial is shaken or tilted.

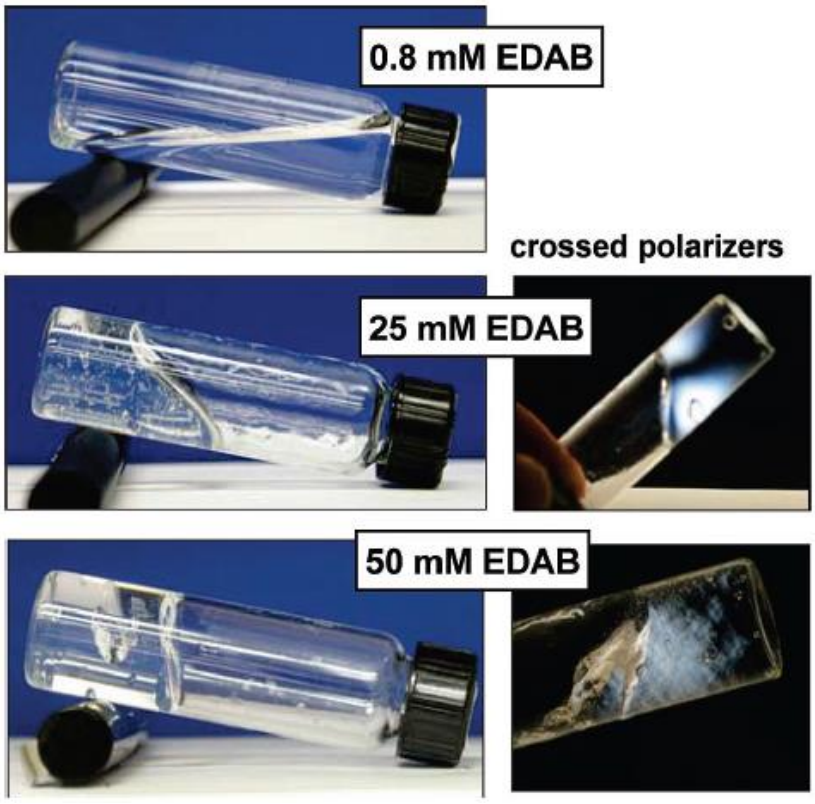


**Figure 1.14**: EDAB solutions at different VES concentrations and under the crossed polarizers (Kumar et al. 2007).

Normally in the oil and gas industry, various additives are added in one treatment fluid, and the interaction between these additives could significantly affect the outcome of the treatment. Thus, the interaction between zwitterionic surfactant and other types of surfactants could be a very good choice to start with. Surface tension, CMC, and viscosity of the fluid are very good parameters to evaluate the interactions between surfactants. The CMC reached the lowest point when the surfactants were mixed at nearly around the concentration when the zwitterionic surfactants counted for 60% of the

total surfactants. The lowest surface tensions and the highest fluid viscosities were also achieved when they were mixed at the same concentration, as shown in **Figure 1.15,** **Figure 1.16,** and **Figure 1.17**.

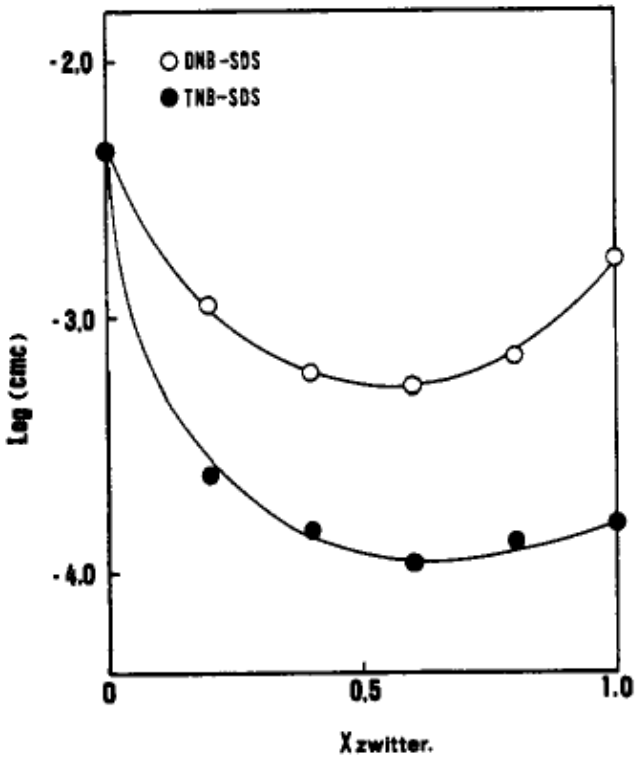


**Figure 1.15**: CMC value as a function of the zwitterionic surfactant fraction in an anionic and zwitterionic surfactant mixing solution (Iwasaki et al. 1991).

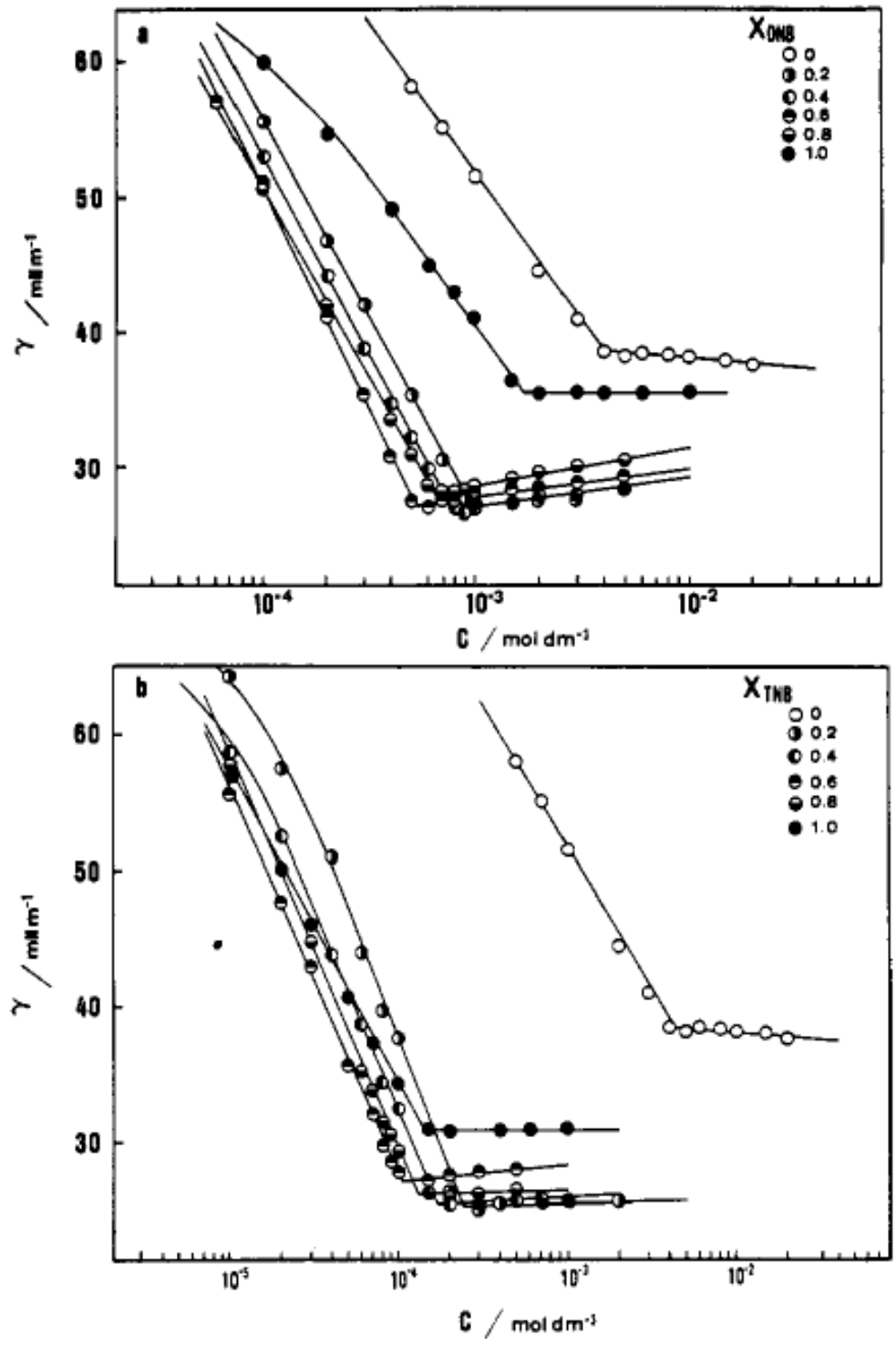


**Figure 1.16**: Surface tension as a function of the VES concentration and zwitterionic VES fraction (Iwasaki et al. 1991).

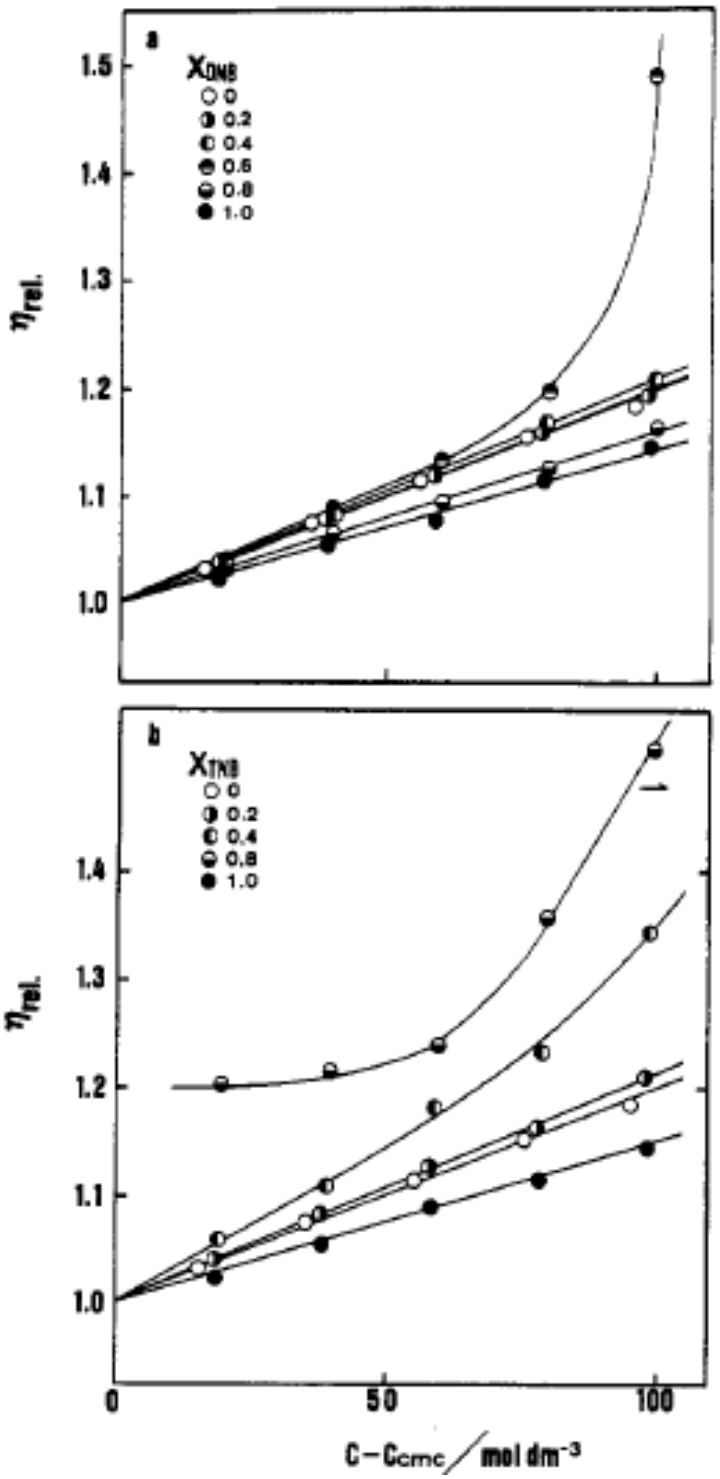


**Figure 1.17**: Viscosity as a function of the VES concentration and zwitterionic VES fraction (Iwasaki et al. 1991).

Not only the anionic surfactant was investigated, the effect of the cationic surfactant was also well studied when it was mixed in a solution containing zwitterionic surfactant, as shown in **Figure 1.18**. The original rheological behavior of the zwitterionic surfactant followed the non-Newtonian fluid, as it was shear thinning. With the addition of anionic surfactant, the zero viscosity of the fluid increased at relatively lower anionic surfactant concentration. However, over dosing of the anionic surfactant reduced the overall fluid viscosity. Meanwhile, the introduction of cationic surfactant decreased the fluid viscosity immediately after it was mixed with the zwitterionic surfactant based solution, as shown in **Figure 1.19**.

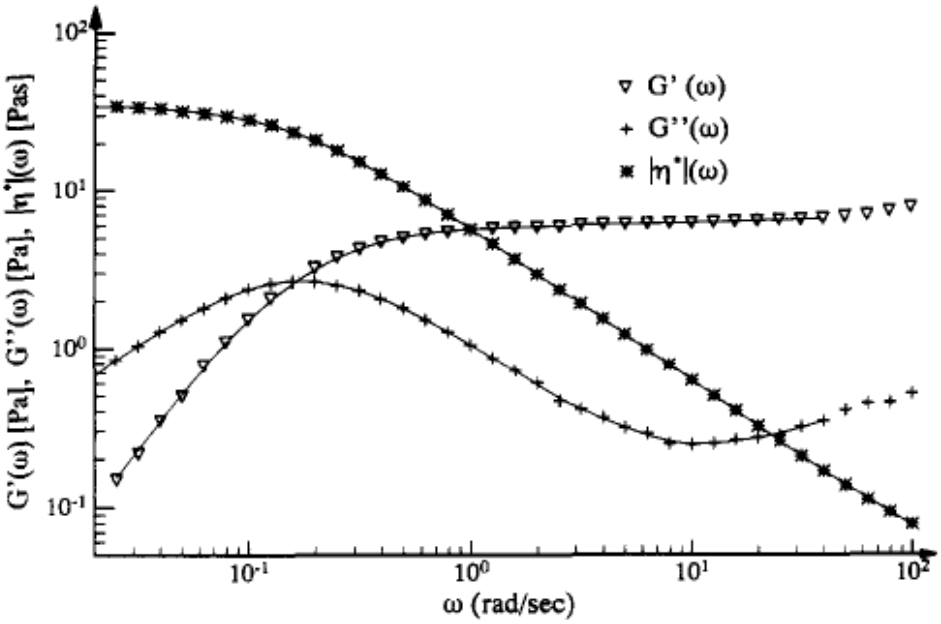


**Figure 1.18**: Absolute value of viscosity, storage modulus, and viscous modulus as a function of rotating speed (Hoffmann et al. 1992).

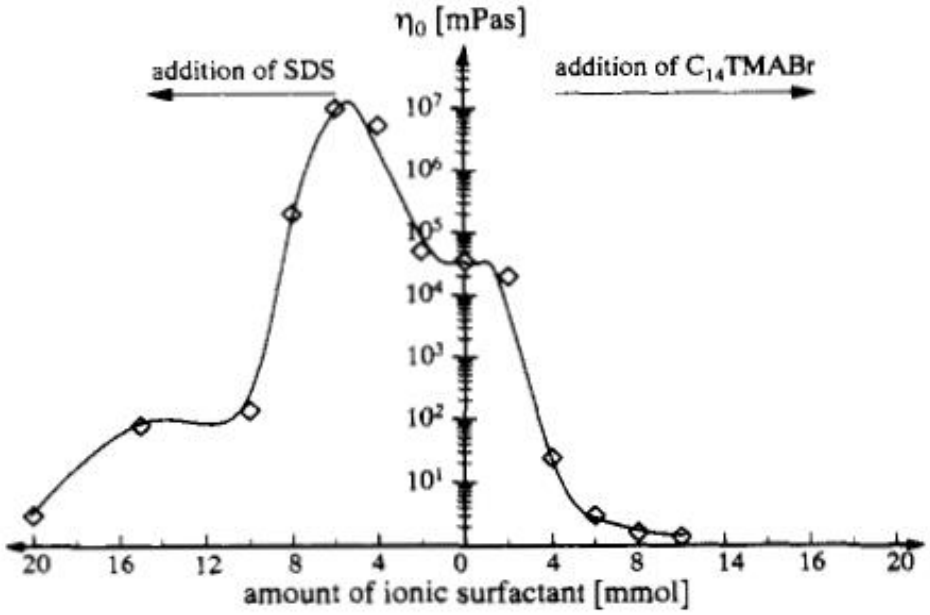


**Figure 1.19**: Effects of anionic surfactant and cationic surfactant on the viscosity of zwitterionic surfactant solutions (Hoffmann et al. 1992).

The behavior of the fluid can be further changed with the introduction of hexanol. Micelles no longer exist and instead, the surfactants are assembled in single and multi-lamellar vesicles as is shown in a freeze fracture diagram. The electron micrograph, **Figure 1.20**, shows that at the concentration of the sample the vesicles are more or less densely packed. Because of their charge, the bilayers furthermore repel each other and the vesicles cannot pass each other in shear flow without being deformed.

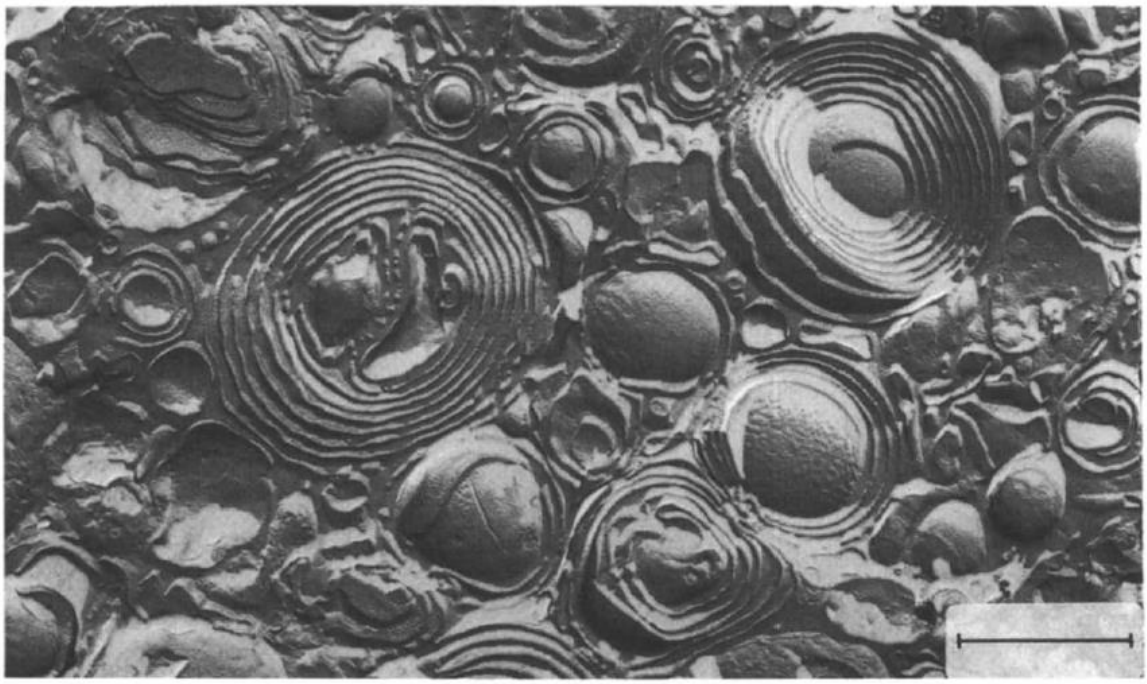

**Figure 1.20**: TEM images of VES vesicles with the presence of hydrocarbon and hexanol, bar =1 μm (Hoffemann 1994).

However, if a long chain cationic VES is mixed with a short chain cationic surfactant, vesicles formed initially could be transferred to wormlike micelles, **Figure 1.21**. This can help the solution to achieve the drag reduction function.

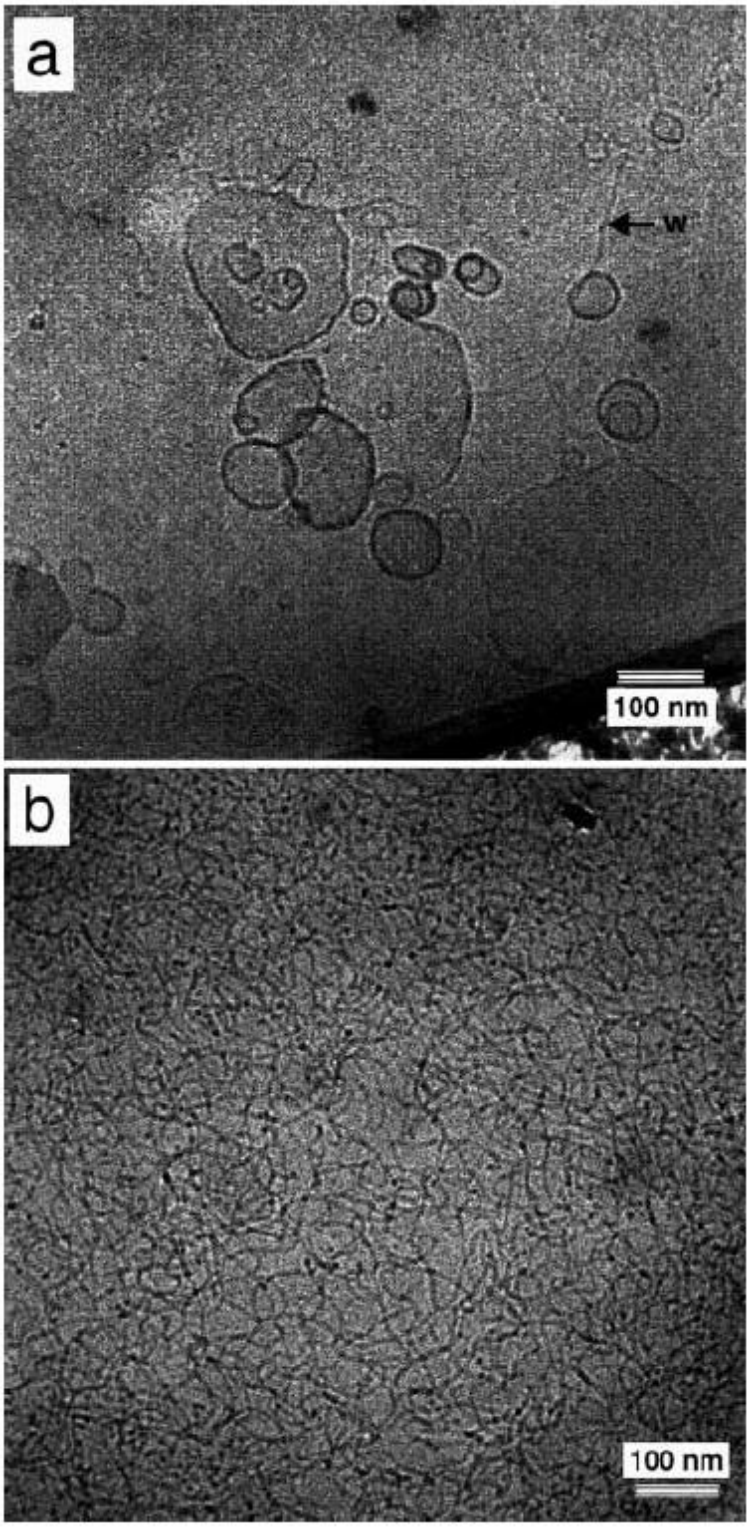


**Figure 1.21**: Transition from vesicles to wormlike micelles (Lin et al. 2000).

Other than the samples listed above, it is also worth investigating when the cationic surfactant and the anionic surfactant are mixing. The fluid viscosity tended to increase with the introduction of a small amount of the anionic surfactant into the cationic surfactant based solution. After it reached the critical ratio, the fluid viscosity started to decrease with increment of anionic surfactant ratio. The reduction of the fluid viscosity was much more significant than the increment of the fluid viscosity before the ratio reached the critical value, as shown in **Figure 1.22**. When the ratio was fixed, the addition of both surfactants increased the apparent viscosity of the fluid. However, when the concentration was above the critical concentration, the fluid viscosity started to decrease with the additional amount of surfactants. The reduction of the fluid viscosity was not as significant as the increment of the fluid viscosity before the overall surfactant concentrations reached the critical point, as shown in **Figure 1.23**.

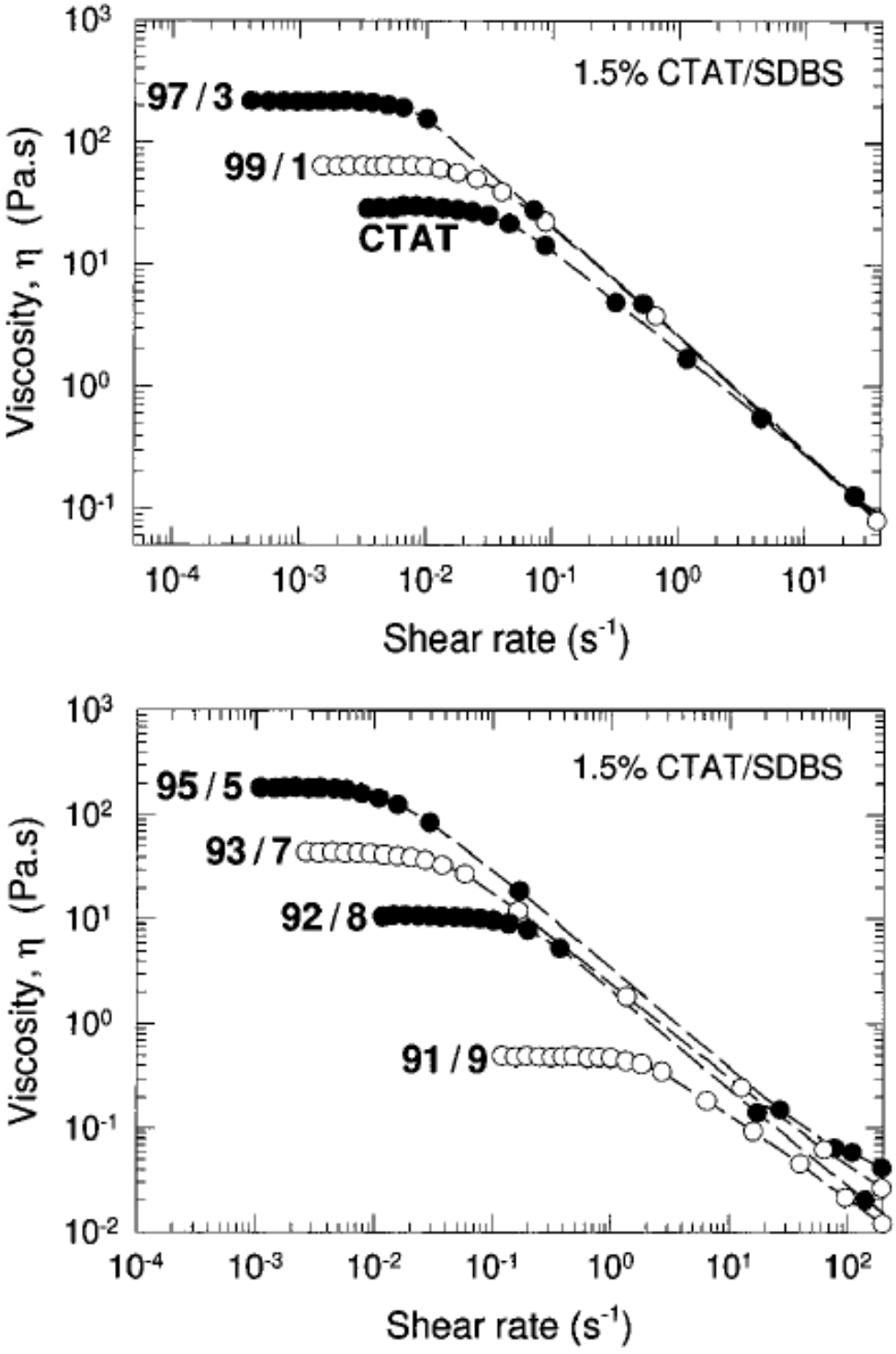


**Figure 1.22**: Viscosity of solutions with constant overall cationic and anionic mixing of surfactant concentrations and various ratios of cationic surfactant (Koehler et al. 2000).

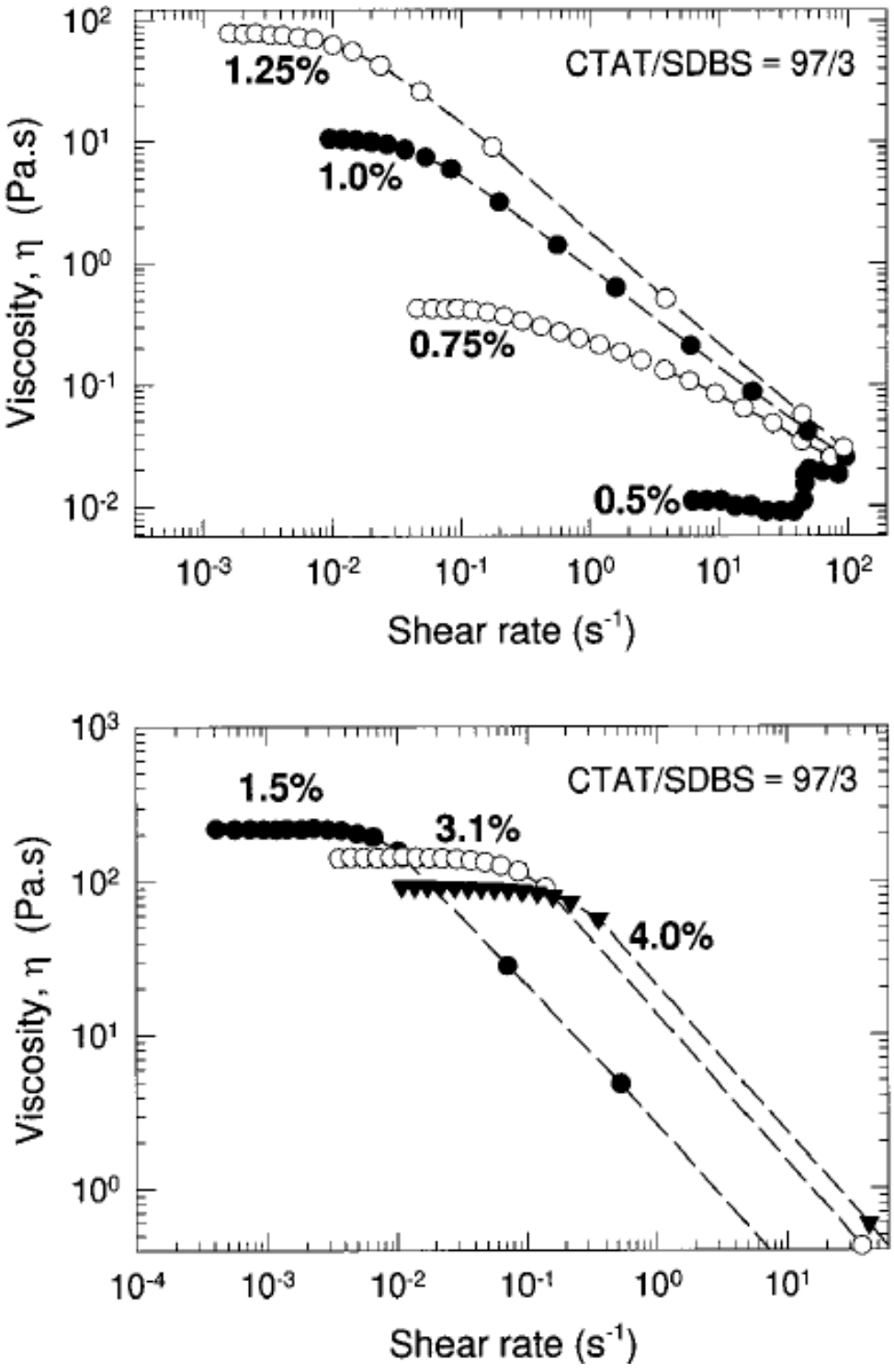


**Figure 1.23**: Viscosity of solutions with constant cationic and anionic surfactant mixing ratios and various overall surfactant concentrations (Koehler et al. 2000).

It is always well known that the VES solutions are shear thinning under most conditions. However, when the surfactant concentration is low, the fluid becomes shear thickening with wormlike micelles forming in the solution, **Figure 1.24**. The apparent viscosity of the fluid increased dramatically when the shear rate was above the critical shear rate. Meanwhile, with constant shear rate, the apparent viscosity of the fluid pumped increased after shearing at about 150 seconds. In addition, it was proven that it was the stress, rather than the shear rate, that really affected the behavior of the VES-based fluids. The mechanism is that shear thickening occurs through the heterogeneous nucleation of viscous structures at moderate stresses and through the homogeneous nucleation at high values of stress, as explained in **Figure 1.25**. In regime I, a relatively low-viscosity phase that exhibits shear thinning is observed, consistent with the shear alignment of the micelles. In regime II, a viscous phase is observed to co-exist with the less viscous phase of regime I. The viscous phase is generated by shear, and nucleates heterogeneously from the inner wall in regime II. Regime II is observed under steady state conditions only when the externally applied stress is held constant; coexistence is observed only under transient conditions when the shear rate is held constant. In regime III, the viscous phase nucleates homogeneously and fills the entire volume of the flow cell.

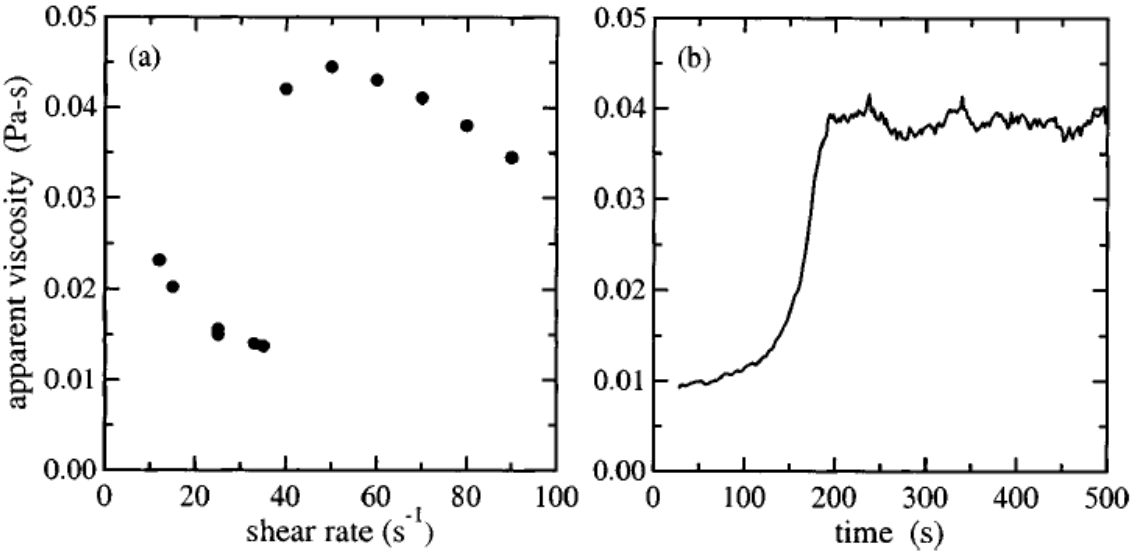


**Figure 1.24**: Shear thickening of diluted VES-based solutions as the increase of shear rate and fixed shear rate mix over time (Hu et al. 1998).

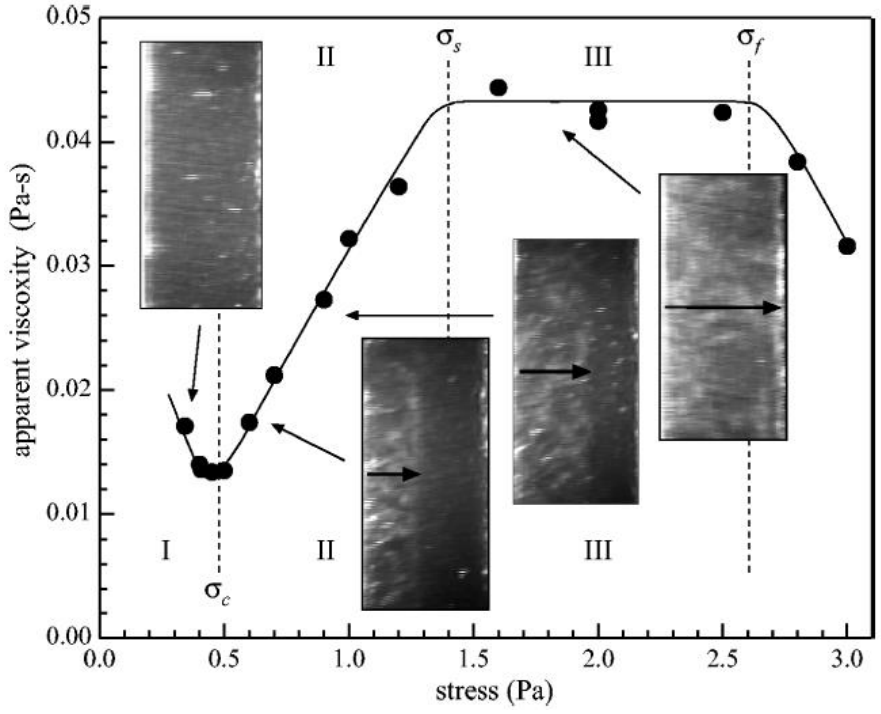


**Figure 1.25**: Shear thickening and phase behavior change of diluted VES-based solutions as the shear stress increases (Hu et al. 1998).

Another patent was published in 2001 regarding the application of a carboxybetaine viscoelastic surfactant. The rheology properties of the VES-based fluid were very well studied at different temperatures (**Figure 1.26**) and concentrations of VES (**Figure 1.27**). The patent mainly claimed the application of the VES solution in the area of solid suspension.

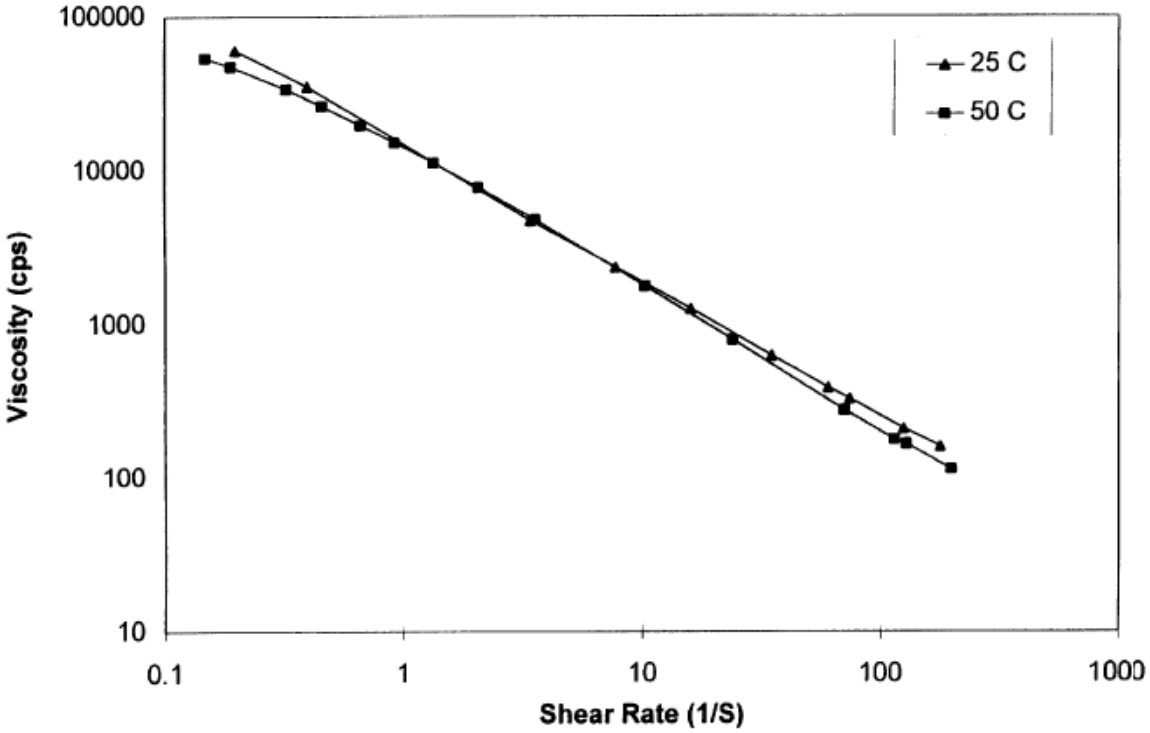


**Figure 1.26**: Effects of temperature on the viscosity of VES-based fluids for solid suspension application (Dahayanake et al. 2001).

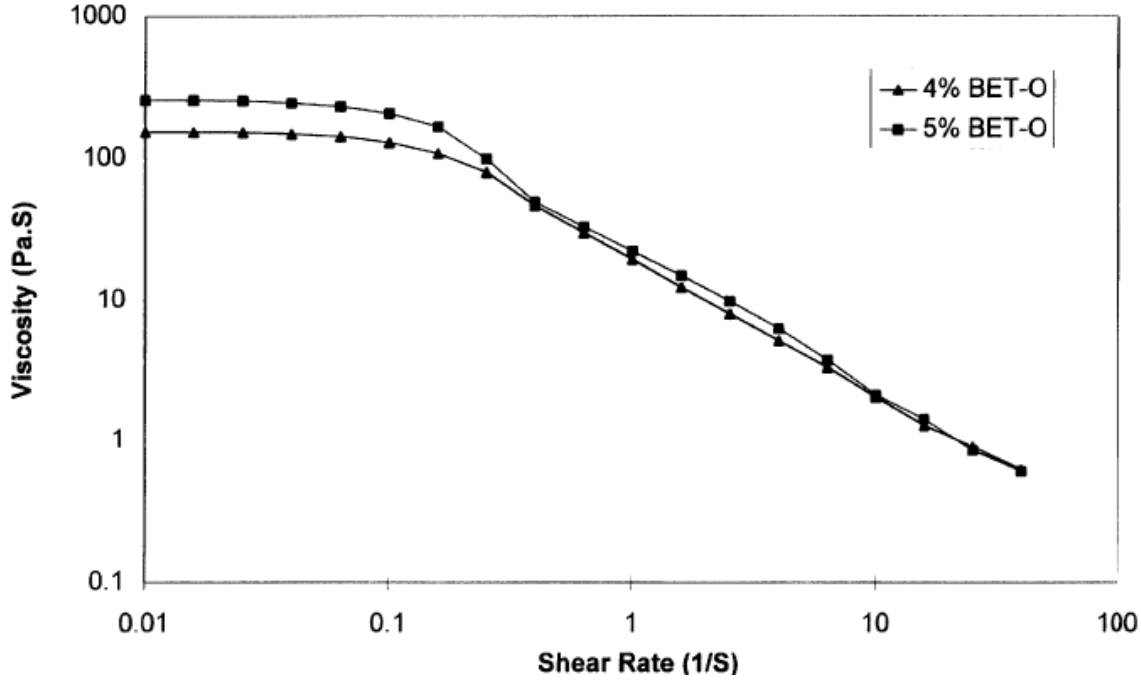


**Figure 1.27**: Effects of VES concentration on the viscosity of VES-based fluids for solid suspension application (Dahayanake et al. 2001).

The counterions used in the VES micelle formation can result in different ways of packing, as shown in **Figure 1.28**. The counterions can be divided into two main categories: penetrating and nonpenetrating. The representative of the penetrating ions is salicylate. The bulky benzene ring can penetrate the head group area, not only changing the distance between the polar head groups, but also increasing the average volume per surfactant. Meanwhile, chloride, a representative of the nonpenetrating ions, adsorbs only at the interface of the micelle and the water phase and affects only the surface area per surfactant molecule. Thus, a lower concentration of penetrating counterions is needed to drive the growth of the micelles. Some other factors could significantly affect

the micelle formation and stability. The alkyl group, for example, can favor the formation of the micelles by increasing the length. In addition, VES with longer chains can form micelles that are more stable than that formed with shorter chains. By incorporating a double bond in the long alkyl chain (carbon number larger than 16), the solubility of the VES can be significantly increased. In addition, a cis double bond is preferred as the kink in the hydrocarbon chain of the cis double bond increases the volume occupied by the hydrocarbon tail, which results in large end cap energy and favors micelle growth, as shown in **Figure 1.29**.

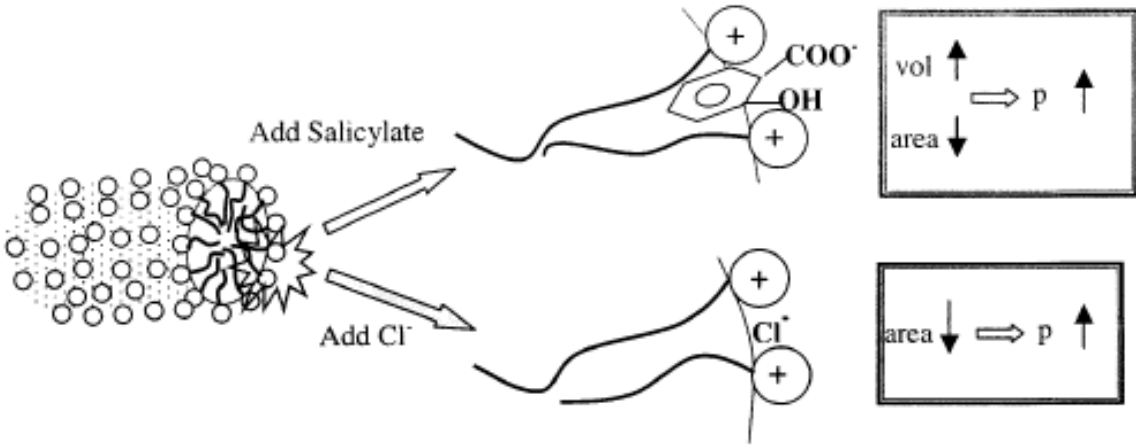


**Figure 1.28**: Effects of size of counterion species on the micelles formed by VES (Qi and Zakin 2002).

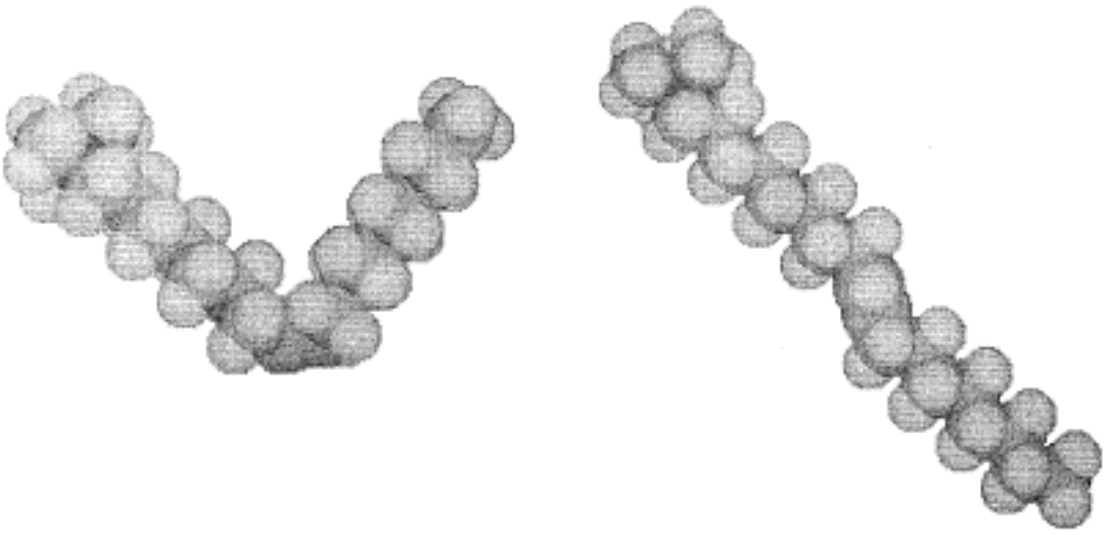


**Figure 1.29**: Effects of the cis and trans structure in the alkyl group on the micelles formed by VES (Qi and Zakin 2002).

Then, another patent was filled aiming for the application of a carboxybetaine in the area of drilling, completion, and stimulation of wells in the oil and gas industry. The advantage of the VES was that it could tolerate high concentrations of salts. However, the temperature at which the highest viscosity was achieved was still lower than 200 ℉, which limited the area where the fluid could be used, as shown in **Figure 1.30**.

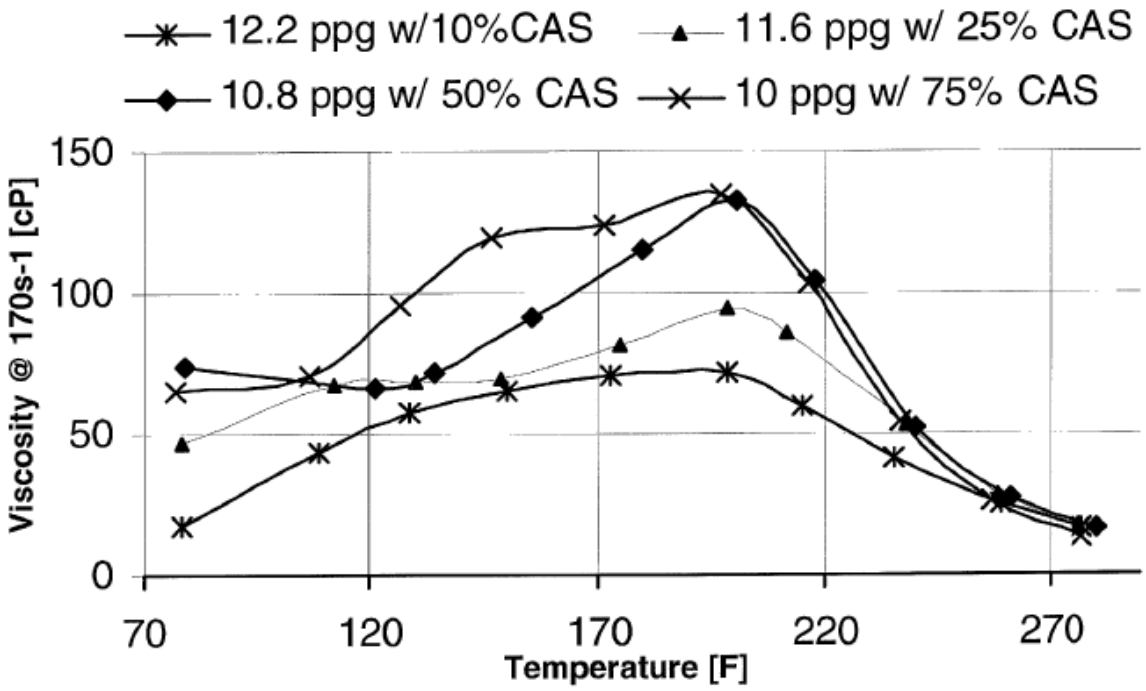


**Figure 1.30**: Effects of temperature on the viscosity of high salinity VES-based fluids (Lungwitz et al. 2002).

As mentioned before, the gel network that was formed by the wormlike micelles of the VES can be broken into sphere micelles via the addition of hydrocarbons, **Figure 1.31**. If there is an excess amount of hydrocarbon that is more than what can be solubilized in the VES solution, there will be a phase transition, resulting a dilute phase and a denser phase, **Figure 1.32**.

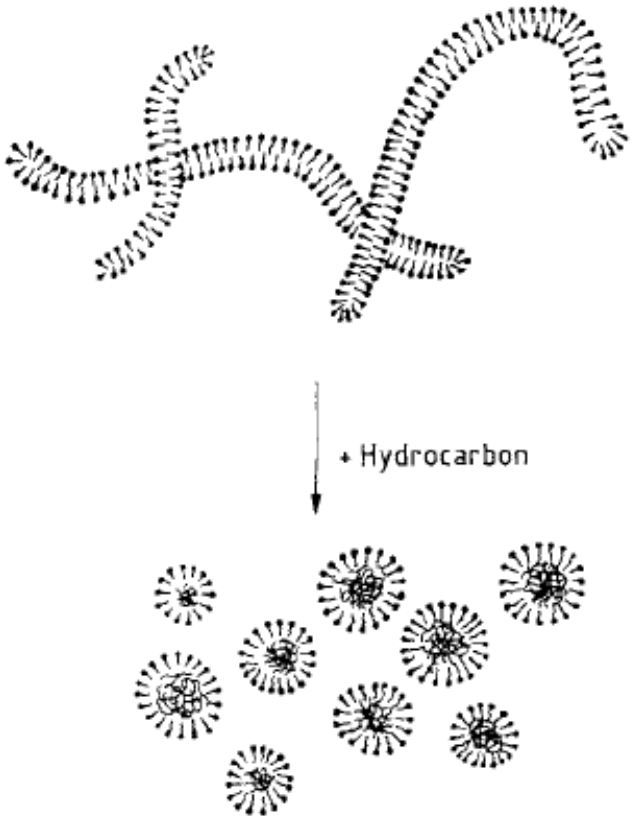


**Figure 1.31**: Breaking down of wormlike micelles formed by VES via the addition of hydrocarbon (Hoffmann and Ebert 1988).

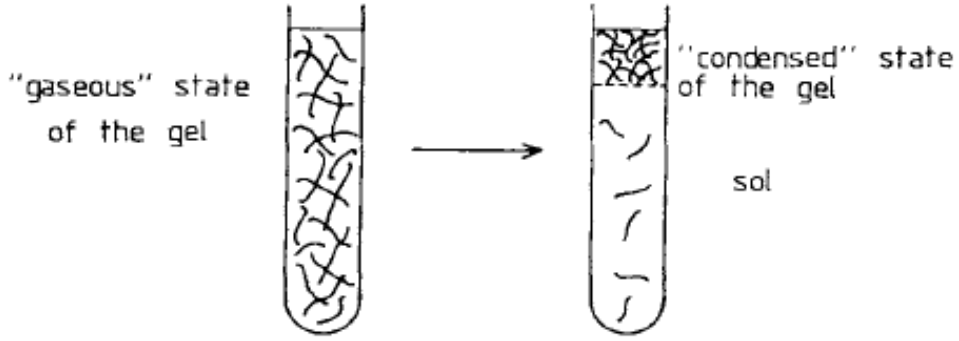


**Figure 1.32**: Phase separation of VES-based wormlike micelles solutions with the addition of an excess amount of hydrocarbon (Hoffmann and Ebert 1988).

The rheological properties of the VES-based fluid were analyzed with the presence of other additives. The effects of alcohols were investigated, as they are very important additives during oil and gas production to prevent emulsion, hydrate formation, etc. With the addition of the alcohols, the viscosity of the VES-based fluid decreases, as shown in **Figure 1.33**. Moreover, longer chain alcohols can reduce the fluid viscosity further.

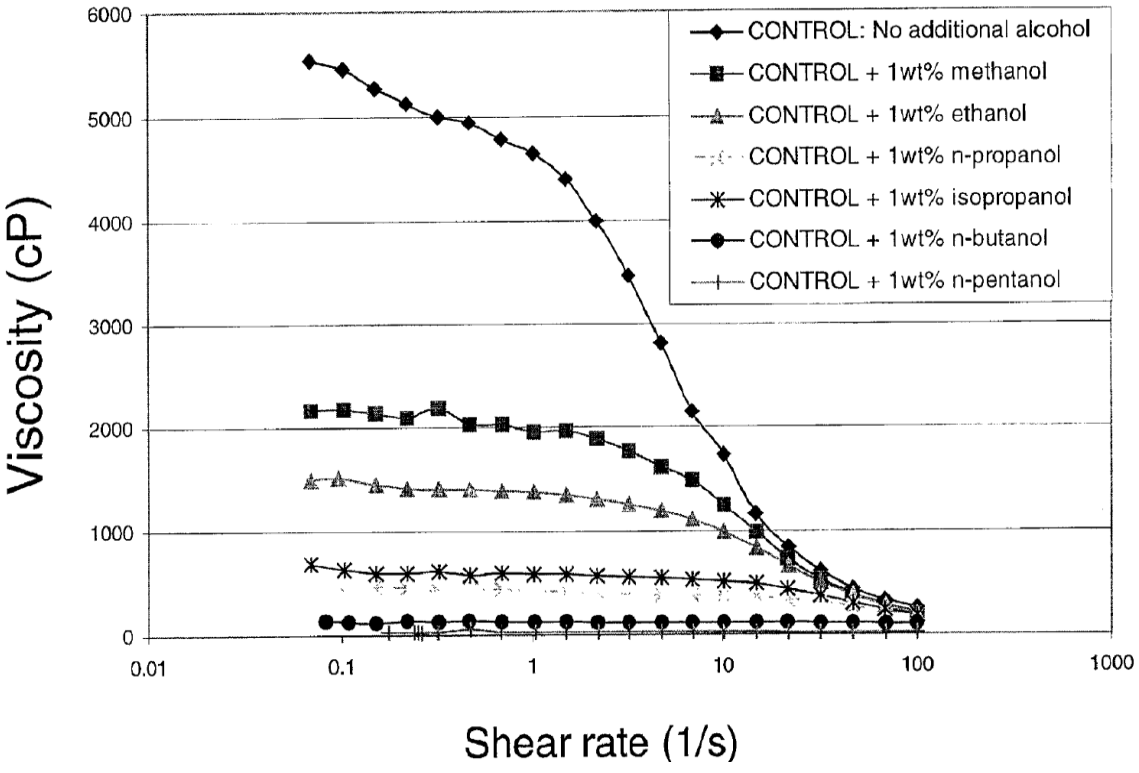


**Figure 1.33**: Effect of alcohol on the viscosity of the VES-based fluid (Nelson et al. 2005).

With development in the research of the VES-based fluid, more theoretical analysis of the wormlike micelles have been conducted, as shown in **Figure 1.34**. The characteristic length was described by various parameters, including the overall radius of gyration $R_g$, the contour length L, the persistence length $l_p$, and the cross-section radius $R_{cs}$.

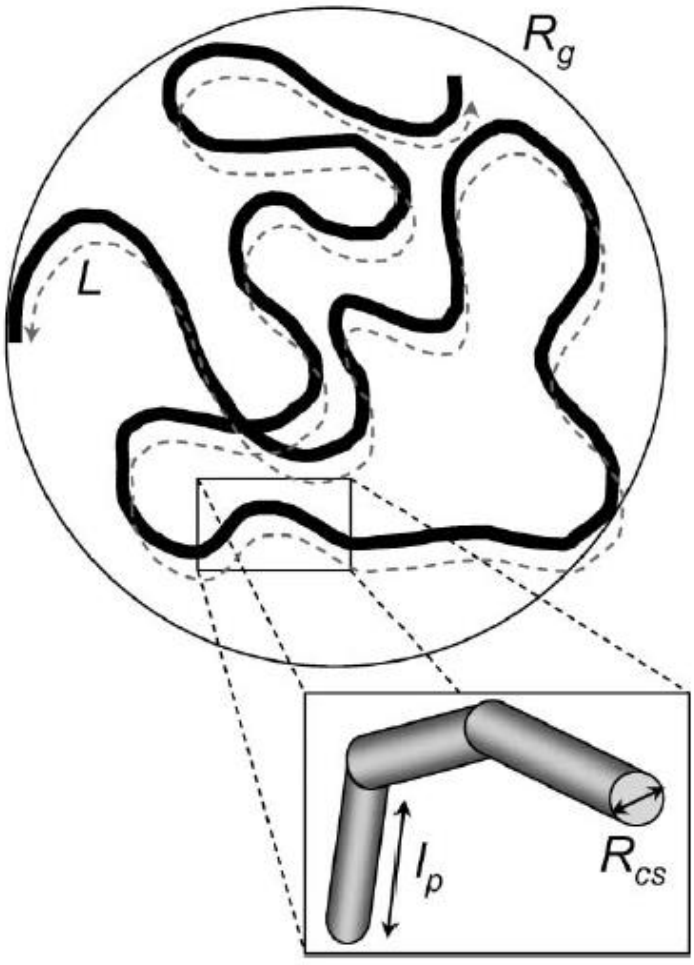


**Figure 1.34**: Parameters to describe the wormlike micelle structure (Dreiss 2007)

Since the VES-based fluids are non-Newtonian fluids, the traditional Darcy's equation for fluid flow through porous media is no longer applicable. Thus, a resistance coefficient was introduced, which can be expressed as $\Lambda = \mu_{app}/\mu$ (Rothstein 2008).

Ultra-long-chain VES was synthesized through the following scheme (**Figure 1.35**). Tertiary ammine intermediates were prepared by amidation of ultra-long-chain fatty acids directly with N,N-dimethyl-1,3-propanediamine, without solvent, at 160–165 ℃. The resulting products were quaternized by 1,3-propanesultone at around 80–85 ℃ in ethyl acetate to obtain a series of ultra-long-chain amidosulfobetaines. The ultra-long chain VES can tolerate high temperature as explained before. With the addition of the sulfonate group, the stability of the micelles formed by the VES molecules is even better compared to the conventional VES. Similarly, some other synthesis routes were proposed (**Figure 1.36**) (Wang et al. 2013).

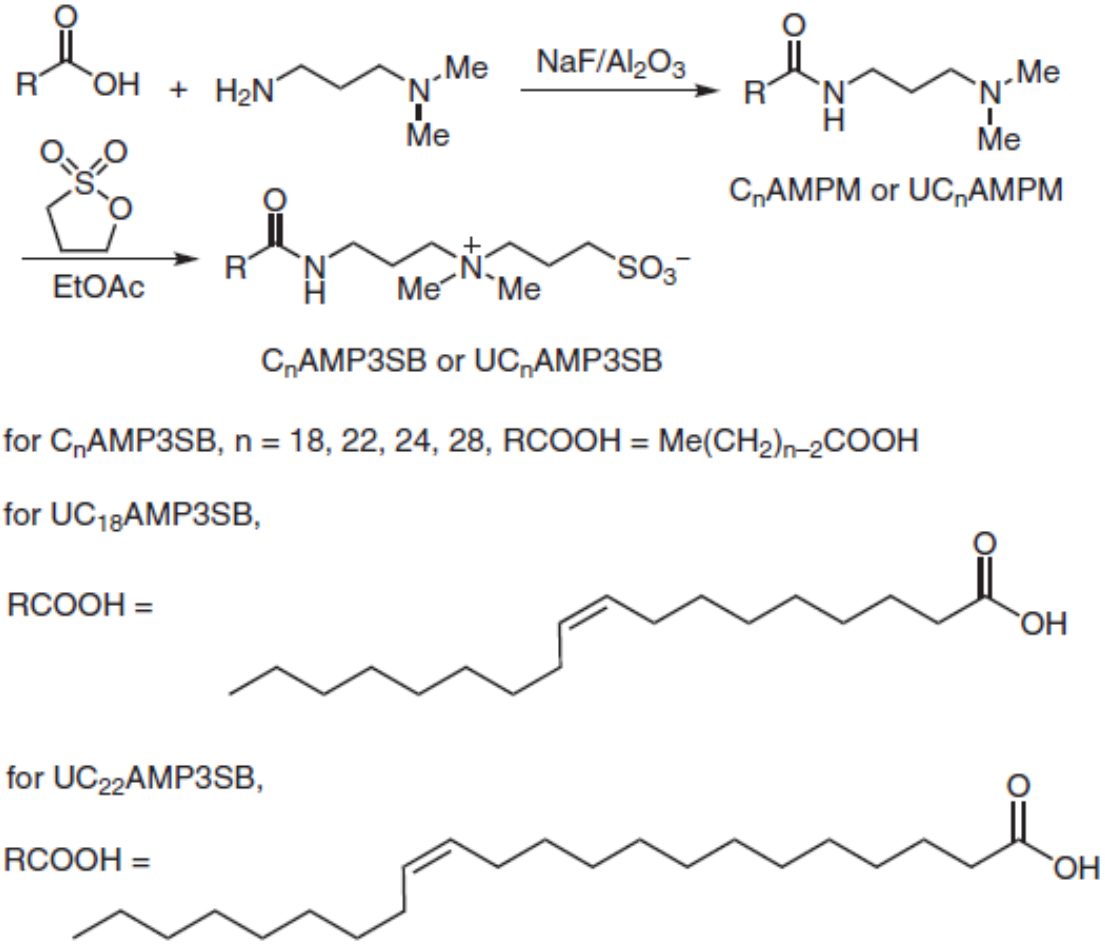


**Figure 1.35**: Synthesis route of amidosulfobetaine surfactants (Chu and Feng 2009).

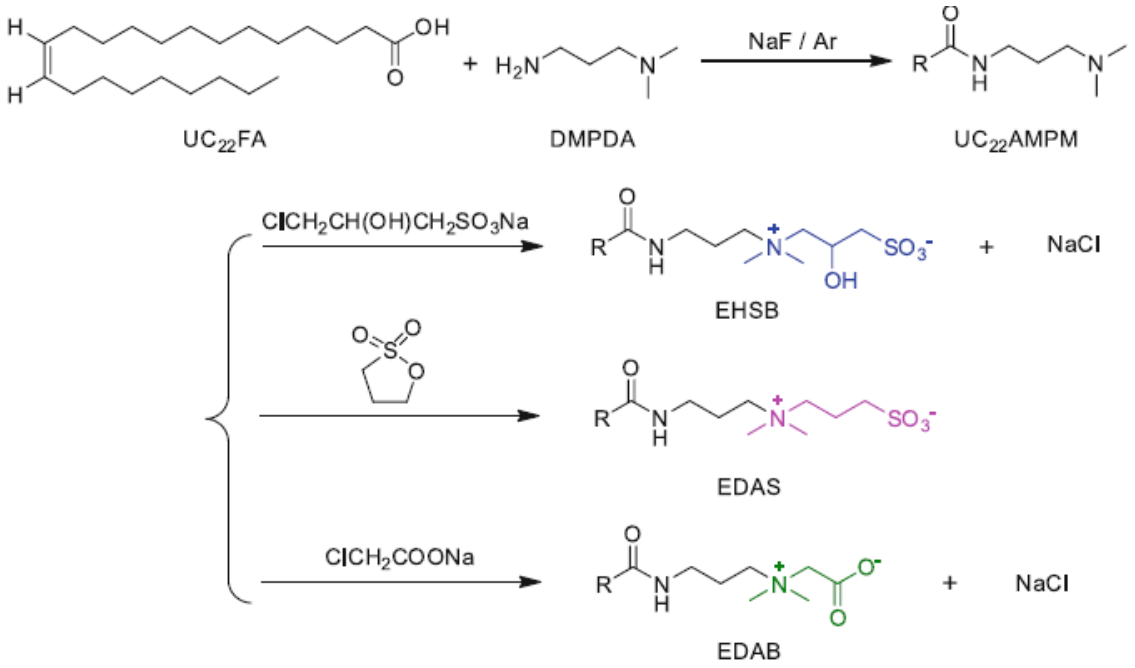


**Figure 1.36**: Synthesis route of erucyl amidobetaines (Wang et al. 2013).

One of the amidosulfobetaine was further investigated in this work. Thus, VES with similar structures were further investigated. Similar to the other VES, temperature and VES concentration were the main factors affecting the rheological properties of the VES-based solution. A higher temperature lowers the CMC of the VES and the surface tension of the fluid, **Figure 1.37**. A higher VES concentration increases the viscosity of the VES-based fluid, **Figure 1.38**. However, unlike the other VES, the addition of NaCl and change of pH at constant NaCl concentration did not affect the viscosity of the VES-based fluid, **Figure 1.39**. Surprisingly, change of fluid pH does not significant change the fluid viscosity as well, **Figure 1.40**. Although there exists a cis double bond in the alkyl chain of the VES, the solubility of the VES remained poor inside pure water. With

the assistance of salt, the solubility of the VES could be significantly increased via the abrupt decrease in Krafft temperature, **Figure 1.41**.

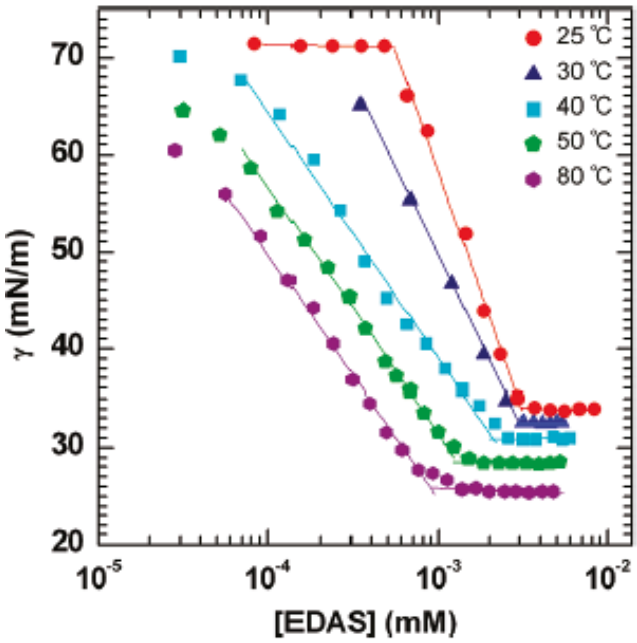


**Figure 1.37**: Surface tension plotted as a function of EDAS concentration at various temperatures (Chu et al. 2010).

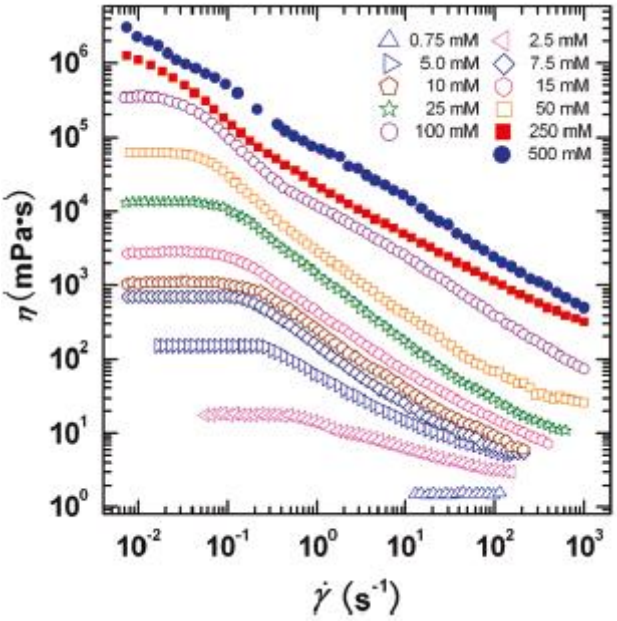


**Figure 1.38**: Apparent viscosity as a function of shear rate for various EDAS concentrations at 25 ℃ (Chu et al. 2010).

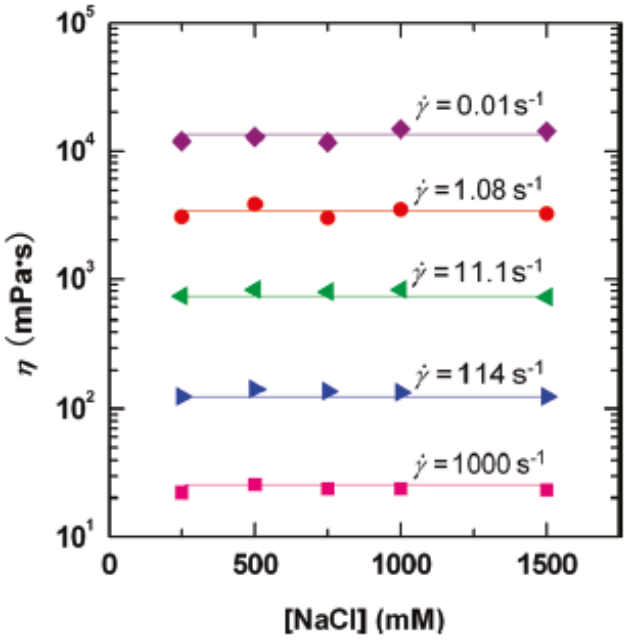


**Figure 1.39**: Viscosity as a function of NaCl concentration for EDAS solutions at their natural pH values at 25 ℃ (Chu et al. 2010).

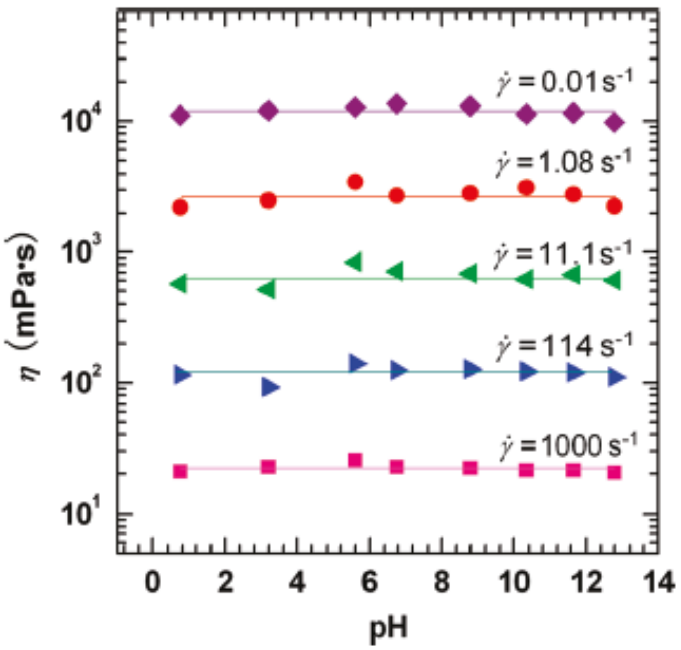


**Figure 1.40**: Viscosity as a function of pH for EDAS fluids at 25 ℃ (Chu et al. 2010).

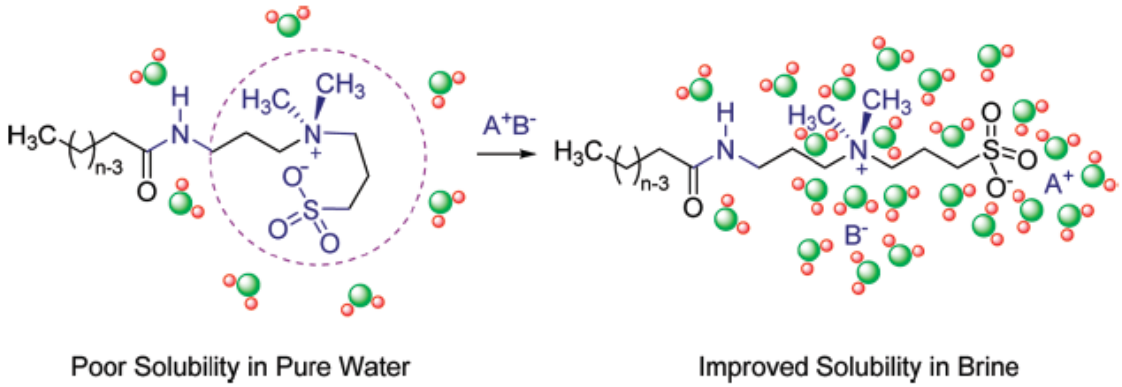


**Figure 1.41**: Schematic illustration of the solubility increase of the long-chain amidosulfobetaines by adding salt (Chu and Feng 2012).

## 1.6 Application of Chelating Agents in Well Stimulation

HCl was cheap and widely used. However, in high temperature wells, the high reactivity between HCl and almost all objectives present in the reservoir could lead to a quick expense of the acid and stimulation outcomes below expectation. To overcome the high reactivity, some alternatives were provided. Formic acid, acetic acid, and other weak organic acids were applied to achieve similar levels of stimulation outcomes. One of the highlights was the introduction of chelating agents. Ethylenediaminetetraacetic acid (EDTA) was first introduced by Fredd and Fogler (1998) to stimulate carbonate reservoirs. During the treatment, no face dissolution occurred even though the injection rates were very low. The stimulation fluid was even capable of creating wormholes at higher pH values. This reduced the potential needs for corrosion inhibitors, iron control agents, antisludge agents, and many other additives. Furthermore, deep penetration of the wormholes could easily bypass the damaged zone and significantly increase well productivity.

Chelation involves the formation or presence of two or more separate coordinate bonds between a polydentate (multiple bonded) ligand and a single central atom. The ligands are usually organic compounds named chelating agents. Citric acid, lactic acid, and many other weak organic acids are good representatives of chelating agents. However, the low solubility of the corresponding calcium salts limits the upper concentration of which these chelating agents can be applied. Calcium EDTA salt is instead, very soluble in water. Thus, EDTA was widely used in various fields due to its high complexity with metal ions. In the oil and gas industry, it is usually used as an iron

control agent, scale inhibitor, corrosion inhibitor, water clarifier, etc. However, low solubility of $H_4$EDTA in acidic solutions and poor biodegradability limits its applications. Thus, a series of new chelating agents were developed to overcome various deficiencies of previously employed ones. Nitrilotriacetic acid (NTA) is less expensive than EDTA, which is more economically beneficial. However, its complex with iron is less stable and it is considered as carcinogen. Diethylenetriaminepentaacetic acid (DTPA) can form a complex with metal ions that are 100 times more stable than an EDTA-based complex. 1,2-cyclohexylenedinitrilotetraacetic acid (CTDA) was also evaluated as a potential stimulation fluid, which can achieve breakthrough with a minimal volume of injection (Fredd and Fogler, 1997)

Hydroxyethylethylenediaminetriacetic acid (HEDTA) and hydroxyethyliminodiacetic acid (HEIDA) were developed and evaluated as alternatives that are soluble in an acidic environment (Freiner et al. 2000) Other than that, HEIDA exhibits the characteristics of being completely biodegradable, which suggests that it could be used as a "green" oilfield chemical even if it is not as effective as EDTA and HEDTA (Freiner 2001). Both HEDTA and HEIDA are capable of creating wormholes at temperatures up to 400 ℉ (Freiner et al. 2001). GLDA was developed recently and test results indicated that it is highly soluble even though the pH of the fluid is less than 2 (LePage 2011). GLDA is also completely compatible with other acid systems. Because it was manufactured based on L-glutamic acid, the chelating agent is completely biodegradable with extremely low toxicity.

After the development of GLDA, evaluation of GLDA was conducted (Mahmoud et al. 2011d). GLDA was able to create wormholes in carbonate rocks at the pH of 1.7, 3, and 13, respectively. The reaction was much faster when the fluid pH was 1.7 since it combined both acid dissolution and the chelation of calcium. Meanwhile, the concentration of complex calcium was the highest when the pH was 13. NaCl can accelerate the reaction when used in GLDA treatment fluid with a pH of 1.7. HEDTA was more effective in capturing calcium cations when compared to GLDA and HEIDA. A smaller volume of the treatment fluid was needed when GLDA was injected at 2 $cm^3$/min. Later on, effects of the initial pH, temperature, and other factors were examined for GLDA-based carbonate treatments (Mahmoud et al. 2010a). Not only being effective in calcite formation, GLDA was also capable of creating wormholes in dolomite cores. Unlike HCl, no face dissolution was noticed when using GLDA at high temperatures. Lower pH values and higher temperatures resulted in a quicker breakthrough and less consumption of GLDA. For further optimization of GLDA-based treatment fluids, tests were conducted with various injection rates, initial GLDA concentrations, and rock lithology (Mahmoud et al. 2010b). The optimum concentration of GLDA to create wormholes in carbonate formations was 20 wt%. In Pink Dessert limestones, the optimum injection rate was 3 $cm^3$/min. While in Indiana limestones, the optimum injection rate was 1 $cm^3$/min. The authors further investigated the effects of temperature and the initial pH of the GLDA-based treatment fluid. Parallel coreflood tests were also conducted to investigate the diverting ability of GLDA (Mahmoud et al. 2011e). Optimum injection rates are affected by the initial pH and the length of the core,

but not the temperature. Without the help of the diverting agents, GLDA was able to stimulate both high permeability and low permeability cores within a certain initial permeability ratio. The reaction kinetics between GLDA and calcite was investigated (Rabie et al. 2011). Hydrogen ion attack is the main reaction at low pH, while the chelation reaction was not significantly influenced by the rotating speed. Then, stimulation of dolomite with GLDA was analyzed and compared with HCl (Mahmoud et al. 2011a). There was no optimum injection rate, and the lower injection rate was preferred to reduce the overall injection volume without face dissolution. Calcium is easier to chelate by GLDA, but there is no significant preference compared to magnesium. Usually, in field applications, the formation is not 100% water saturated but partially saturated with residue oil or gas. GLDA was compared to HEDTA and EDTA at these conditions (Mahmoud et al. 2011b). GLDA performed the best overall, and the residue oil and gas had no adverse effects on the treatment conducted with GLDA. A systematic study indicated that GLDA was a very good alternative for HCl when treatments were conducted at high temperatures and low injection rates (Mahmoud et al. 2011c).

## 2. PERFORMANCE OF AMINE OXIDE-VES-BASED ACID IN STIMULATION*

### 2.1 Background

These series of tests were based on a recently developed VES with the backbone structure shown in **Figure 2.1**. The new VES had a better solubility in water and the chain length was slightly larger, which made the formation of micelles favorable. In this work, the best formula that could be used as self-diverting in-situ gelled acid was investigated.

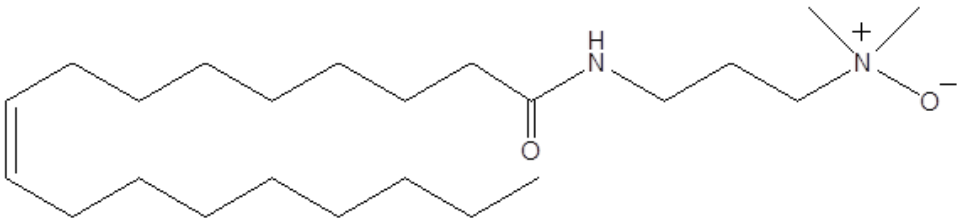


**Figure 2.1**: Chemical structure of the amine oxide viscoelastic surfactant.

### 2.2 Materials

Hydrochloric acid (ACS reagent grade) was titrated using a 1N sodium hydroxide solution to determine its concentration, and the concentration was found to be

---

*Reprinted with permission from "An Experimental Study of a New VES Acid System: Considering the Impact of $CO_2$ Solubility" by Gomaa, A.M., Wang, G., and Nasr-El-Din., H.A., 2011. SPE-141298-MS. SPE International Symposium on Oilfield Chemistry, 11-13 April, The Woodlands, Texas, USA. Copyright 2011 by Society of Petroleum Engineers.

36.8 wt%. All acid solutions were prepared using deionized (DI) water with a resistivity of 18.2 MΩ·cm at room temperature. Surfactants and other additives were all oilfield chemicals, and were used without further purification. Calcium carbonate powders were obtained by crushing the Pink Dessert limestone cores used in this study.

Cylindrical core plugs were cut from two blocks: Pink Dessert limestone and Austin Chalk. Pink Dessert limestone that had a permeability of 80 md was used to represent the high permeability formation, while Austin chalk with a permeability of 4 md was used to represent the low permeability formation. Cores were cut to a length of 6 and 1.5 in. in diameter.

## 2.3 Acid Preparation

VES-based acid solutions were prepared by mixing the corrosion inhibitor and HCl acid with water. Then, the VES was added slowly into the acid. The final solution was mixed for 30 minutes and centrifuged for another 30 minutes at 4500 rpm to remove air bubbles. Powders of Pink Dessert limestone were used to neutralize the VES-based acid to a pH value of 4.5. Centrifuge techniques were also applied to remove air bubbles and excess amounts of calcium carbonate powders.

## 2.4 Equipment

Viscosity measurements were conducted with a HP/HT viscometer at 300 psi and temperature range of 75-250 ℉, as shown in **Figure 2.2**. All treatment fluids were mixed using a magnetic stirrer. The coreflood setup (**Figure 2.3**) was constructed to simulate

matrix stimulation treatments. A backpressure of 1,100 psi was applied to keep most of the $CO_2$ in the solution. Pressure transducers were connected to a computer to monitor and record the pressure drop across the core during the experiments. A Teledyne ISCO D500 precision syringe pump, which had a maximum allowable working pressure of 2,000 psi, was used to inject the acid into the cores. Based on the maximum pump pressure and the backpressure, the maximum pressure drop across the core was 900 psi. pH values for the core effluent samples were measured using an Orion 370 PerpHecT Ross Electrode (**Figure 2.4**). To determine the residue HCl concentration, 1 $cm^3$ solution was taken from each sample and titrated with 1N sodium hydroxide. Calcium concentrations were measured using an atomic absorbance spectrometer (AAnalyst 700-flame type, **Figure 2.5**). A X-ray Computed Tomography (CT) machine was used to scan the cores before and after treatment.

**Figure 2.2:** High pressure high temperature rheometer.

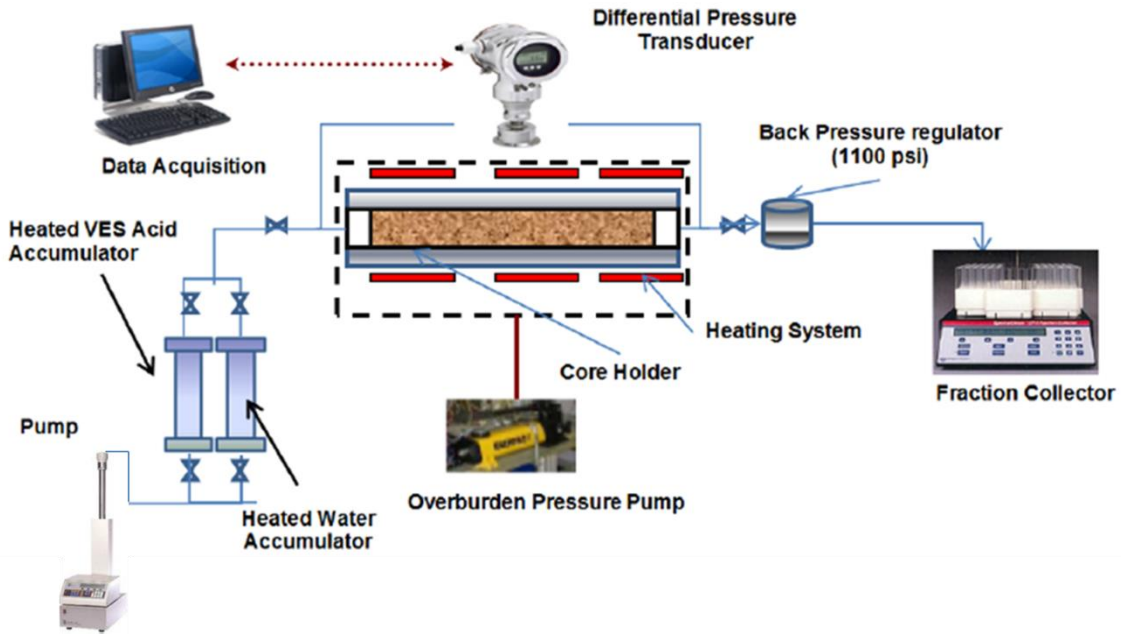


**Figure 2.3:** Coreflood setup.

**Figure 2.4:** pH meter.

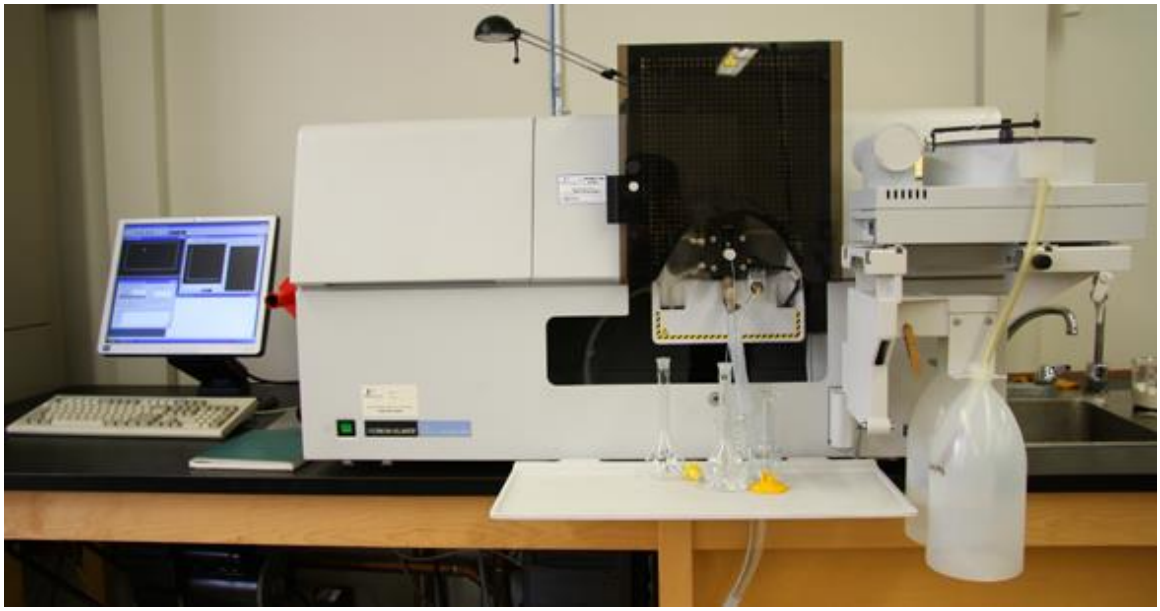

**Figure 2.5:** Atomic absorption spectroscopy.

## 2.5 Core Preparation

The following procedures were followed to prepare the core samples:

1. The cylindrical cores were dried at 250 ℉ for 6 hours. Then, the cores were immersed in DI water under a vacuum for 24 hours to insure full saturation. Porosities of the cores were calculated based on the weight differences before and after saturation and the density of the DI water.

2. The DI water saturated cores were CT scanned before the treatment, and the CT number was found to be 2,000-2,200 for Pink Dessert limestone and Austin Chalk, and 1,700-1,800 for Indiana limestone.

3. The cores were then placed inside the core holder, and DI water was injected at different flow rates (5, 10, and 20 $cm^3$/min) to calculate the initial core permeability.

4. The core was examined using a CT scan to characterize the wormholes after treatments. Cores were water saturated during the scanning.

## 2.6 Experimental Procedures

During the rheological property measurements, apparent viscosities of the fluids were measured at various shear rates. The measurements were conducted in the order of ascending shear rates from 0.1 to 1,000 $s^{-1}$ at room temperature. Then, the shear rate was fixed at 100 $s^{-1}$ by increasing the test temperature from 75 to 250 ℉. When measuring the storage modulus G' and the viscous modulus G", the first series of tests were conducted by increasing the frequency from 0.3 to 5 Hz. Then, the moduli were measured at 1 Hz by increasing the temperature from 75 to 220 ℉. A pressure of 300 psi was applied during high temperature measurements.

During the coreflood with VES-based 5 wt% HCl acid, the core was placed inside the coreholder and a backpressure of 1,100 psi was applied. The overburden pressure was set at 2,000 psi. After all the wire lines were well connected, DI water was injected at a constant rate until the pressure drop across the core was stable. Then, half a pore volume of core effluent sample was collected as a background. Injection fluid was switched to the VES-based acid at the same flow rate in the same flow direction. Core effluent samples were collected with test tubes every quarter of a pore volume. When the pressure drop across the core reached zero, which indicated the occurrence of a breakthrough, the injection fluid was switched back to water. When no more bubbles

were noticed in the core effluent sample, the injection stopped as the core was already fully saturated again with DI water.

## 2.7 Results and Discussion

### 2.7.1 Rheological Properties of VES-Based Acids

**Figure 2.6** shows the viscosity of live VES-based acid as a function of HCl concentration. It is important to highlight that the VES-based acid system has its maximum viscosity at an initial HCl concentration of 5 wt%. The viscosity behavior of the VES-based acid system was measured at a HCl concentration of 5 wt%. The composition of the 5 wt% HCl VES-based acid was shown in **Table 2-1**. **Figure 2.7** shows the viscosity of VES-based acid at live and partially neutralized conditions as a function of the shear rate, while **Table 2-2** gives the values of power law parameters (K and n). The viscosity of the VES acid at the live condition was higher than at the partially neutralized condition. As the acid reacted with the formation, the HCl concentration was reduced, and the viscosity of the partially neutralized acid decreased as shown in **Figure 2.6.**

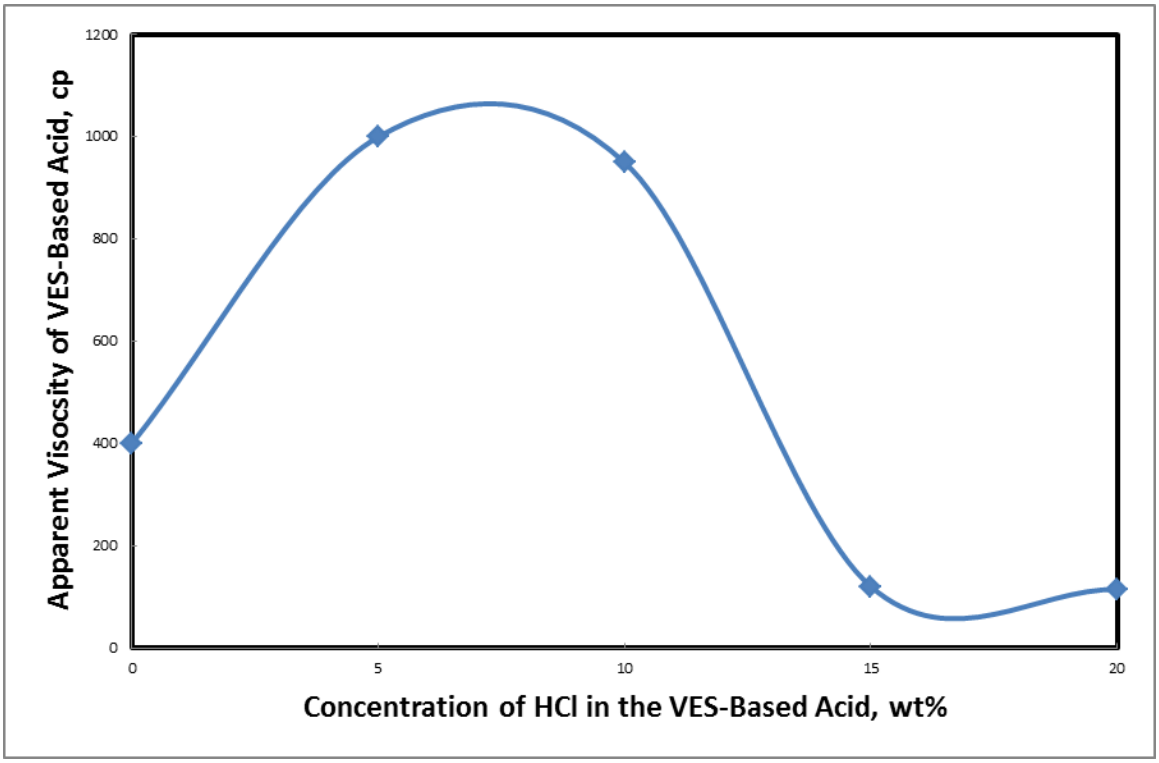


**Figure 2.6:** Apparent viscosities of live VES-based acid were measured at various HCl concentrations. Tests were conducted at 1 $s^{-1}$ and 28 ℃.

| TABLE 2-1: FORMULA OF THE VES-BASED ACID WITH 5 WT% HCL | |
|---|---|
| **Component** | **Concentration** |
| Hydrochloric Acid | 5 wt% |
| Surfactant | 5 vol% |
| Corrosion Inhibitor | 0.5 vol% |

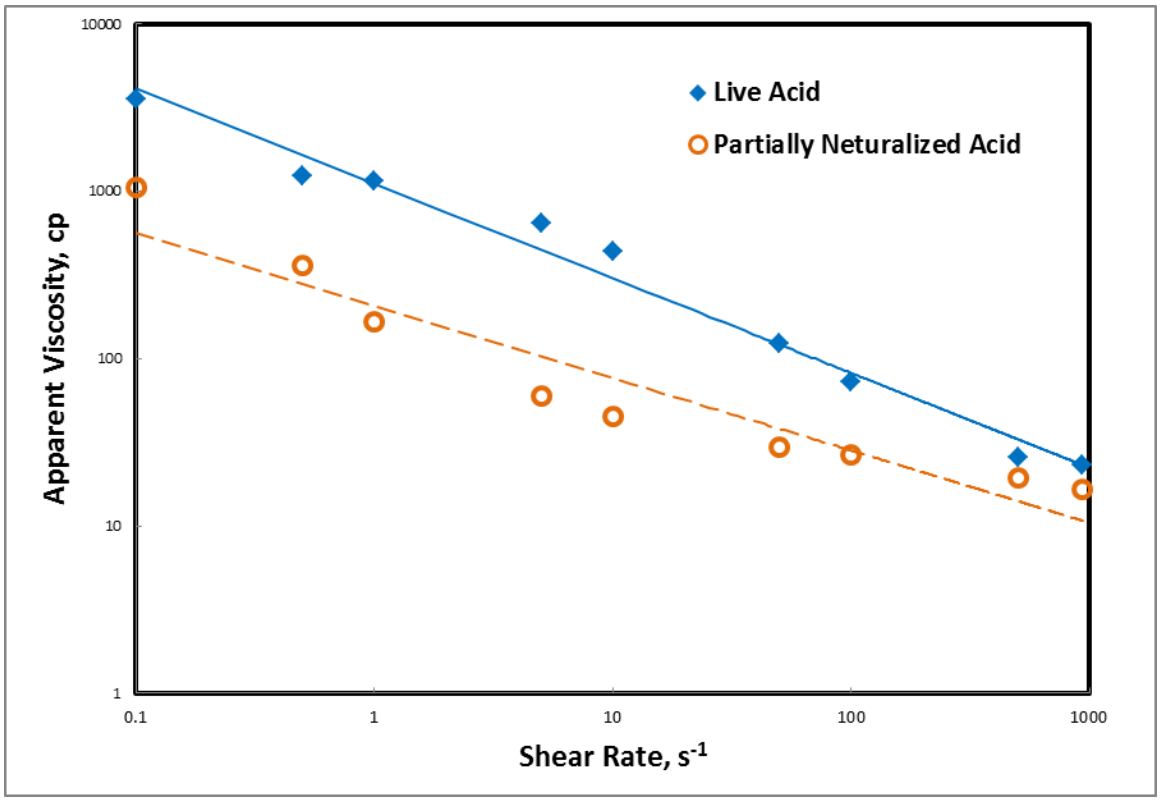


**Figure 2.7:** Apparent viscosities of live and spent acid at 25 ℃ and various shear rates. The initial HCl concentration was 5 wt%.

**TABLE 2-2: POWER-LAW PARAMETERS FOR VES-BASED 5 WT% HCL SOLUTION AT 25 ℃.**

| | K, mPa.s$^n$ | n | $R^2$ |
|---|---|---|---|
| Live acid | 1114.7 | 0.434 | 0.98 |
| Partially neutralized | 208.2 | 0.567 | 0.91 |

The effects of temperature on the viscosity of live and partially neutralized acids were investigated at shear rates of 100 $s^{-1}$, where the acid solution was examined in the

temperature range of 75 to 250 ℉ (**Figure 2.8**). The viscosity of the live acid increased with the temperature to a maximum value of 120 cp at 100 ℉, after which the live acid viscosity decreased to nearly zero at 250 ℉. The viscosity of the partially neutralized acid increased to a value of 60 cp at 120 ℉. After that, it decreased to 11 cp at 250 ℉. The partially neutralized acid ended with a viscosity higher than the live acid. The overlap in the viscosity between live and partially neutralized acids is obtained at 140 ℉.

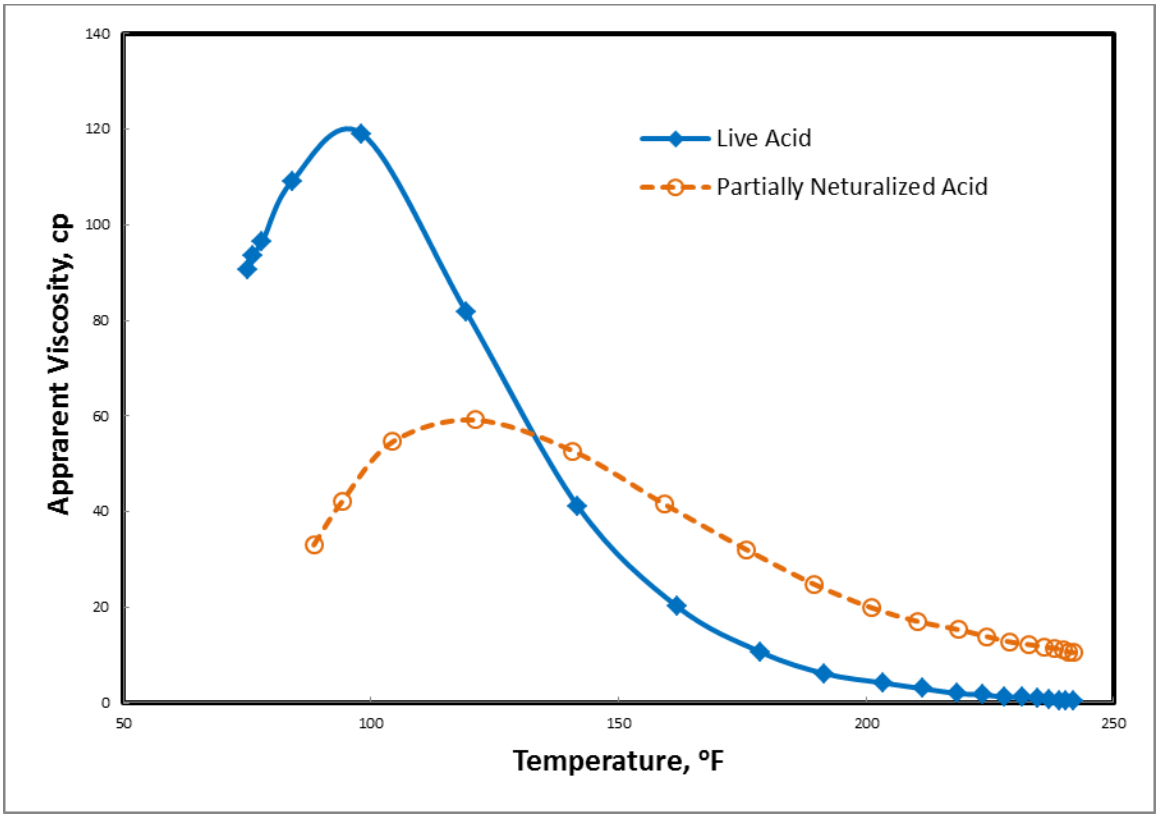


**Figure 2.8:** Apparent viscosities of live and spent acid at 100 $s^{-1}$ and under various temperatures.

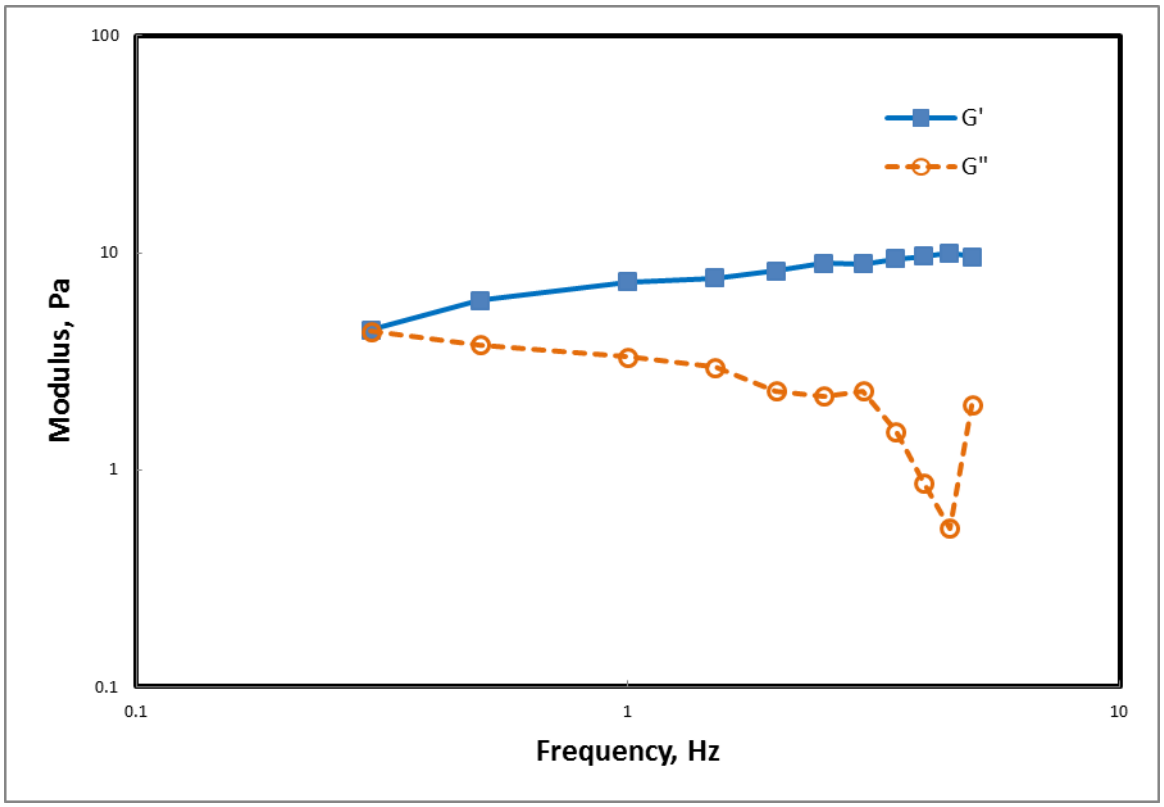


**Figure 2.9:** G' and G" of live VES acid system as a function of frequency at 28°C.

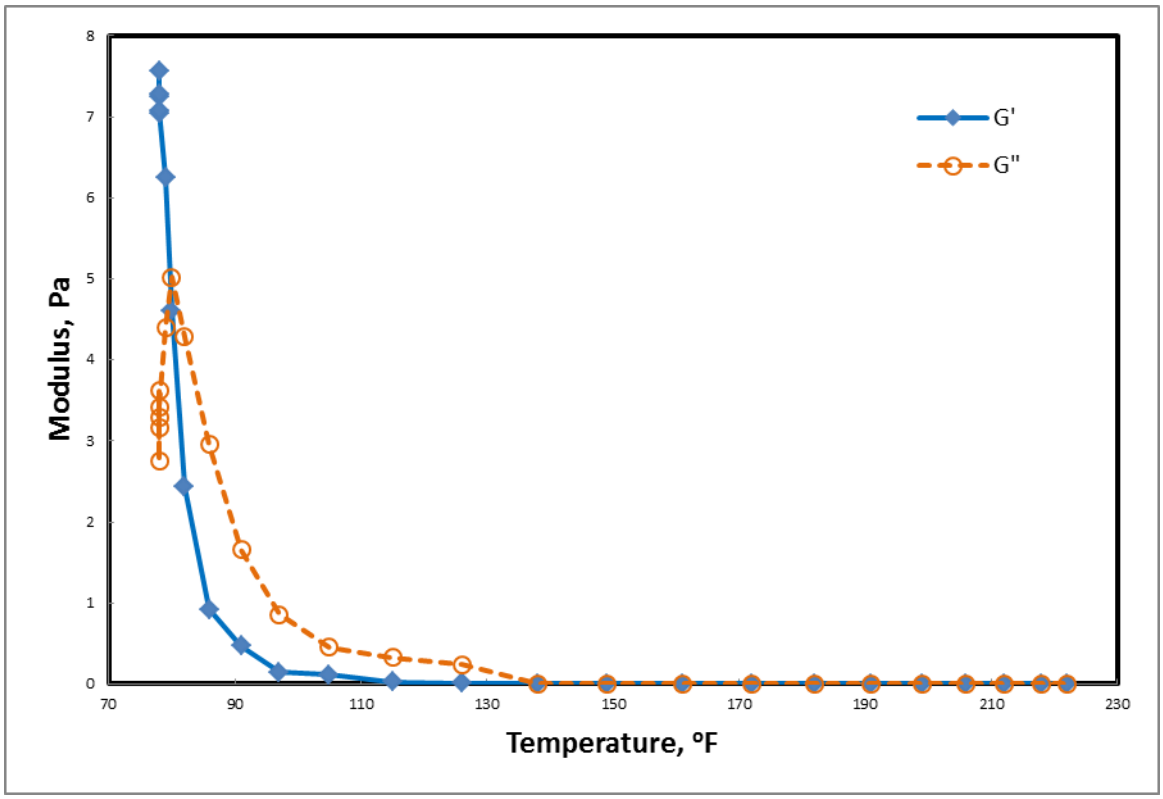


**Figure 2.10:** G’ and G” of live VES acid system as a function of temperature at 1 Hz.

**Figure 2.9** shows the elastic modulus (G’) and viscous modulus (G”) of the live acid as a function of frequency. G’ was dominated over the G” at all frequency ranges. As the frequency increased, the G’ slightly increased while the G” significantly decreased (**Figure 2.9**). It is important to highlight that the elastic properties of the VES-based acid increased by frequency. This means that better elastic properties of the system occurs by increasing the injection rate. **Figure 2.10** shows the change in the elastic and viscous moduli as the temperature increases. The elastic modulus decreased

when temperature increased, while the viscous modulus increased initially with the temperature, then decreased again.

### 2.7.2 Coreflood Experiments with 5 wt% HCl VES-Based Acid

Eight experiments were conducted with the 5 wt% HCl VES-based acid system at injection rates ranging from 0.5 to 20 $cm^3$/min using 80 md Pink Dessert limestone cores (**Table 2-3**). All of the eight experiments were conducted at room temperature while the pressure drop across the core was monitored. New identity cores were used in each experiment. Analysis of the density, the calcium, and the surfactant concentrations in the effluent samples was used to conduct material balance on both calcium and surfactant.

**Figure 2.11** shows the change in the normalized pressure drop as a function of the cumulative volume injected for core #1 and #2, which were treated with an injection rate of 0.5 and 1 $cm^3$/min, respectively. The normalized pressure drop was defined as the ratio of the pressure drop during acidizing to the initial pressure drop during water injection. A 5.1 PV slug of the VES-based acid was injected through core #1 until the acid breakthrough occurred while a 2.9 PV slug of the VES-based acid was injected through core #2. In both cores, as the acid entered the core, the pressure drop increased due to the higher acid viscosity (**Figs. 2.8 and 2.9**). The pressure drop increased in a linear behavior until acid breakthrough occurred. However, the normalized pressure drop of core #1 was higher than core #2. The normalized pressure drop at the injection rate of 0.5 $cm^3$/min was increased to 40 times what it was before acid breakthrough, while it

was 5 times what it had been when the injection rate increased to 1 $cm^3$/min. Because VES-based acids are non-Newtonian shear thinning fluids, increasing the shear rate by increasing the injection rate will reduce the viscosity of the solution. Therefore, the viscosity of the VES at core #1 was higher than was noted for core #2.

**TABLE 2-3: SUMMARY OF COREFLOOD EXPERIMENTS**

| Core # | Pore Volume $cm^3$ | Initial Permeability md | Injection Rate $cm^3$/min | Volume of Acid Used at Breakthrough PV |
|---|---|---|---|---|
| 1 | 39.52 | 81.9 | 0.5 | 5.1 |
| 2 | 38.72 | 84.0 | 1.0 | 2.9 |
| 3 | 39.46 | 81.9 | 2.5 | 2.1 |
| 4 | 42.78 | 82.7 | 5.0 | 1.9 |
| 5 | 46.93 | 76.8 | 7.5 | 1.7 |
| 6 | 39.93 | 82.7 | 10.0 | 1.8 |
| 7 | 43.65 | 82.5 | 15.0 | 2.2 |
| 8 | 44.37 | 87.3 | 20.0 | 2.6 |
| 9 | 25.05 | 4.3 | 1 | 1.7 |
| 10 | 28.08 | 4.2 | 5 | 1 |
| 11 | 26.48 | 4.1 | 10 | 1.3 |

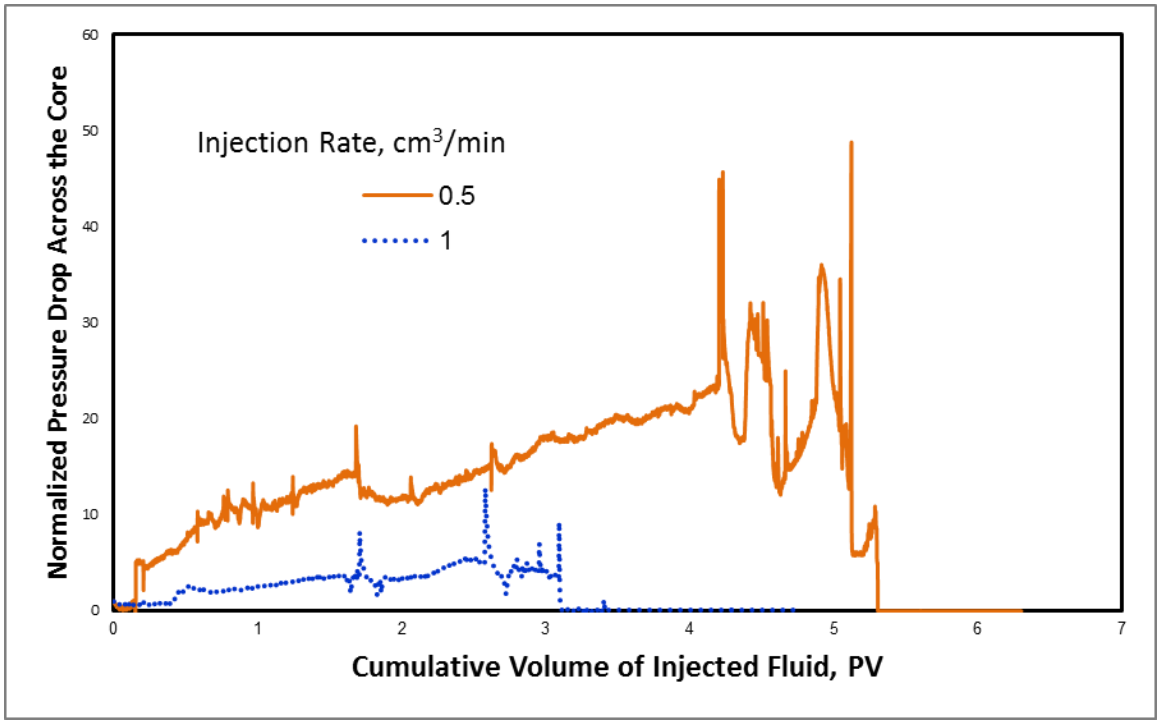


**Figure 2.11:** Normalized pressure drop across the core during the VES-based acid injection at 0.5 and 1 $cm^3$/min, respectively.

**Figure 2.12** shows the normalized pressure drop of cores #3 and #6 where the VES-based acid system was injected at rate of 2.5 and 10 $cm^3$/min, respectively. The volume of the acid needed to achieve acid breakthrough in the cores #3 and #6 were 2.1 and 1.8, respectively. At higher injection rates, the performance of the pressure drop was notably different from that observed at lower injection rates (**Figure 2.11**). The pressure drop of the VES-based acid can be divided into two regions. The first one is that the pressure drop increased when the VES entered the core due to the higher acid viscosity. Therefore, in this region the pressure drop at a rate of 2.5 $cm^3$/min, was higher than at 10

$cm^3$/min. The first region takes nearly 0.5 to 0.75 PV (**Figure 2.12**). The second region was observed when the pressure drop decreased sharply to a value similar to the starting value, and then increased slightly to a constant value before the acid breakthrough. The sharp decrease that was observed in the pressure drop across the core was due to the creation of the wormhole. In the second region, the pressure drop of core #3 (higher rate) is less than core #6 (lower rate). At higher injection rates, the VES-based acid system was not able to build up enough of the pressure needed to achieve the diversion.

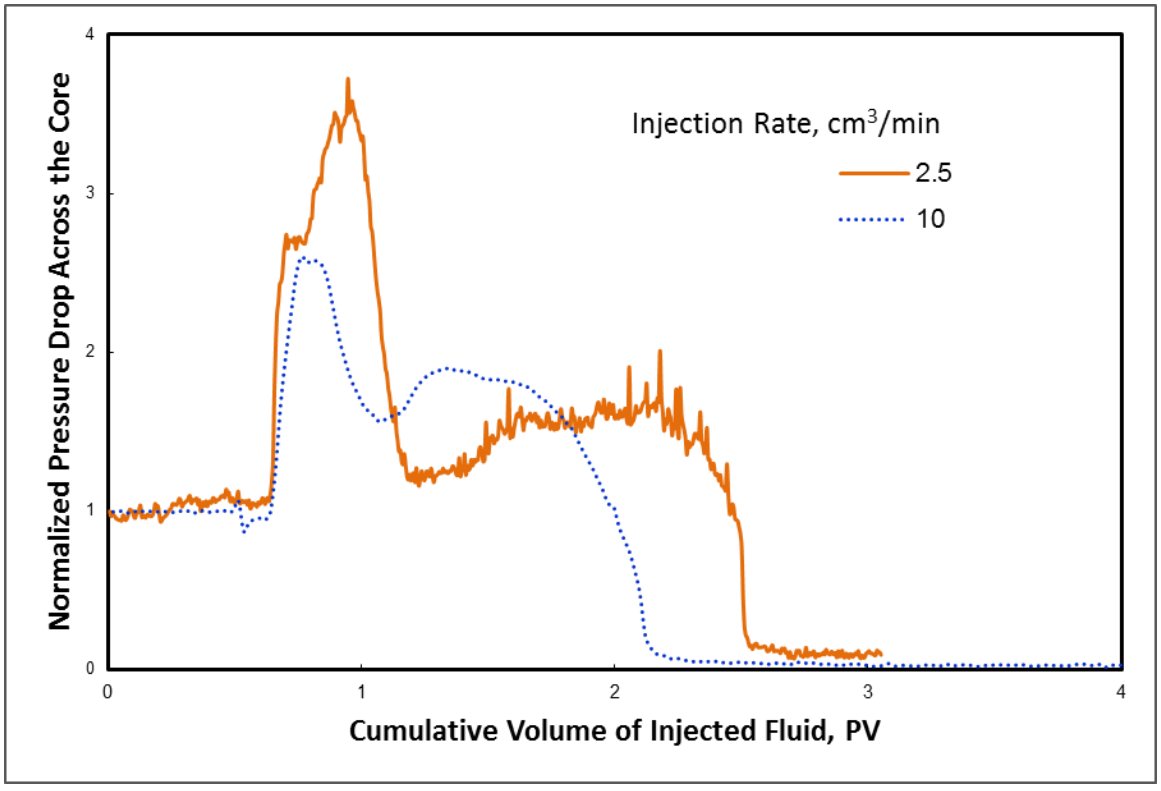


**Figure 2.12:** Normalized pressure drop across the core when the VES-based acid system was injected at 2.5 and 10 $cm^3$/min, respectively.

Three experiments were conducted with 5 wt% VES acid systems at injection rates of 1, 5, and 10 $cm^3$/min using 4 md Austin chalk cores #9, 10, and 11, respectively. **Figure 2.13** shows the normalized pressure drop for cores #9, 10, and 11 as a function of the injected pore volume at room temperature. The pressure drop increased only for the core #9 that treated with 1 $cm^3$/min. However, the pressure drop of core #11 behaved as a regular acid where it decreased linearly until acid breakthrough (**Figure 2.13**).

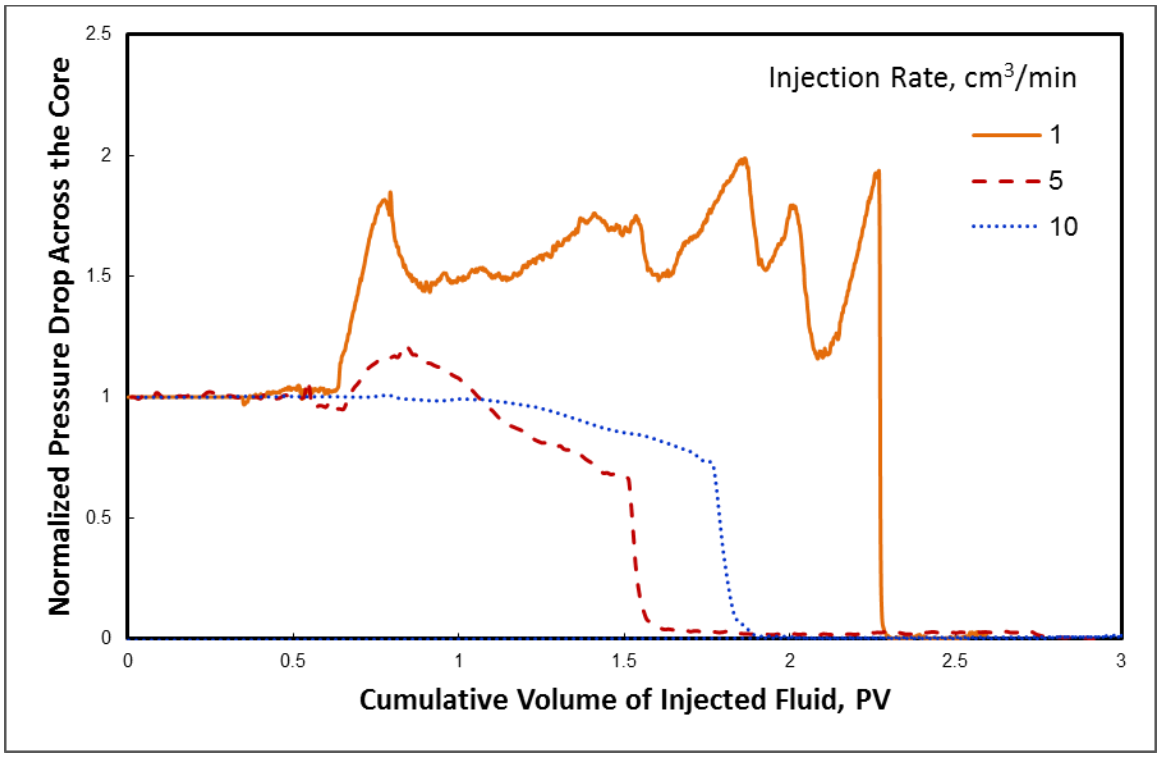


**Fig 2.13:** Normalized pressure drop across the core when the VES-based acid was injected into cores with lower initial permeability at 1, 5, and 10 $cm^3$/min, respectively.

The effects of the initial core permeability can be shown in the pore throat (thread) diameter where it was decreased by the reduction in permeability. A smaller pore volume was noted for the Austin chalk cores (**Table 2-3**). Therefore, the same volume of acid can penetrate deeper in the lower permeability formations than in the higher permeability formations. The consumption of the acid in the low permeability zone was higher. Therefore, the VES-based acid neutralized faster in the low permeability cores than in the high permeability zones. This reduced the viscosity of the VES acid faster (**Figs. 2.6** and **2.7**). Therefore, the performance of the VES in the low permeability core was nearly the same as regular acid.

Wormhole propagation is defined by the ratio of the created wormhole length to the acid volume required to create this wormhole. For certain core lengths, the wormhole propagation can be evaluated by the volume of acid required to breakthrough. The wormhole propagation decreased as the acid volume to breakthrough increased. **Figure 2.14** shows the effect of the VES-based acid injection rate on the acid pore volume to breakthrough for low and high permeability cores. Based on the classification of Bazin et al. (1999), three regions were obtained when VES-based acid systems were applied in 80 md cores (**Figure 2.14**): Region I at the injection rate less than 0.5 $cm^3$/min, Region II in the range between 0.5 and 7.5 $cm^3$/min, and Region III, at injection rates higher than 7.5 $cm^3$/min. At low injection rates (Regions I and II), VES acid was consumed faster than at higher injection rates, which reduced the viscosity of the acid. However, the low shear rate environment that was obtained at the low injection rates enhanced the viscosity of the acid that would reduce the wormhole propagation (**Figure 2.7**). At the

beginning of the acid injection, a fast growth of the wormhole tip occurred as it was noted by Bazin et al. (1999). Then, as acid injection continued, the wormhole extension in length occurred slowly with severe branching, which occurred at the wormhole tip and an increase in the wormhole diameter. At high injection rates (Region III), the formation of wormholes was faster and wormholes propagated with an almost fixed diameter. Very fine branches were formed around the main wormhole channel (Bazin et al. 1999).

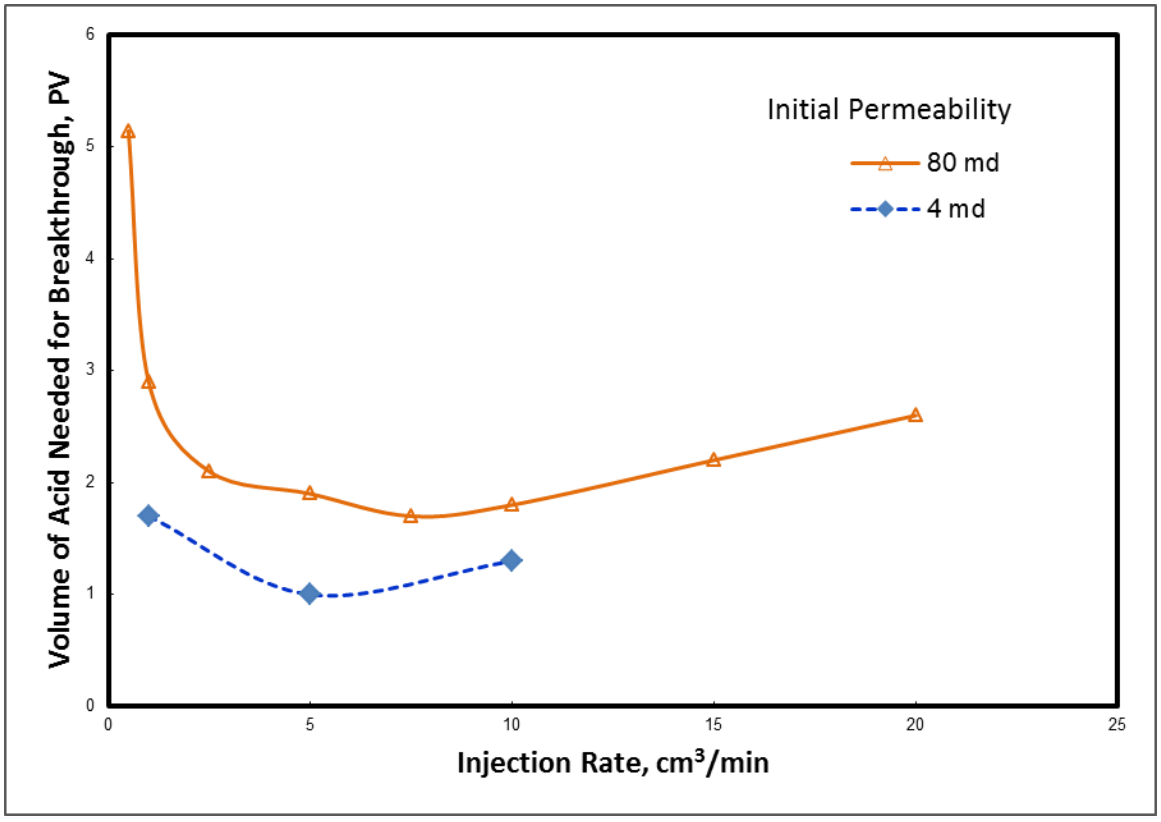


**Figure 2.14**: Volume of the VES-based acid required to achieve breakthrough as a function of the injection rate.

For low permeability cores, smaller acid pore volumes were needed to achieve breakthrough (**Figure 2.14**) and there was no pressure drop build up (**Figure 2.13**). These results confirmed that VES-based acid was not able to form a gel even at low injection rates. This gives the VES-based acid system a unique advantage in that in low permeability cores there will be no damage due to the small volume of acid injected.

**Figure 2.15** shows the pH values and densities of the core effluent samples as a function of the cumulative volume injected in the core that was treated at 5 $cm^3$/min. The initial pH value was nearly 7.0, which is the DI water injected before the acid treatment. After the injection of 1.4 PV of acid solution, the pH started to decrease and reached 5 at the point that acid injection was stopped due to acid breakthrough and was followed by water injection. However, the pH increased as the injected water increased. Calcium was detected in the core effluent sample at the same time that the pH values began to decrease (**Figure 2.16**). However, by observing pH and acid concentration measurements, there was no indication that there was live acid or surfactant. That means there was a breakthrough of calcium ions from the core while acid and surfactant were still propagating inside the core. In all coreflood experiments, calcium ions reached to a maximum value of 30,000 to 40,000 mg/l just before the acid breakthrough, while calcium cations started to come out of the core after around 1.5 PV of the VES-based acid injection (**Figure 2.17**).

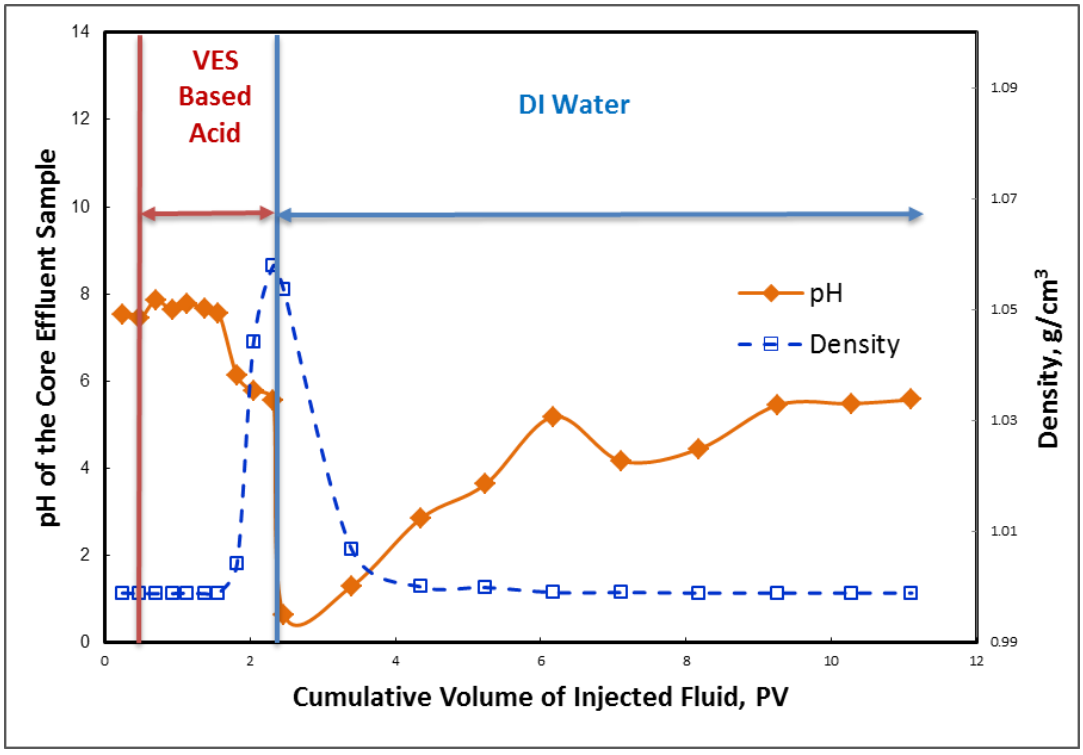


**Figure 2.15:** pH value and density of the core effluent samples when the coreflood test was conducted at 5 $cm^3$/min.

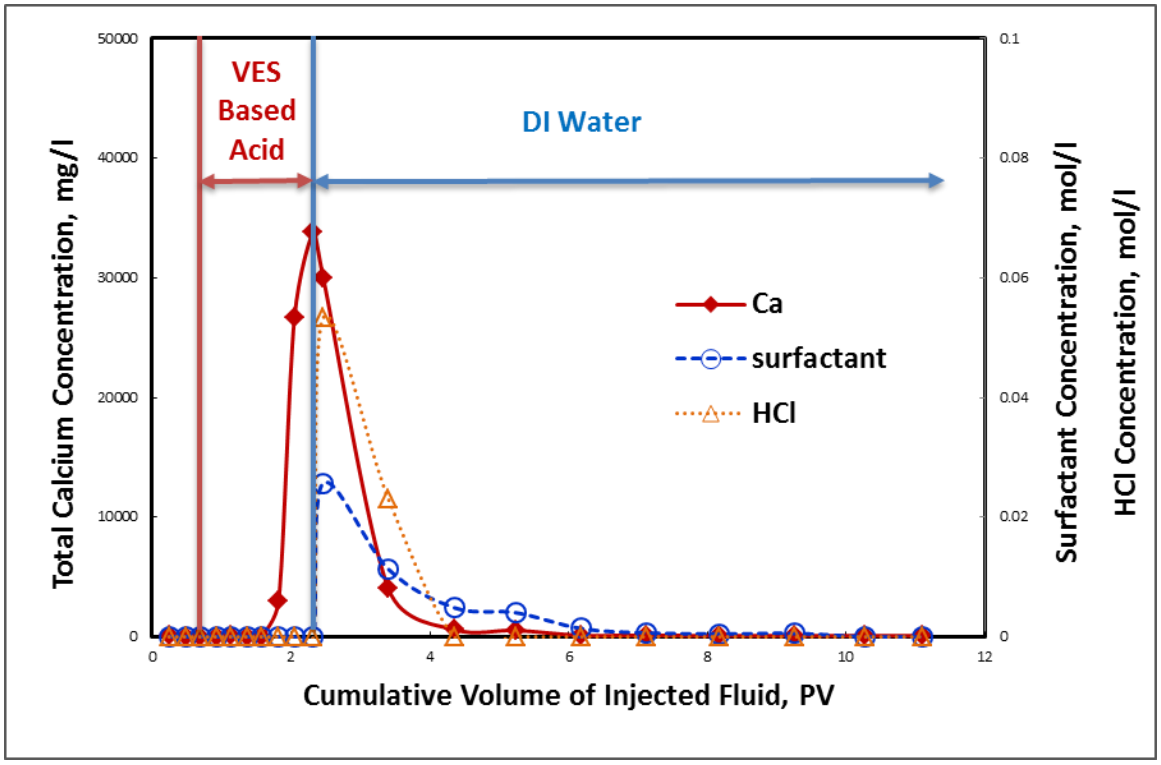


**Figure 2.16:** Calcium ions, surfactant, and acid concentrations in the core effluent samples when the coreflood tests were conducted at 5 $cm^3$/min.

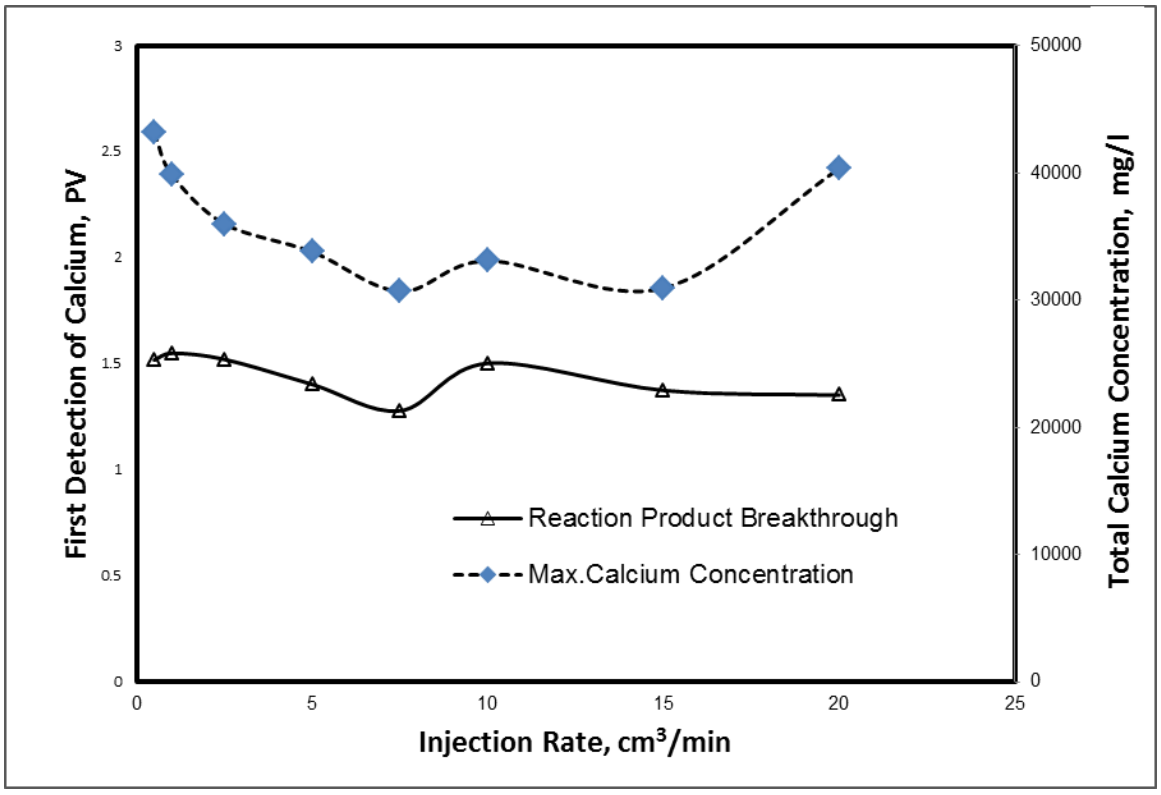


**Figure 2.17:** Volume of VES-based acid needed to achieve breakthrough and maximum calcium concentration before breakthrough in the high permeability cores.

The weights of the collected samples were measured, and the collected volumes of the samples were calculated from the sample density and weight. Using the surfactant concentration of each sample and its volume, the amount of surfactant in moles was calculated. Finally, the summation of all of the samples in each experiment was calculated to determine the amount of surfactant that came out of the core. **Table 2-4** gives the summary of the surfactant material balance. At the optimum injection rate, a minimum of 60.7 and 33.3 mol% of surfactant remained inside the high and low

permeability cores, respectively. The low permeability cores had less remaining surfactant. However, there was a surfactant loss inside the core for each of the experiments even after the injection of 10 PV of water.

To cover the whole core, 30 slices with 2 mm thickness and 5 mm separation between each slice were selected. In the processing step, the binary image data, collected by the CT-scanner, was processed with a SUN workstation using the petrophysical CT-scanning software, ImageJ. Analysis of ImageJ showed a cross-sectional area for each slice along the core length. This enabled us to show the difference in the shape of the wormhole when VES acid was injected at various flow rates. **Figure 2.18** shows the results from the CT scan for the tested cores at injection rates of 0.5, 5, 10, and 20 $cm^3$/min. Phase dissolution was observed in all cores where it was significant, at injection rates less than 1 $cm^3$/min and rates higher than 10 $cm^3$/min. It was unpredicted that the VES has its maximum face dissolution at the injection rate of 20 $cm^3$/min (**Figure 2.18**), where nearly a half of the core face was dissolved by the acid.

| TABLE 2-4: SUMMARY OF VES MATERIAL BALANCE | | | | |
|---|---|---|---|---|
| **Core #** | **Injected VES mole** | **Collected VES mole** | **Retained VES mole** | **Retained VES %** |
| 1 | 0.0129 | 0.0012 | 0.0117 | 90.70 |
| 2 | 0.0072 | 0.0014 | 0.0058 | 80.56 |
| 3 | 0.0053 | 0.0016 | 0.0037 | 69.81 |
| 4 | 0.0052 | 0.0017 | 0.0035 | 67.31 |
| 5 | 0.0051 | 0.002 | 0.0031 | 60.78 |
| 6 | 0.0046 | 0.0015 | 0.0031 | 67.39 |
| 7 | 0.0062 | 0.001 | 0.0052 | 83.87 |
| 8 | 0.0074 | 0.0009 | 0.0065 | 87.84 |
| 9 | 0.0027 | 0.0015 | 0.0012 | 44.44 |
| 10 | 0.0018 | 0.0012 | 0.0006 | 33.33 |
| 11 | 0.0022 | 0.0013 | 0.0009 | 40.91 |

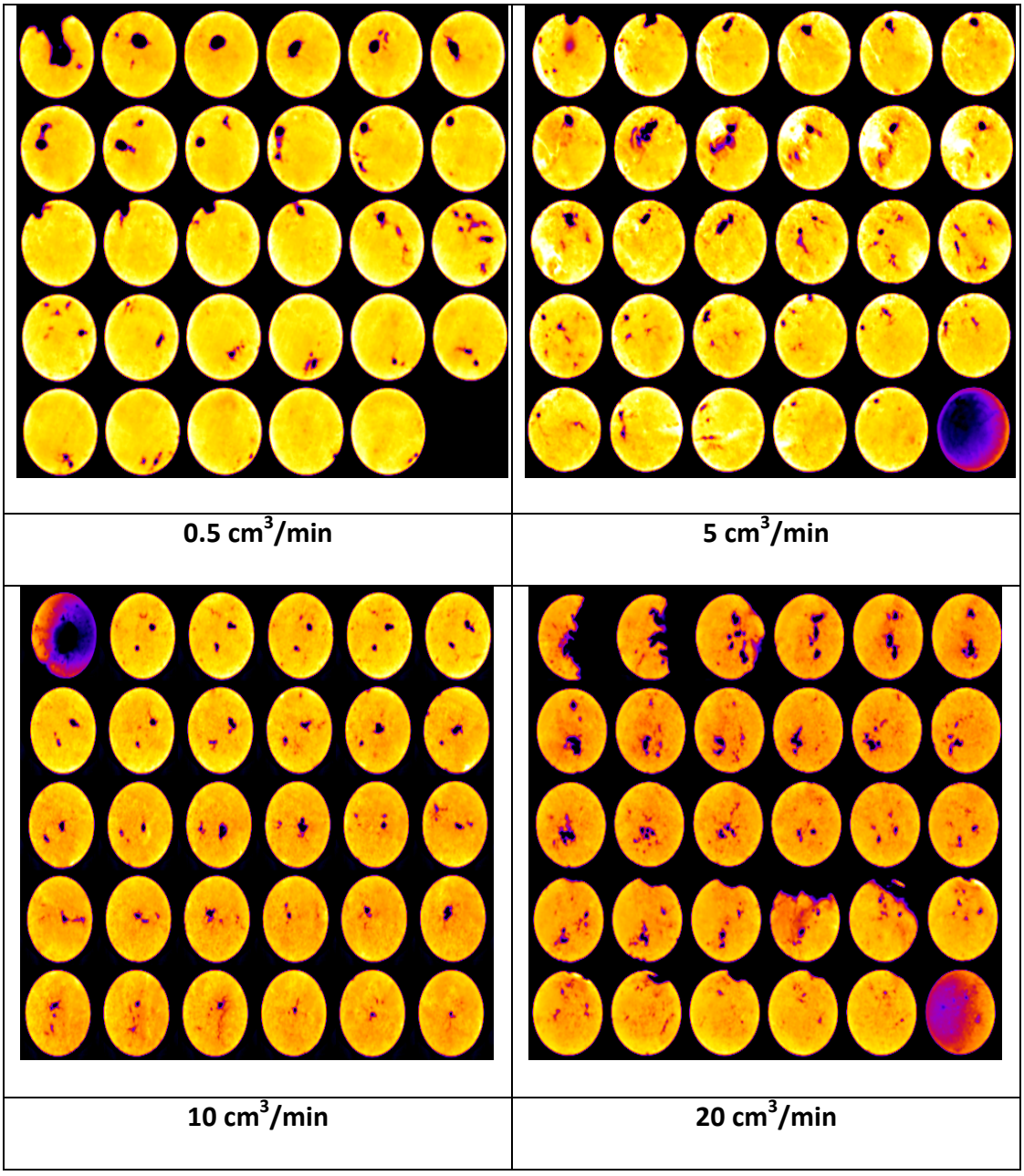


**Figure 2.18:** CT scan images of the Pink Dessert limestone cores after acid treatment.

At the low injection rate of 0.5 $cm^3$/min, one dominant wormhole was created in the first half of core while wormholes branching into multi-wormholes were obtained in

the second half of the core. Increasing the injection rate increased the branches of the wormhole in the first half of the treated core and reduced the diameter of the wormhole.

## 2.8 Conclusions

After a series of measurements of rheological properties of the VES-based acids and coreflood tests with the VES-based acid injections into two different carbonate rocks at various injection rates, the following conclusions can be drawn:

1. At ambient conditions, the viscosity of the live VES-based acid was higher than that of the partially neutralized (pH 4.5). At temperatures greater than 140 ℉, the viscosity of partially neutralized acid was higher than the live acid.
2. G' of the live VES-based acid was dominant at ambient temperature, while when temperature increased to 85°F, G" became the dominant characteristic of the live VES acid.
3. Among various concentrations of HCl at room temperature, the 5 wt% HCl VES-based acid had the highest viscosity.
4. VES-based acid was only able to build up the pressure drop across the core at injection rates less than 1 $cm^3$/min when it was injected into 80 md permeability cores. However, at injection rates of 1 $cm^3$/min and higher, VES was not able to build up any pressure drop across the core when it was injected inside 4 md cores.
5. Acid pore volume to breakthrough and the amount of VES retained in the core were reduced when low permeability cores were used.

6. Calcium propagated faster than the HCl, while the surfactant propagated with the same rate as HCl. In addition, the pore volume needed to detect the calcium and the maximum calcium concentrations were not dependent on the acid injection rate.
7. CT scans confirmed that wormhole branches were observed at the second half of the core.

# 3. FORMATION DAMAGE CAUSED BY THE RETENTION OF VES*

## 3.1 Background

The retention of the VES inside the formation could adversely affect the stimulation outcome after acidizing treatment. Even with a post-flush of mutual solvent, a significant amount of VES was still trapped inside the pores. It has been suggested that the internal breaker can solve this problem or that the VES gels can be broken down with the hydrocarbon production. However, the damage caused by the retained VES has not been well addressed. Thus, the purpose of this section was to evaluate the formation damage caused by the retained VES via a series of coreflood tests.

## 3.2 Materials and Equipment

The HCl acid, the corrosion inhibitor, and the VES are the same as used in the previous session, and also the exact same Pink Dessert limestone cores were used in this study. The same coreflood setup was used, and the core effluent samples were analyzed with density meter, pH meter, and AA to acquire the fluid density, pH, and concentration of the calcium cation. As before, the two-phase titration method was used to determine the concentration of the VES that got out of the core after treatment. The VES-based

*Reprinted with permission from "Effect of Initial HCl Concentration on the Performance of New VES Acid System" by Wang, G., Gomaa, A.M., and Nasr-El-Din., H.A., 2011. SPE-143449-MS. SPE European Formation Damage Conference, 7-10 June, Noordwijk, The Netherlands. Copyright 2011 by Society of Petroleum Engineers.

acid solutions were prepared in a similar way with only the HCl and/or corrosion inhibitor concentrations being different.

### 3.3 Experimental Procedure

Similar procedures were followed when higher concentrations of HCl were used to stimulate the cores. However, only a quarter-pore volume of the treatment fluid was injected to assure that the $CO_2$ was fully dissolved. DI water was injected in the same direction after the acid treatment. When the pressure drop across the core stabilized and there was no more generation of bubbles, the injection stopped since the system already reached equilibrium.

### 3.4 Results and Discussion

Several coreflood experiments were conducted with higher concentrations of the HCl VES-based acid system at an injection rate ranging from 0.5 to 5 $cm^3$/min using Pink Dessert limestone cores (**Tables 3-1&3-2**). The composition of the VES-based acid used in the tests was listed in **Table 3-3**. All of the experiments were conducted at room temperature while the pressure drop across the core was monitored. A new core was used in each experiment. Density, calcium, and surfactant concentrations in the effluent samples were analyzed to conduct material balance on both calcium and surfactant.

| TABLE 3-1: SUMMARY OF THE COREFLOOD TESTS | | |
|---|---|---|
| **Experiment #** | **Injection Rate, $cm^3$/min** | **VES-Based Acid Injected, PV** |
| 1 | 5 | 0.25 |
| 2 | 2 | 0.25 |
| 3 | 1 | 0.25 |
| 4 | 0.5 | 0.25 |
| 5 | 5 | 0.25 |
| 6 | 5 | 0.25 |
| 7 | 0.5 | 0.25 |

| TABLE 3-2: SUMMARY OF CORE PROPERTIES | | | | |
|---|---|---|---|---|
| **Experiment #** | **Pore Volume, ml** | **Porosity, %** | **Initial k, md** | **Final k, md** |
| 1 | 47.70 | 27.5 | 69 | 178 |
| 2 | 41.14 | 23.7 | 66 | 94 |
| 3 | 45.60 | 26.2 | 62 | 102 |
| 4 | 44.42 | 25.6 | 66 | 44 |
| 5 | 45.31 | 26.1 | 69 | 69 |
| 6 | 48.09 | 27.7 | 72 | 80 |
| 7 | 48.44 | 27.9 | 65 | 81 |

| TABLE 3-3: FORMULA OF THE VES-BASED ACID EXAMINED | | | |
|---|---|---|---|
| **Experiment #** | **HCl, wt%** | **VES, vol%** | **Corrosion Inhibitor, vol%** |
| 1 | 20 | 5 | 1 |
| 2 | 20 | 5 | 1 |
| 3 | 20 | 5 | 0.3 |
| 4 | 15 | 5 | 0.3 |
| 5 | 15 | 5 | 0.3 |
| 6 | 10 | 5 | 0.3 |
| 7 | 10 | 5 | 0.3 |

**Figure 3.1** shows the change in the normalized pressure drop as a function of the cumulative injected volume for experiments #1 to #3 that were treated with the initial acid concentration of 20 wt% HCl. The normalized pressure drop is defined as the ratio of the pressure drop during acidizing to the initial pressure drop during water injection. To observe the VES retention inside the core, 0.25 PVs of VES-based acid was injected in all experiments. Acid was injected at rates of 5, 2 and 1 $cm^3$/min, respectively. There was no significant pressure buildup, which indicated that no surfactant gel was formed during the treatment even if when the corrosion inhibitor was reduced from 1 to 0.3 vol%.

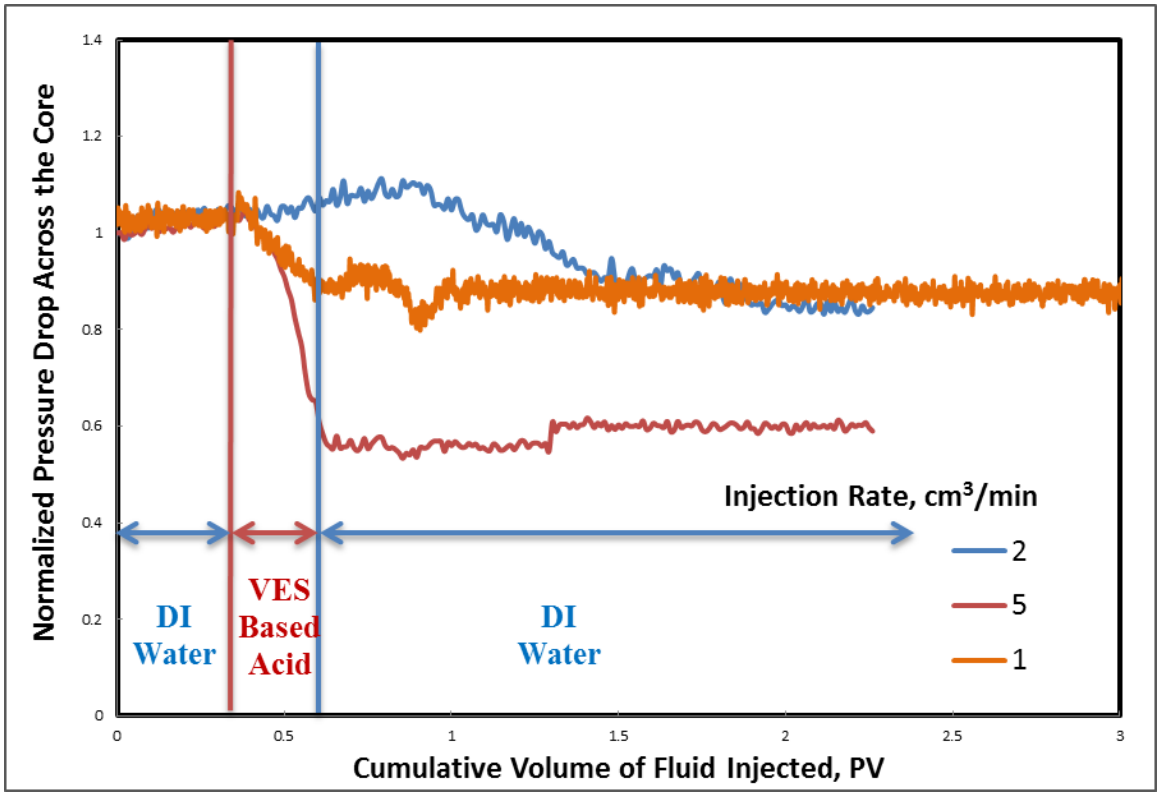


**Figure 3.1:** Normalized pressure drop across the core when 0.25 PV of VES-based 20 wt% acid was injected into the carbonate cores at various rates.

Experiment #4 and #5 were treated with 15 wt% HCl. There was no more than 20% pressure buildup during the whole process (**Figure 3.2**). The VES-based acid was more viscous than water, and a higher pressure was needed to pump the fluid at the same injection rate. The effect was eliminated by the following injection of water and the pressure drop returned to the initial status. When the carbonate rock was treated with 15 wt% HCl, no benefit was gained. Similar cases showed up again when we further reduced the concentration of HCl to 10 wt% (**Figure 3.3**). There was no pressure

buildup at all when the injection rate was low, and a small peak was observed when acid was injected at 5 $cm^3$/min. In this case, the VES-based acid system was unable to build up the pressure drop, which indicated that there was no chance for the occurrence of diversion. It only acted like an acid without any additives for diversion, and based on **Table 3-2**, the improvement of permeability was not significant sometimes causing formation damage.

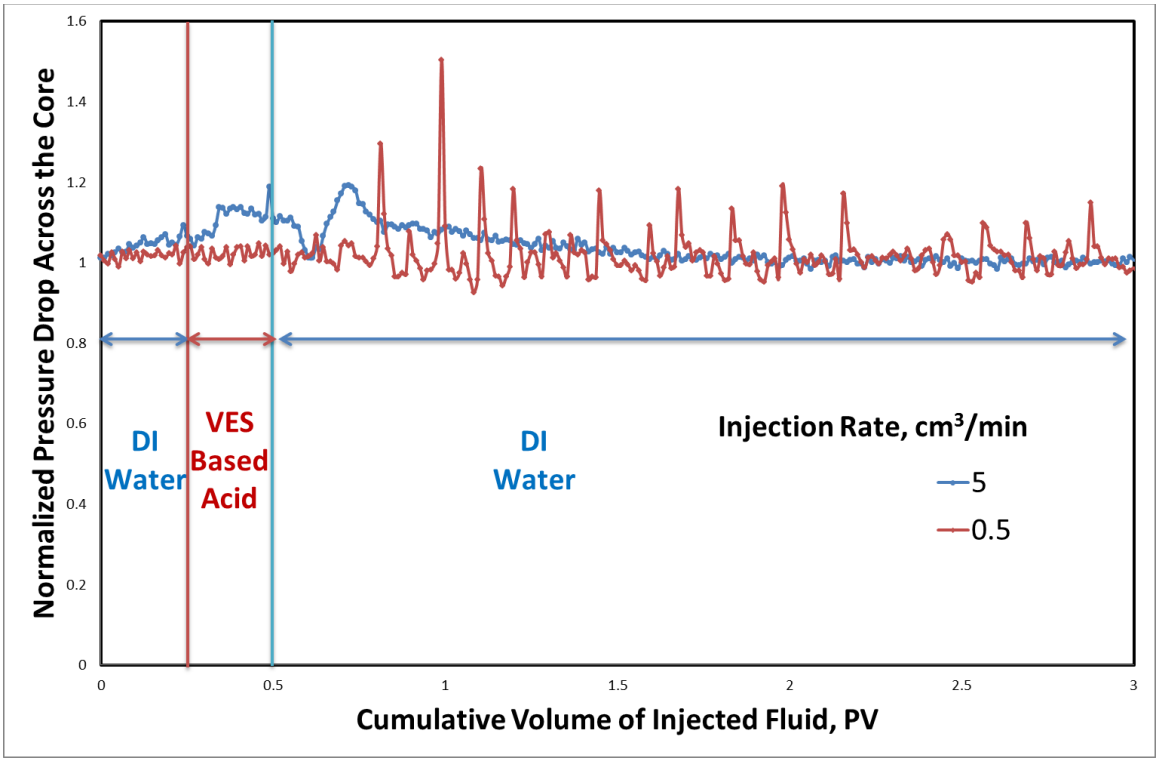


**Figure 3.2:** Normalized pressure drop across the core when 0.25 PV of VES-based 15 wt% HCl acid was injected into the carbonate cores at various rates.

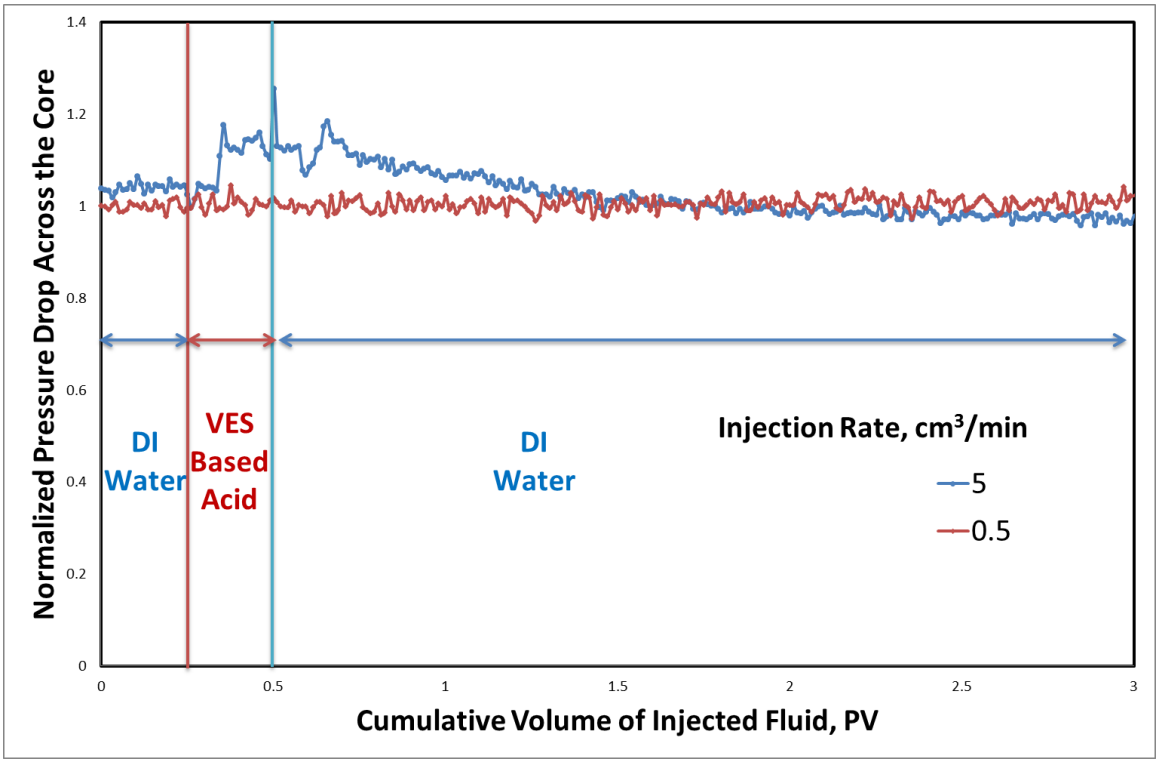


**Figure 3.3:** Normalized pressure drop across the core when 0.25 PV of VES-based 10 wt% HCl acid was injected into the carbonate cores at various rates.

**Figure 3.4** shows the pH values and densities of the core effluent samples as a function of the cumulative volume injected for the core that was treated with 20 wt% HCl at the injection rate of 5 $cm^3$/min. The initial pH value was nearly 7.8. After the injection 10 $cm^3$ of the acid solution, the pH started to decrease. Since no breakthrough occurred during the whole process, the lowest pH of the effluent sample was around 6.4, and the acidity was from the dissolution of $CO_2$ generated from the acid and the carbonate reaction. When $CO_2$ was all taken away by the injection water, pH started to increase again to around 7.0. Calcium (in the form of $Ca^{2+}$) was detected in the core

effluent sample after 0.5 pore volume of water injection when pH values started to decrease (**Figure 3.5**). Meanwhile, surfactant concentration started to increase which means that calcium cations and the surfactant propagated with the same velocity. However, this was not a pattern. In the other experiments, there were gaps between the occurrence of calcium and the surfactant (**Table 3-4**), which means the surfactant did form gel structures during the treatment, and the gel slowed down the surfactant concentration by increasing the apparent viscosity of the fluid.

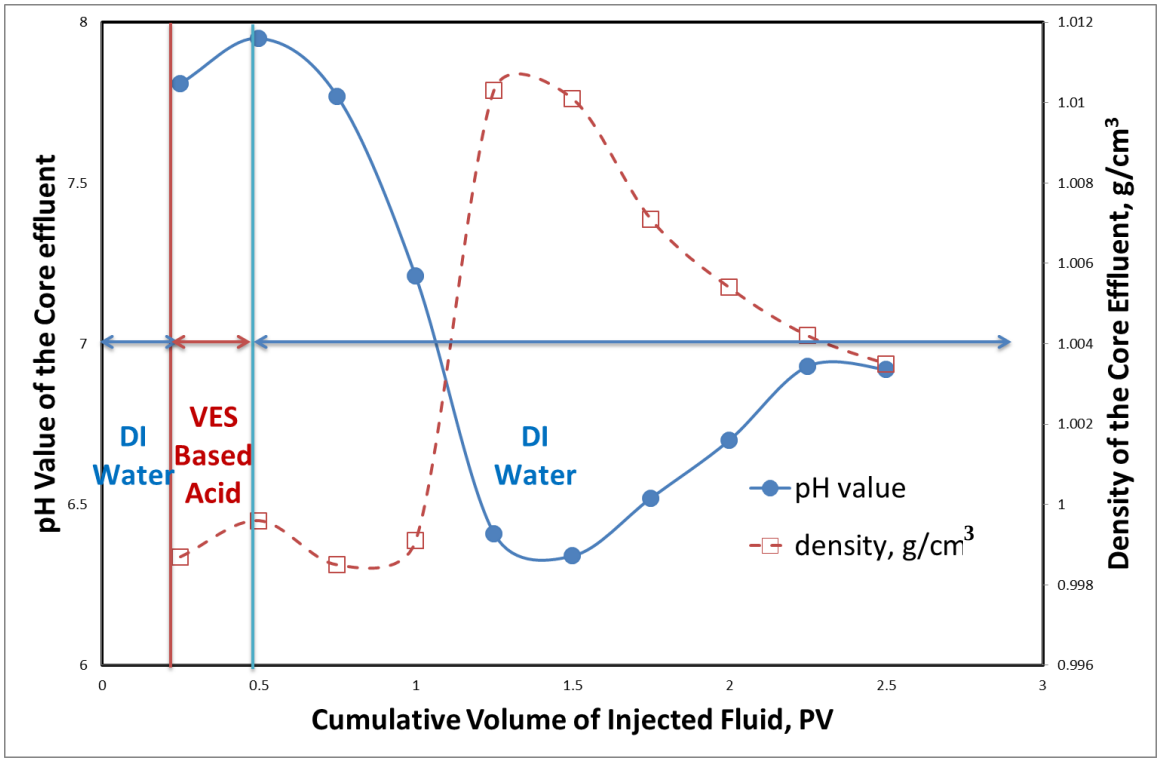


**Figure 3.4:** Analysis of the pH and density of the core effluent when the core was treated with 20 wt% HCl at 5 $cm^3$/min.

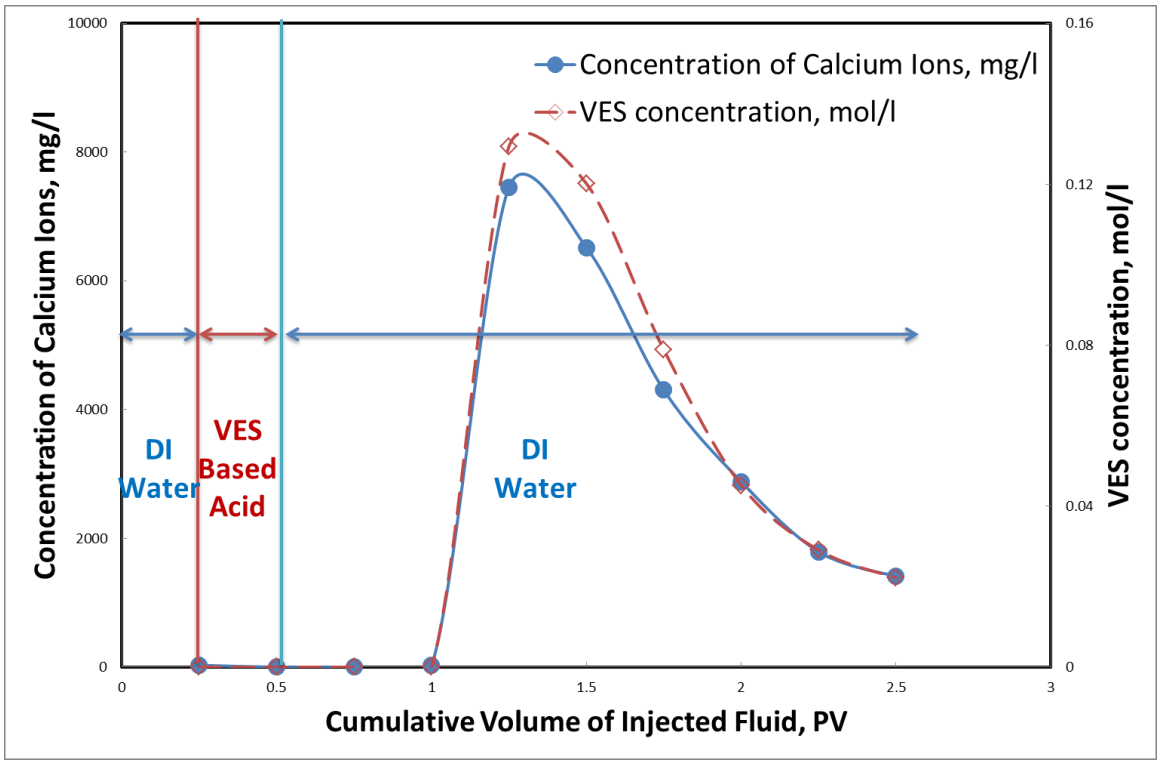


**Figure 3.5:** Analysis of the concentration of calcium ions and VES of the core effluent when the core was treated with 20 wt% HCl at 5 $cm^3$/min.

The weight of the collected samples was measured, and the collected volume of the samples was calculated from the sample density and weight. Using the surfactant concentration of each sample and its volume, the amount of surfactant, in volume, was calculated. Finally, the summation of all samples in each experiment was calculated to determine the amount of surfactant that came from the core. **Table 3-5** gives the summary of the surfactant material balance. At higher concentrations of HCl, about 90% of the surfactant injected remained inside the cores. For lower HCl concentrations, especially for low injection rates, no surfactant was detected in the effluent sample and

100% retention occurred. Even though wormholes were created, the permeability did not correspondingly increase, which means the surfactant caused formation damage. Further treatment, such as injection of mutual solvent, should be applied.

**TABLE 3-4: TIME OF OCCURRENCE OF CALCIUM IONS AND VES**

| Experiment # | Initial $Ca^{2+}$ PV | Maximum $Ca^{2+}$ PV | Initial VES PV | Maximum VES PV |
|---|---|---|---|---|
| 1 | 1.25 | 1.5 | 1.5 | 1.75 |
| 2 | 1.25 | 1.25 | 1.25 | 1.25 |
| 3 | 1 | 1.25 | 1 | 1.25 |
| 4 | 1.5 | 2 | No | No |
| 5 | 1.25 | 1.5 | 1.75 | 2.25 |
| 6 | 1.5 | 2.5 | 3 | 3 |
| 7 | 1.75 | 2 | No | No |

To cover the whole core, 29 slices with 2 mm thickness and 5 mm separation between each slice were selected. In the processing step, the binary image data collected by the CT-scanner was processed with a SUN workstation using the petrophysical CT-scanning software ImageJ. Analysis of ImageJ showed a cross-sectional area for each slice along the core length. This enabled us to show the difference in the shape of the wormhole when VES acid was injected at various flow rates with different acid

compositions. **Figure 3.6** shows the results from the CT scan for the tested cores treated with 20, 15, and 10 wt% HCl, respectively. Phase dissolution was noted when injection rates were less than 1 $cm^3$/min. Multiple wormholes were observed only at the very beginning, while at the end, only one dominant wormhole was observed.

**TABLE 3-5: MATERIAL BALANCE OF VES AFTER TREATMENT**

| Experiment | Injected, $cm^3$ | Collected, $cm^3$ | Retained, $cm^3$ | Retained ratio, % |
|---|---|---|---|---|
| 1 | 1 | 0.174 | 0.826 | 82.60 |
| 2 | 0.5 | 0.0534 | 0.4466 | 89.32 |
| 3 | 0.5 | 0.0403 | 0.4597 | 91.94 |
| 4 | 0.5 | 0.0551 | 0.4449 | 88.98 |
| 5 | 0.5 | 0 | 0.5 | 100 |
| 6 | 0.5 | 0.0130 | 0.487 | 97.40 |
| 7 | 0.5 | 0.00225 | 0.49775 | 99.55 |
| 8 | 0.5 | 0 | 0.5 | 100 |

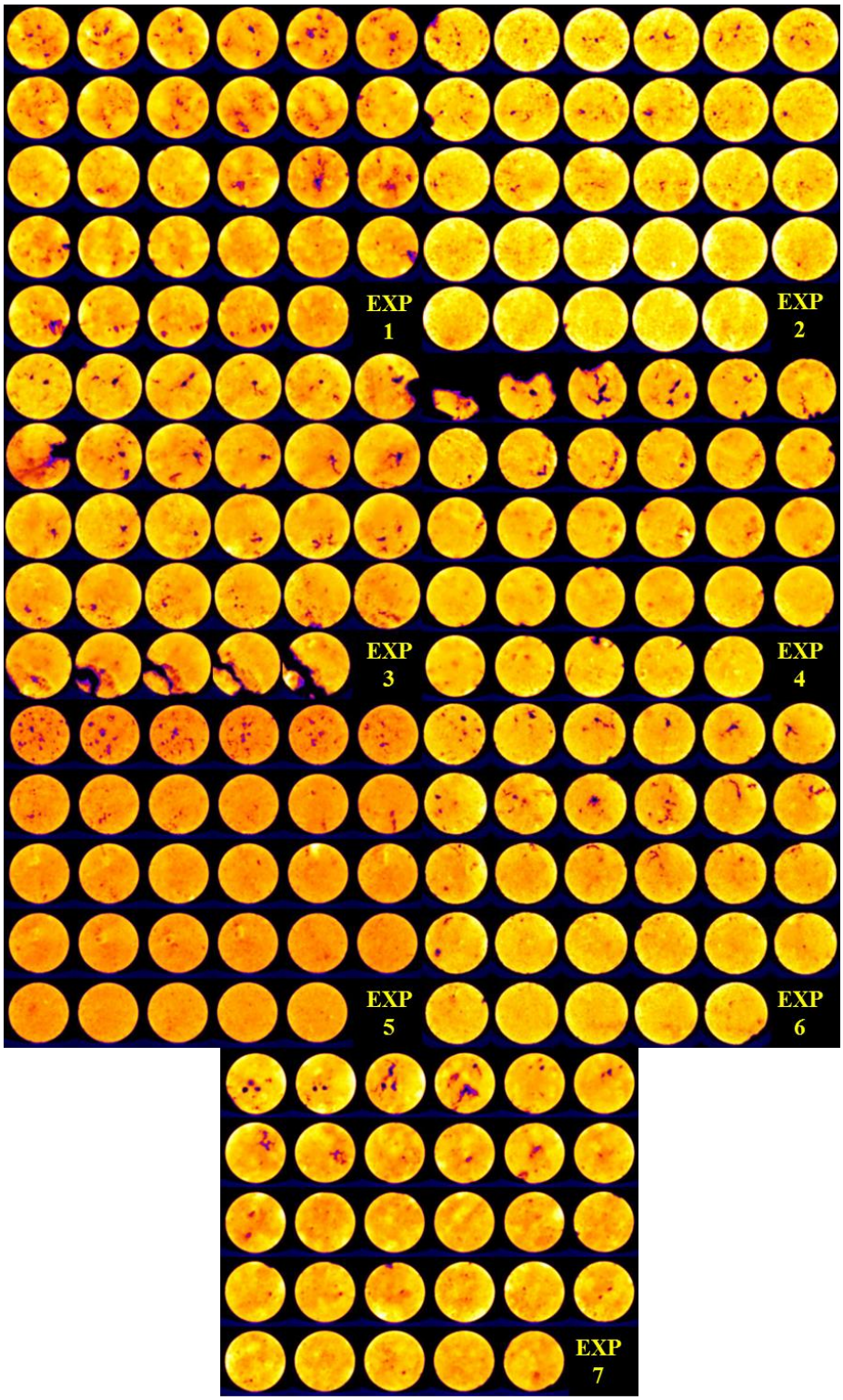


**Figure 3.6:** CT scan images of the cores after treatment of VES-based acids.

As seen in **Figure 3.1**, for 20 wt% HCl based VES solutions, only a small pressure buildup was observed when the injection rate was 2 $cm^3$/min. After checking the cores, it is clear that at the injection rate of 2 $cm^3$/min the number of wormholes in the first section was much less. This meant that the acid had fewer pathways to propagate than the others did, and a small pressure buildup was achieved. The one with the injection rate of 5 $cm^3$/min had the best permeability improvement. Although the overall acid-rock reaction rate was lower, it had a higher injection rate, which significantly increased the stress on the core. The core was treated with this stress for more than 20 minutes, and the overall structure was not as tight as it had been. So, a much more significant permeability improvement was observed. There was almost no time gap between the detection of calcium and the surfactant for experiments with the injection rates of 2 and 1 $cm^3$/min. This was due to a lack of a significant amount of gel being formed and a lack of pressure buildup being observed. However, when the injection rate was 5 $cm^3$/min, a small gap of about 0.25 PV was observed. This was due to the higher adsorption of surfactant on the surface of the rock when higher stress was applied. The higher percentage of adsorption delayed the propagation of the surfactant and a gap occurred without any gel formation. A specific phenomenon for the coreflood test with the injection rate of 2 $cm^3$/min was that the initial detection of the calcium and the surfactant was also their highest concentration. Fewer wormholes were responsible for this. For the other experiments, they have multiple channels to transport the reaction product and the traveling velocity between each channel was not exactly the same. Therefore, there was a gap between the first detection and the peak. For the conditions

with fewer wormholes, almost all the channels were transporting with similar speeds and there was no chance to create the gap. The amount of retained VES in the core increased with a decrease in injection rates. Although the test that was injected at 1 $cm^3$/min was the lowest injection rate, less corrosion inhibitor made the HCl more reactive than in the other cases. More space was created, which helped to be remove the VES from the treated formation.

For cores treated with 15 wt% HCl based VES solution, **Figure 3.2**, a small increase in pressure drop was obtained after the treatment, which indicated that formation damage occurred. The 100% retained VES was the source of the formation damage. A smaller amount of calcium indicated a slower reaction, and the most reaction occurred on the surface due to less stress from the lower injection rate. Therefore, a severe washout was observed as shown in **Figure 3.6**. A small pressure buildup was obtained for the core treated with the injection rate of 5 $cm^3$/min. This was considered a sign of diversion and the CT scan confirmed this sign since it had much more wormholes than the others. Meanwhile, diverting captured more calcium ions during the process, and it took time to deform the VES gel. That was the main reason that a gap of 0.5 PV was shown between the first detection of calcium and the VES. The higher maximum calcium concentration compared to the one with the lower injection rate was due to the high stress caused by the higher injection rate. More calcium was washed off rather than reacted. The larger area created by the multiple wormholes covered by the same amount of acid solution made the wormholes shorter. Although there were multiple wormholes

and a larger calcium amount in the effluent sample, the improvement of permeability was zero because of the 97.4% retention of the VES.

For the cores treated with 10 wt% HCl based VES solution, **Figure 3.3**, a similar small pressure buildup was observed when the injection rate was 5 $cm^3$/min. Unfortunately, especially for the first third, the core was totally destroyed after taken from the core holder. That could be a similar case compared to the one treated with 15 wt% HCl based VES solution. The gap between the initial detection of calcium and the VES increased to 1.5 PV, which was a sign that the delay due to the gelation was more significant. In addition, the possible multiple wormholes gave it a larger gap of 1 PV between the first detection and the maximum calcium concentration. The permeability of the core increased a little at the end, which implied that even with formation damage from the VES (99.6% as shown in **Table 3-5**), the system was still able to stimulate the formation. For the core treated with the injection rate of 0.5 $cm^3$/min, a similar phenomenon was observed as there was no pressure drop change and there was 100% VES retention. Moreover, the length of the wormhole was shorter since the acid concentration was lower.

## 3.5 Conclusions

According to the coreflood tests conducted and the analysis of the core effluent samples, the following conclusions can be draw:

1. VES acid was not able to build up a pressure drop across the core when it was injected inside 70 md permeability cores at various acid concentrations and injection rates when only one fourth of the pore volume was injected.
2. At high concentrations of HCl, calcium ions and the VES propagated with the same velocity. When low concentrations of HCl were employed, calcium ions propagated faster.
3. Surfactant retention is higher when the acid concentration and the injection rates were lower. This number could be up to 100%.
4. CT scans confirmed only small and short wormhole branches at the area near the inlet, and one wormhole dominated until the end with a decreasing diameter.

# 4. EFFECTS OF ADDITIVES ON THE PERFORMANCE OF GLDA

## 4.1 Background

GLDA has been well studied to stimulate carbonate and sandstone formations. No GLDA treatment fluids contain other additives. However, it was found that after long term of stabilization, some precipitates appear in the core effluent samples. This means that if excess amounts of GLDA were left inside the formation, some scale problems could occur. Furthermore, even though GLDA reacts with carbonate at a much lower rate compared to HCl, the corrosion from GLDA can still be high enough to cause damage. Thus, a corrosion inhibitor and a cationic surfactant were used to investigate the effects on mitigating potential formation damage.

## 4.2 Materials and Equipment

Monosodium GLDA was titrated with a 0.1M $FeCl_3$ solution and its concentration was 40 wt%. The initial GLDA solution had a pH of 3.8. The cationic surfactant and the corrosion inhibitor were field chemicals and were used as received. Indiana limestone cores with an initial permeability between 1 to 1.5 md were used to represent a low permeability formation. They were cut from the same block and the size was 6 in. length and 1.5 in diameter. The coreflood setup was the same as shown in the previous tests.

## 4.3 Preparation of Treatment Fluids and Experimental Procedure

GLDA treatment fluids were prepared by simply mixing the same weight of DI water and the original 40 wt% monosodium GLDA solutions. The final treatment fluid was 20 wt% monosodium GLDA solution with a pH of 3.9. If additives were added, same volume of DI water was replaced.

During the coreflood test process, DI water was injected at the rate of 2 $cm^3$/min. Then, the heating jacket was turned on and heating continued until the end of the test. At higher temperatures, water exhibits lower viscosity and the pressure drop across the core continued to decreasing until the whole system reached equilibrium. Then, half a pore volume of core effluent sample was collected. Injection fluid was switched to GLDA-based treatment fluid, and the core effluent sample was collected every half a pore volume in the test tubes. The injection fluid was switched back to DI water when breakthrough was achieved. When the fluid became colorless without any bubbles, the injection stopped and the heating system was turned off. The final permeability of the core was measured when the system had completely cooled down.

## 4.4 Results and Discussion

GLDA-based treatment fluid was injected at 2 $cm^3$/min during the tests. All tests were conducted at 300 ℉. The initial and final permeabilities of all cores were measured at room temperature in the opposite direction of the treatment fluid injection. Four experiments were conducted as summarized in **Table 4-1**. Pressure drops across the cores were monitored as shown in **Figs. 4.1-4.4**. CT scan images of the cores were

placed in **Figure 4.5**. All treatments were able to create a dominant wormhole throughout the cores. If the core was only treated by GLDA, 4.24 PVs of treatment fluid were needed, and the ratio between the final permeability and the initial permeability was 1223. When the cationic surfactant was added into the system, the diffusion of the GLDA was slowed, and the reaction between the GLDA and the carbonate rock was slowed as well. Thus, a little more fluid was needed to break through, and the wormhole was not as big as the one treated with GLDA only. Thus, the ratio between final permeability and the initial permeability was 737. When corrosion inhibitor was added into the system, the treatment fluid was retarded and even more treatment fluid was needed to achieve breakthrough. The low number of the ratio between the final and initial permeability was as expected, smaller than the previous tests. When combining both additives in the same tests, certain components in the corrosion inhibitor increased the solubility of the cationic surfactant and reduced the fluid viscosity. Meanwhile, cationic surfactant eliminated the corrosion resistivity of the gradients in the corrosion inhibitor, and faster reaction rates were exhibited during the tests. As the carbonate core is slightly positively charged, the negatively charged product of calcium GLDA has a tendency to attach to the rock surface and causes potential formation damage. The cationic surfactant will compete with the rock and combine with the reaction product. Thus, fewer residues were expected after the test, and its final/initial permeability ratio was the highest.

| TABLE 4-1: SUMMARY OF THE COREFLOOD TESTS | | | | | |
|---|---|---|---|---|---|
| Experiment # | Treatment Fluid | $k_{i,}$ md | $PV_{BT}$ | $k_{f,}$ md | $k_f/k_i$ |
| 1 | GLDA+0.2 vol% S+0.1 vol% CI | 1.40 | 4.75 | 4092 | 2923 |
| 2 | GLDA | 1.53 | 4.24 | 1871 | 1223 |
| 3 | GLDA+0.2 vol% S | 1.27 | 4.58 | 936 | 737 |
| 4 | GLDA+0.1 vol% CI | 1.50 | 4.92 | 546 | 364 |

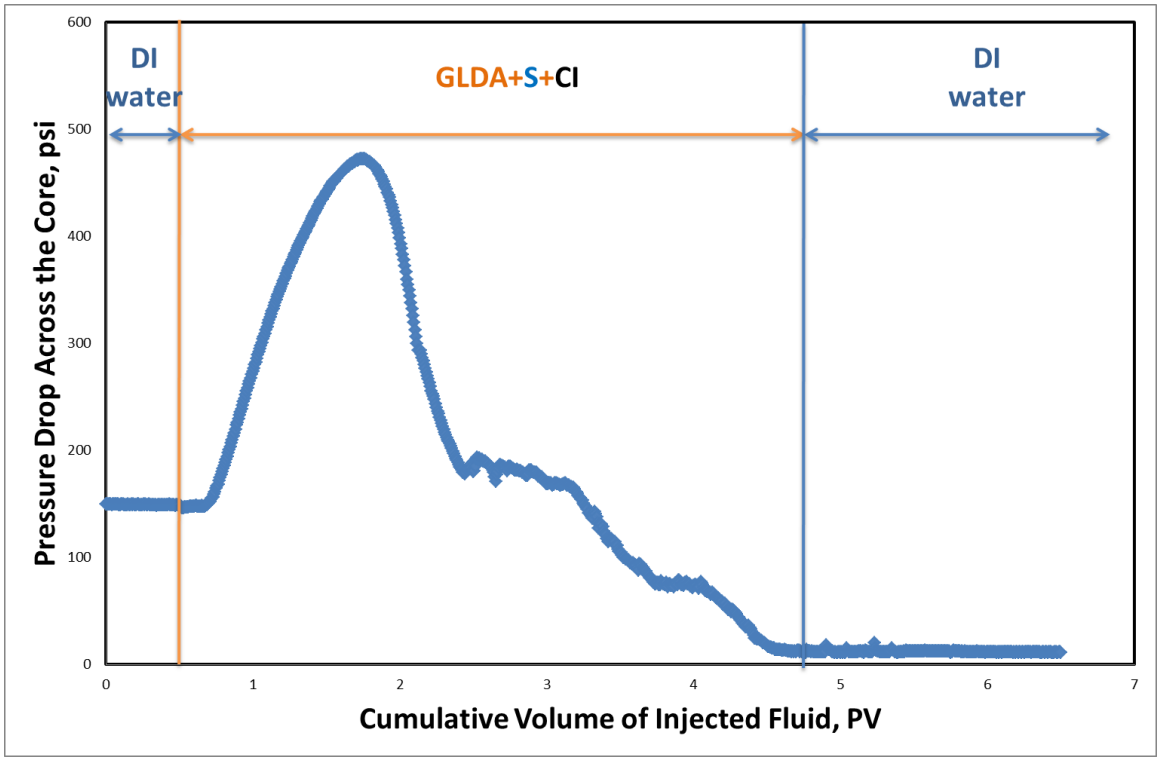


**Figure 4.1:** Pressure drop across the core during GLDA treatment injection with the additives of cationic surfactant and corrosion inhibitor.

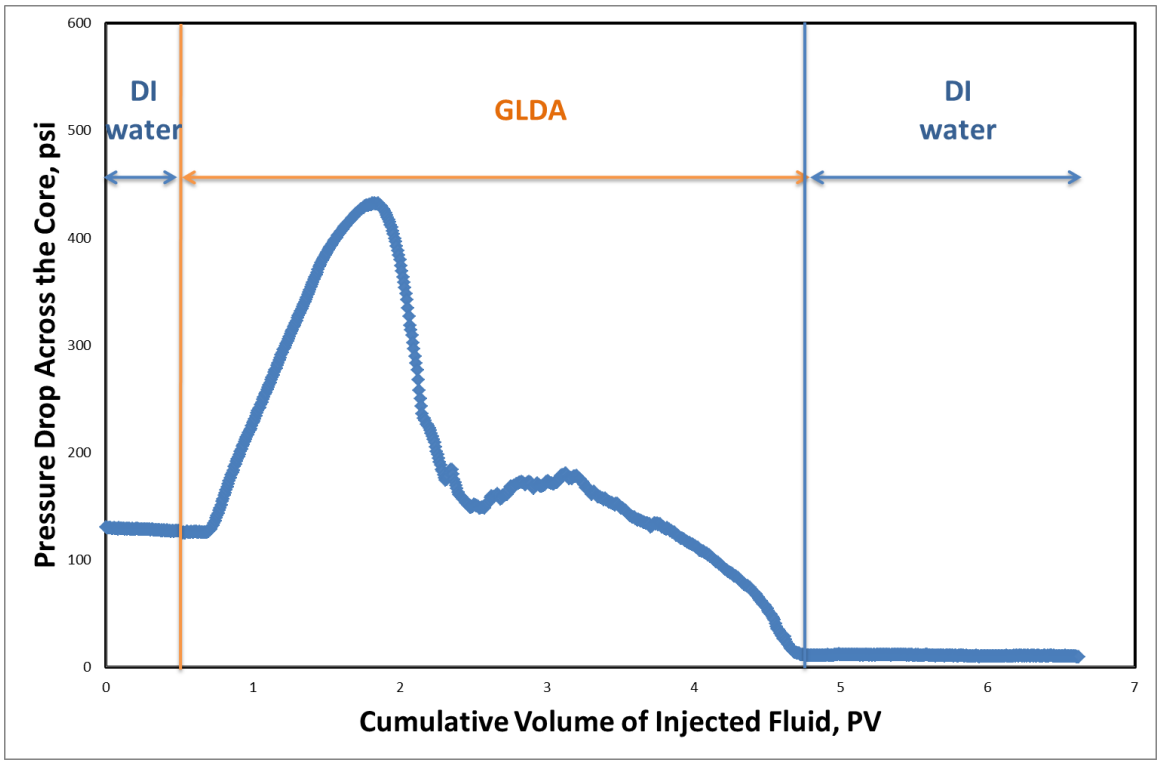


**Figure 4.2:** Pressure drop across the core during GLDA treatment injection.

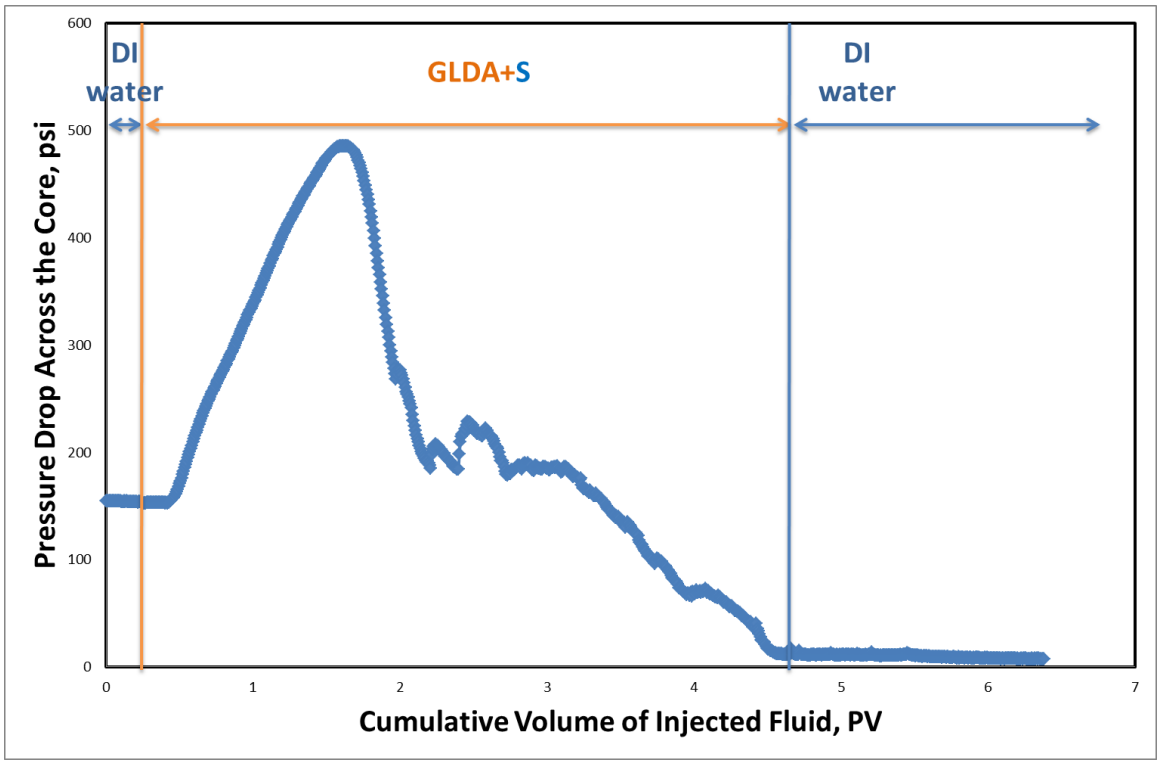


**Figure 4.3:** Pressure drop across the core during GLDA treatment injection with the additive of cationic surfactant.

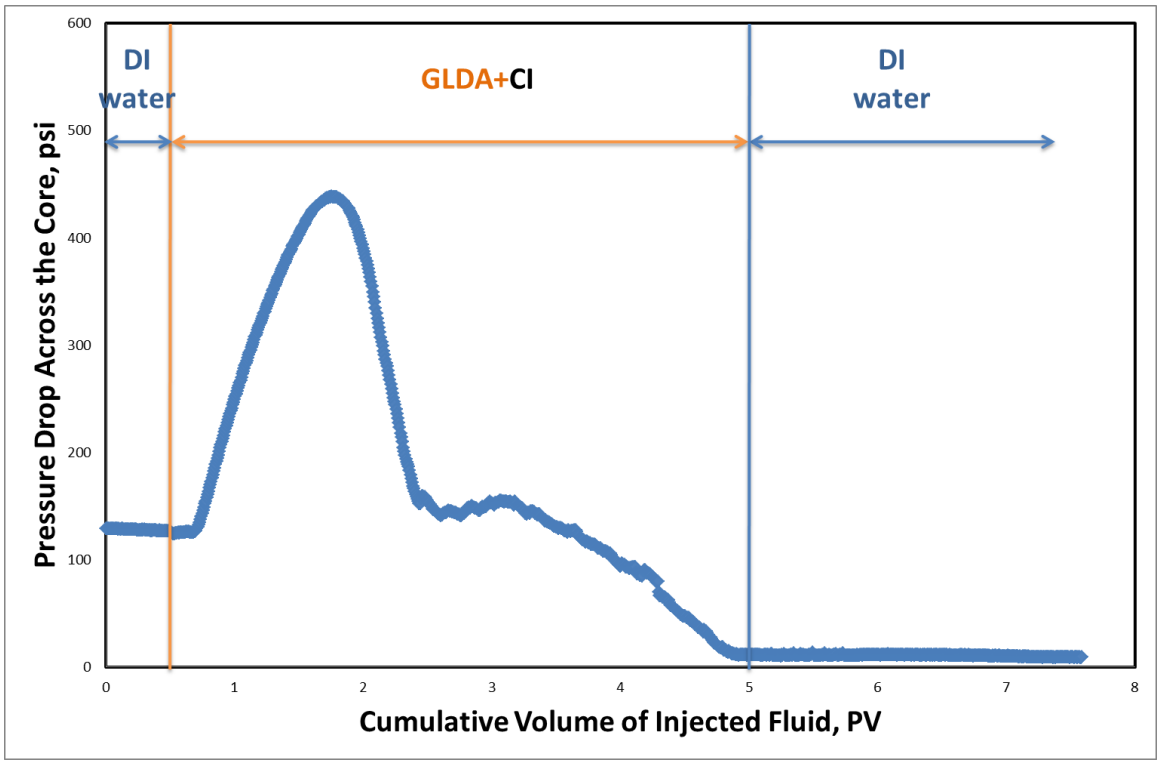


**Figure 4.4:** Pressure drop across the core during GLDA treatment injection with the additive of corrosion inhibitor.

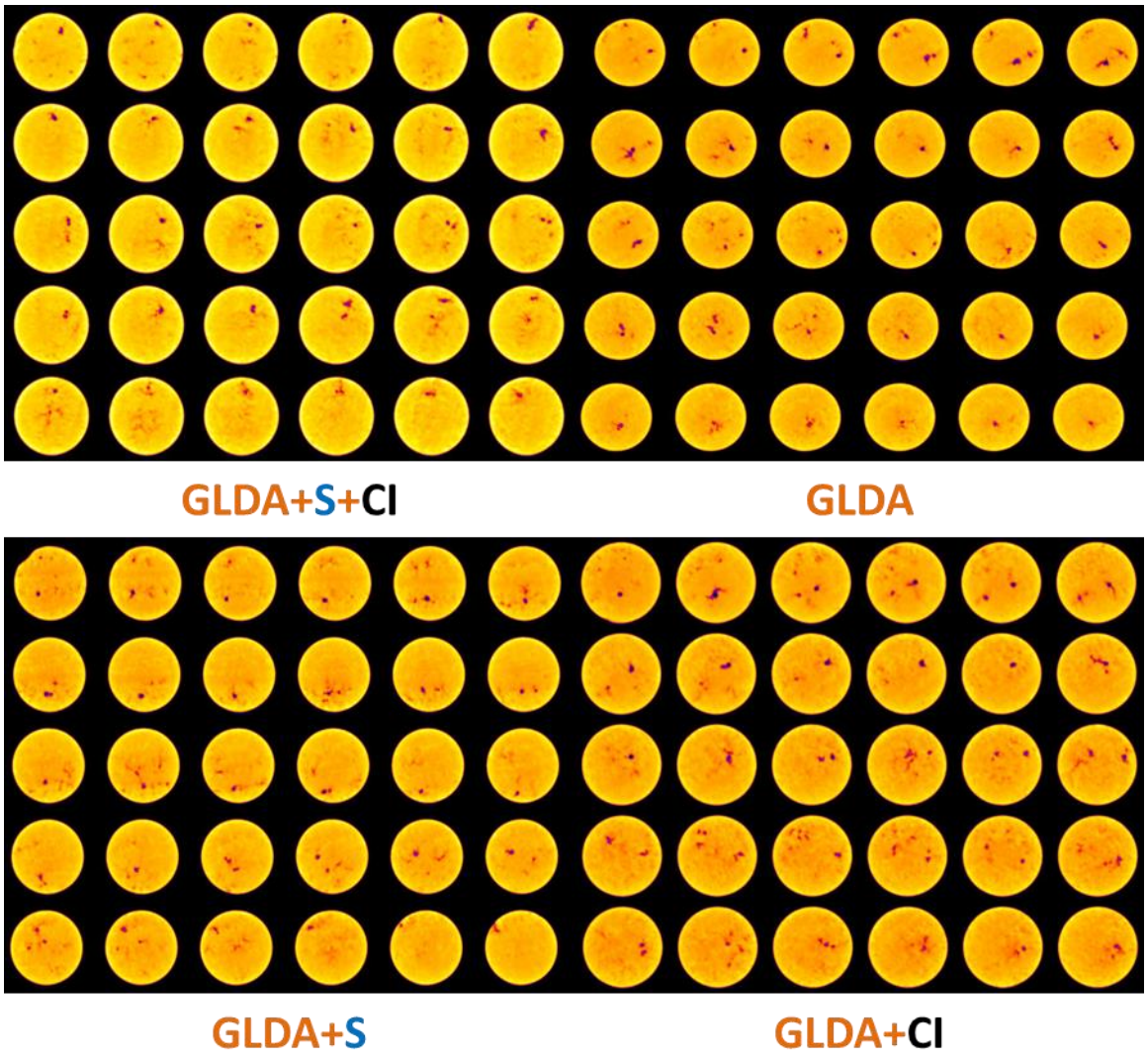


**Figure 4.5:** CT scan images of the Indiana limestone cores after treatment of GLDA-based fluids.

## 4.5 Conclusions

According to the coreflood tests and the CT scan images, the following conclusions can be drawn:

1. Both cationic surfactant and corrosion inhibitor can lower the reaction kinetics between GLDA and the carbonate rock formation. While the treatment with the presence of corrosion inhibitor only provided the lowest stimulation outcome.
2. Combination of the cationic surfactant and the corrosion inhibitor can significantly increase the stimulation outcome. However, more treatment fluid was required to create the same length of the wormholes.

# 5. EVALUATION OF THE VES AIMING FOR HIGH TEMPERATURE APPLICATIONS*

## 5.1 Background

As discussed in the previous sessions, an amine oxide based VES was well studied on its rheological properties and its performance during acidizing in carbonate cores. The VES-based acid can achieve very good diverting ability when injected at a very low rate. However, temperature limited the performance of the VES. Thus, this new VES was invented. The new VES has a longer alkyl chain, which favors the stability of the micelles. Meanwhile, the longer chain also reduces the solubility of the VES and high concentration of salt or acid is required.

## 5.2 Materials and Equipment

Similar to the previous tests to evaluate the amine oxide VES, a HT/HP rheometer and coreflood setup were used. The new VES, a zwitterion surfactant, and three commercial corrosion inhibitors (CI) were used without further purification. CI-A is based on fatty amines. CI-B was designed for brine-acid systems with temperatures up to 350 ℉. CI-C is more effective on protecting high alloy metals at temperatures up to 500 ℉. Main components of the three CI are listed in **Table 5–1**. ACS grade $CaCl_2$ was

*Reprinted with permission from "A New Viscoelastic Surfactant for High Temperature Carbonate Acidizing" by Wang, G., Nasr-El-Din., H.A., Zhou, J., and Holt, S., 2012. SPE-160884-MS. SPE Saudi Arabia Section Technical Symposium and Exhibition, 8-11 April, Al-Khobar, Saudi Arabia. Copyright 2012 by Society of Petroleum Engineers.

used to prepare spent VES-based acid solutions. A 100% pure mutual solvent, ethylene glycol monobutyl ether (EGMBE), was diluted to different concentrations to break the VES gels. Indiana limestone cores, with one set having permeabilities around 5 md and the other set having permeabilities between 50 to 100 md, were used during the coreflood tests. Not only 6-in. cores, but also 20-in. cores were also used to investigate the deep penetration and possible diverting.

**TABLE 5–1: MAIN COMPONENTS OF THE THREE CORROSION INHIBITORS**

| Corrosion Inhibitor-A | Corrosion Inhibitor-B | Corrosion Inhibitor-C |
|---|---|---|
| | Isopropanol | |
| | Aromatic Naphtha | |
| Fatty amines | Naphthalene | |
| Ethoxylated fatty amines | Ethyl octynol | |
| Propargyl alcohol | Propargyl alcohol | Propargyl alcohol |
| Acetic acid | Ethanol | Methanol |
| Formaldehyde | Copper iodide | |
| Water | Dimethyl formamide | |
| | Benzyl chloride | |
| | Ethylene oxide | |
| | Quaternary ammonium salts | |

## 5.3 Acid Preparation

When preparing 100 g of live VES-based acid, 45.1 g of DI water was first weighed in a beaker. Then 1 $cm^3$ of one of the three corrosion inhibitors was added. A magnetic stirrer was used to mix the solution. After 5 minutes, 59.7 g of 36.8 wt% HCl was added to the solution slowly. After another 10 minutes, 4 $cm^3$ of the new VES was slowly added to the acid. Then the acid solution was mixed for 30 minutes before injection. Air bubbles generated during the mixing were removed through centrifuge at 3000 rpm for 20 minutes. The composition of the live 4 vol%-based 20 wt% HCl was listed in **Table 5–2**.

**TABLE 5–2: COMPOSITION OF LIVE VES-BASED 20 WT% HCL**

| Components | Amount |
|---|---|
| Corrosion Inhibitor-C | 1 $cm^3$ |
| VES | 4 $cm^3$ |
| DI Water | 45.1 $cm^3$ |
| 36.8 wt% HCl | 59.7 g |

In a beaker, 5.45 g of $CaCl_2$ was weighed and 46.55 (or 46.8) $cm^3$ of deionized water was added to dissolve the salt. When there was only a transparent colorless solution left in the beaker, 0.5 $cm^3$ (or 0.25 $cm^3$) of a corrosion inhibitor was added into the beaker and mixed with a magnetic stirrer. When the solution was well mixed, 2 $cm^3$

of the new VES was added slowly and mixing stopped until a single-phase fluid was formed. Then the fluid was centrifuged at 3000 rpm for 20 minutes to remove air bubbles that were trapped in the viscous VES solution. The final solution contained 10 wt% $CaCl_2$, 1 (or 0.5) vol% corrosion inhibitor, and 4 vol% VES. Other than 10 wt% $CaCl_2$ in the final solution, another series of solutions were prepared with the $CaCl_2$ concentration of 20 wt%. They represented spent HCl solutions with the initial HCl concentration of 15 wt%. All other components were kept at the same concentrations.

When preparing fluids with mutual solvent, 2.5 $cm^3$ (or 5 $cm^3$) of DI water was replaced by an equal volume of mutual solvent to obtain fluids with 5 vol% (or 10 vol%) MS. All fluid compositions are given in **Table 5–3**.

**TABLE 5–3: COMPOSITION OF VARIOUS SPENT VES-BASED ACID SOLUTIONS**

| Components | Spent 7 wt% VES-Based Acid | Spent 15 wt% VES-Based Acid | Spent 7 wt% VES-Based Acid With MS |
|---|---|---|---|
| Corrosion Inhibitor, $cm^3$ | 0.5 or 1 | 0.5 or 1 | 0 |
| VES, $cm^3$ | 4 | 4 | 4 |
| DI Water, $cm^3$ | 93.1 or 93.6 | 90.1 or 90.6 | 85.1 or 89.6 |
| $CaCl_2$, g | 10.9 | 23.8 | 10.9 |
| 36.8 wt% HCl, g | 0 | 0 | 0 |
| Mutual Solvent, $cm^3$ | 0 | 0 | 5 or 10 |

## 5.4 Experimental Procedure

The viscosity measurements were conducted at four different temperatures: 80, 150, 250, and 325 ℉. After the fluid sample reached the target temperature, the shear rate increased from 0.1 to 1,000 $s^{-1}$ with multiple data points recorded. To evaluate the fluid tolerance to long time heating, a shear rate of 10 $s^{-1}$ was selected and the sample temperature was slowly increased with time. All coreflood tests were conducted the same as the ones described previously. The only difference was that after the acidizing treatment, mutual solvent and DI water was injected in the direction opposite to the acid injection direction.

## 5.5 Results and Discussion

### 5.5.1 Viscosity Measurements

The performance of these three corrosion inhibitors was compared at the same concentration but various temperatures. At room temperature with a CI concentration of 0.5 vol% (**Figure 5.1)**, the addition of CI-A and C both increased the viscosity of the fluid, while CI-B maintained a similar viscosity as that without CI. CI-B contained the highest concentration of alcohol. Meanwhile, other components in CI-B stabilized the wormlike micelles and a similar level of viscosity was obtained. Less alcohol was represented in CI-A and C, and the other components strengthened the wormlike micelles, which led to an increase in the fluid viscosity. However, when the concentration was increased to 1 vol% (**Figure 5.2)**, CI-A and CI-C could not hold a viscosity as high as that of the concentration of 0.5 vol%, and the CI-B based solution

gave a higher viscosity. When the alcohol amount was doubled with a doubled amount of CI-A and C, the effect of the alcohol was much more obvious and the fluid viscosity dropped to a similar level as the control group.

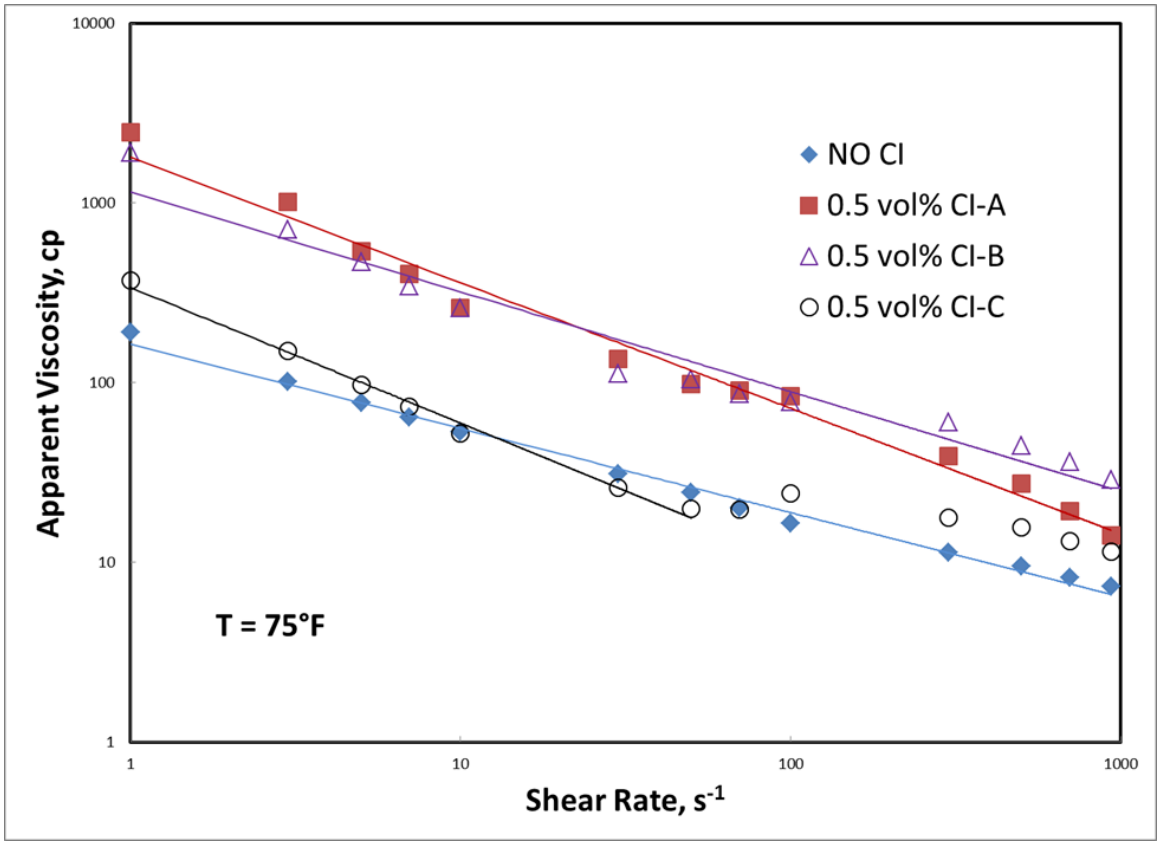


**Figure 5.1:** Effect of 0.5 vol% CI on the viscosity of 4 vol% VES-based fluid at 75 ℉.

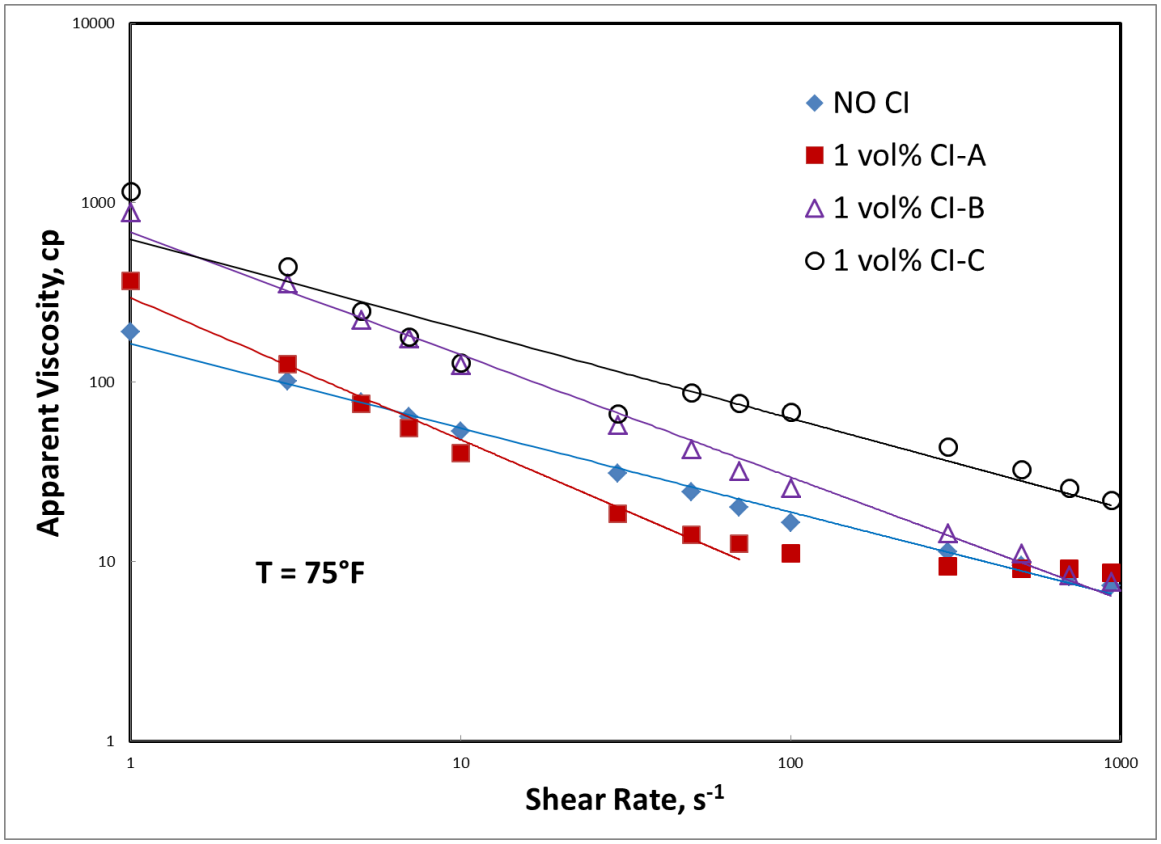


**Figure 5.2:** Effect of 1 vol% CI on the viscosity of 4 vol% VES-based fluid at 75 ℉.

When temperature was increased to 150 ℉ with the concentration of CIs at 0.5 vol%, CI-A significantly increased the viscosity and CI-B maintained the same level of viscosity as the one without CI (**Figure 5.3)**. However, CI-C destroyed the formation of the new VES and dramatically reduced the fluid viscosity due to the temperature sensitive components. When the concentration was increased to 1 vol%, both CI-A and C decreased the viscosity of the fluid. Only CI-B was able to remain at the same level as the one without CI, (**Figure 5.4)**. Similar phenomena were observed as the case at room temperature. A high concentration of alcohol in CI-C prevented the formation of

wormlike micelles at low concentrations. Meanwhile, CI-A, which had the lowest alcohol components, increased the viscosity of the VES-based solution. When the CI concentration doubled, the higher concentration of alcohol in both CI-A and CI-B significantly reduced the amount of wormlike micelles and decreased the fluid viscosity.

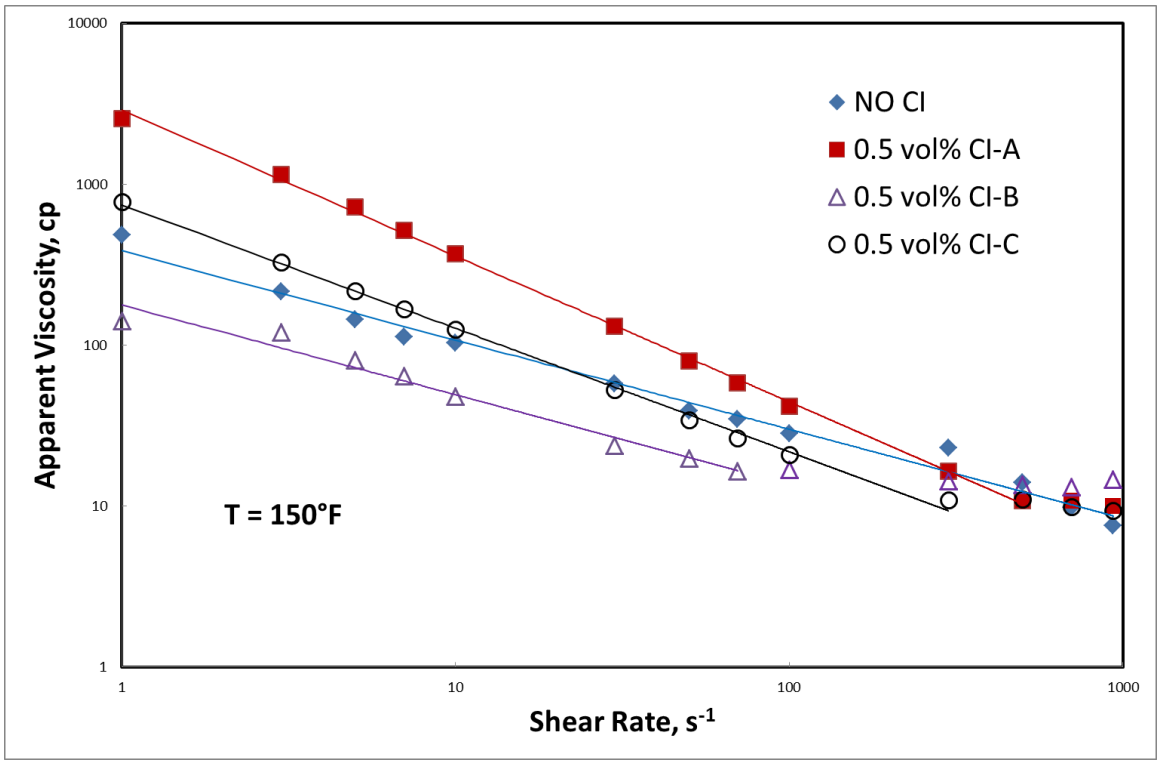


**Figure 5.3:** Effect of 0.5 vol% CI on the viscosity of 4 vol% VES-based fluid at 150 ℉.

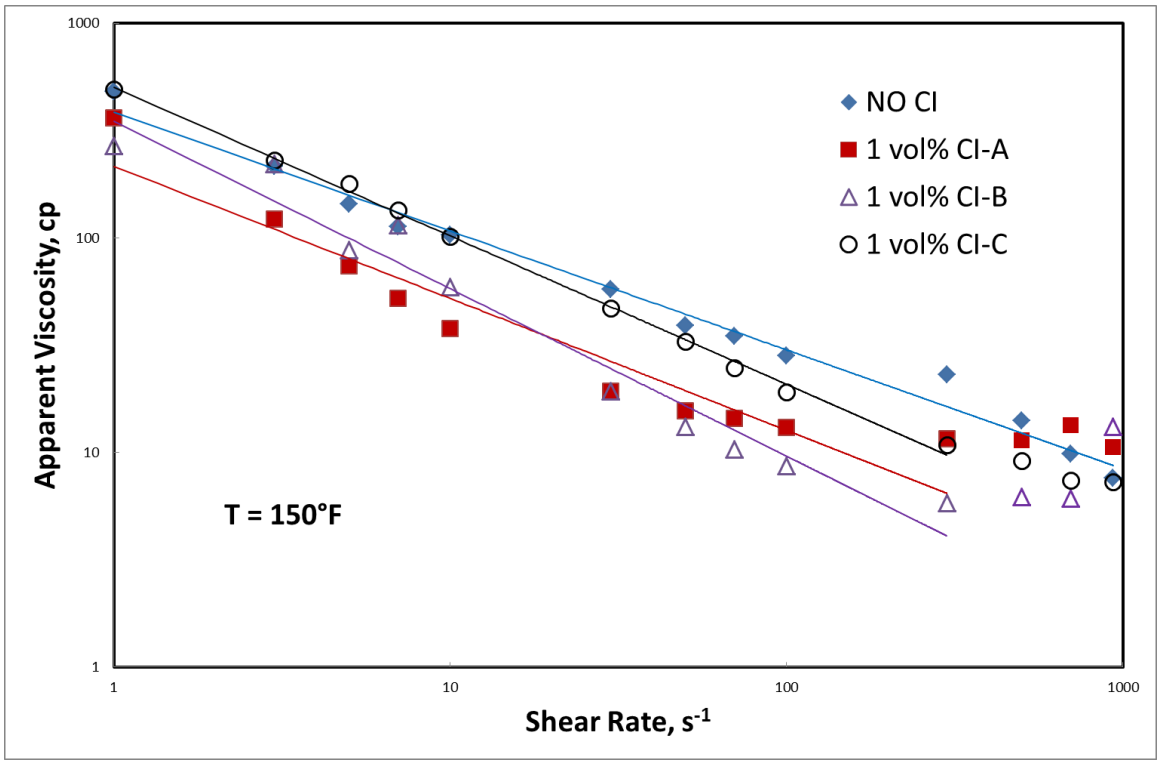


**Figure 5.4:** Effect of 1 vol% CI on the viscosity of 4 vol% VES-based fluid at 150 ℉.

At 250 ℉, at a CI concentration of 0.5 vol% (**Figure 5.5)**, CI-B and C reduced the viscosity of the spent VES-based acid with only CI-A maintaining a similar level to that with no CI. When the concentration of CI increased to 1 vol% (**Figure 5.6)**, none could maintain a similar level of viscosity as the one without CI. CI-B gave the highest viscosity among the three CI. At 250 ℉, because of the special characteristics of the VES molecules, the interaction between the calcium cations and the new VES formed the best wormlike micelles, and we achieved the highest spent acid fluid viscosity. However, the addition of corrosion inhibitors significantly affected the interaction, and only CI-A maintained a similar level of fluid viscosity because of its low composition of alcohol at

0.5 vol% of CI. When the CI concentration increased to 1 vol%, a higher concentration of components other than the alcohol in CI-B further stabilized the wormlike micelles and gave a higher viscosity than the other two. The solution based on CI-A and C could not maintain a similar level of fluid viscosity because of the adverse effect of the alcohol.

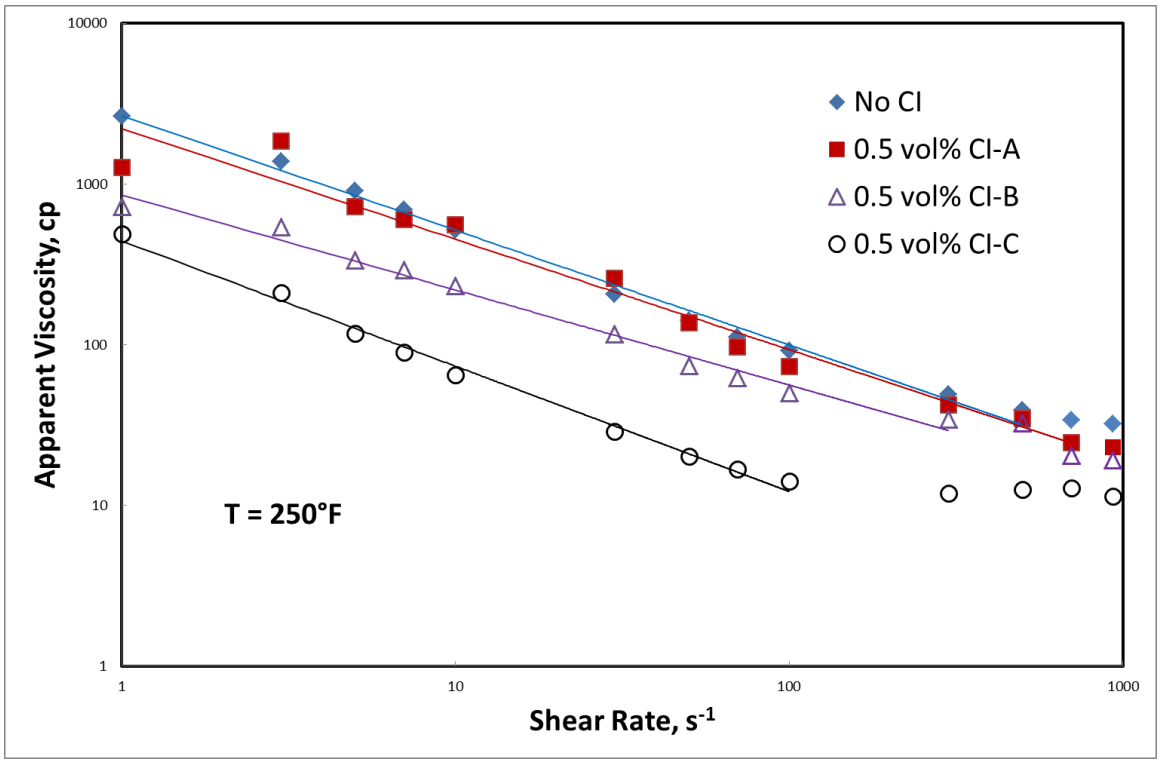


**Figure 5.5:** Effect of 0.5 vol% CI on the viscosity of 4 vol% VES-based fluid at 250 ℉.

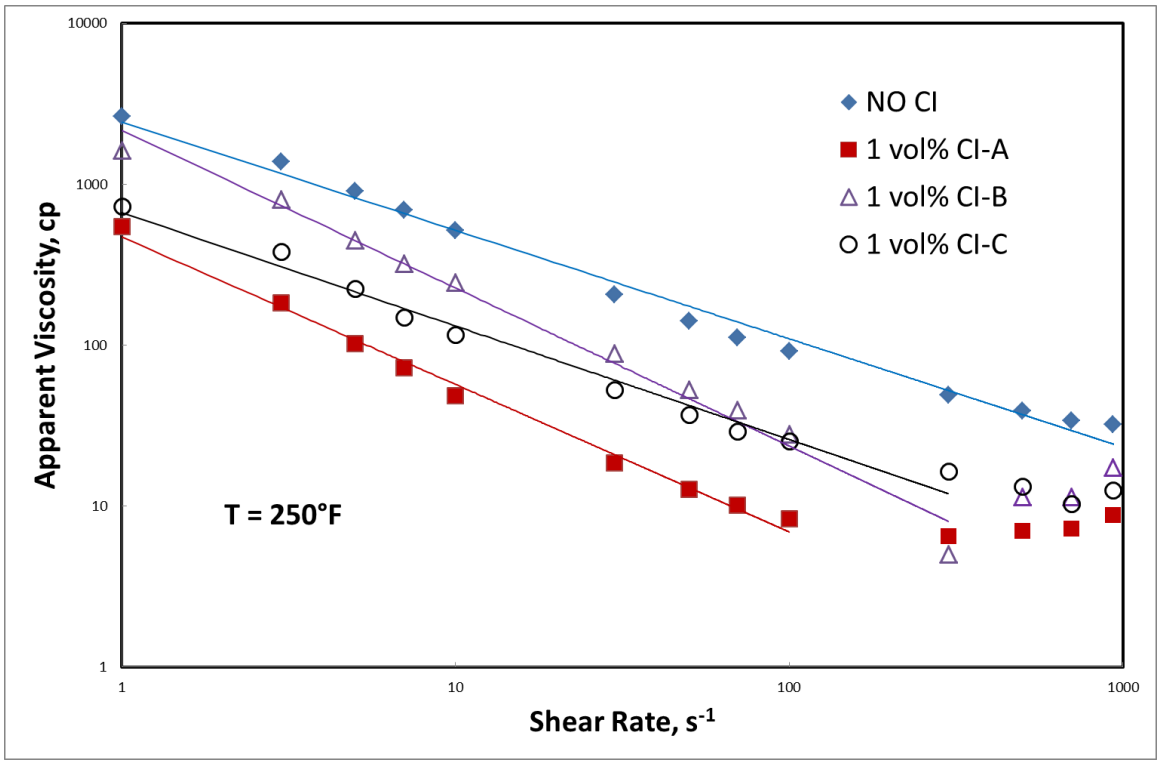


**Figure 5.6:** Effect of 1 vol% CI on the viscosity of 4 vol% VES-based fluid at 250 ℉.

When the temperature increased to 325 ℉, a significant decrease in viscosity was observed even without any CI **(Figs. 5.7 and 5.8)**. The components in the solution could not tolerate such a high temperature, and much fewer wormlike micelles were formed under these conditions. The addition of 0.5 and 1 vol% CI reduced the fluid viscosity, but the differences were not significant since the original viscosity without any CI was low. CI-A gave the highest viscosity among the three CI because it had the lowest alcohol concentration.

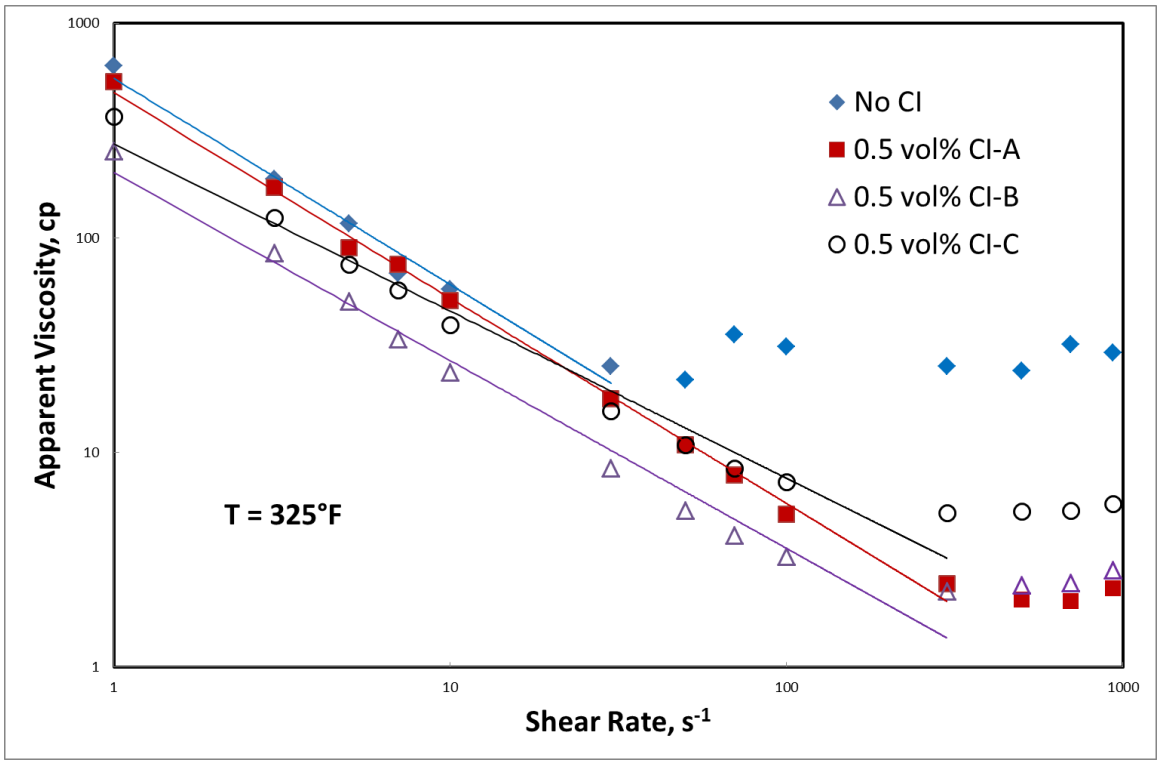


**Figure 5.7:** Effect of 0.5 vol% CI on the viscosity of 4 vol% VES-based fluid at 325 ℉.

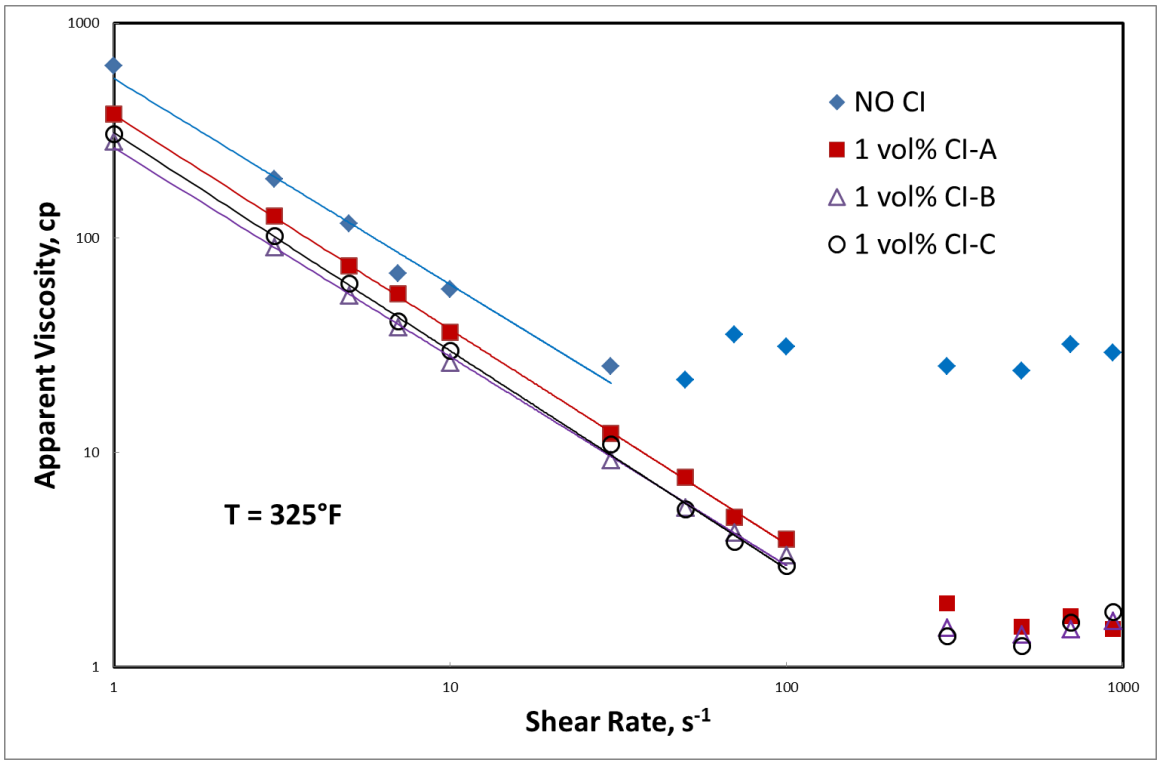


**Figure 5.8:** Effect of 1 vol% CI on the viscosity of 4 vol% VES-based fluid at 325 ℉.

Continuous heating also had a significant effect on the viscosity of the spent VES-based acid. Rather than testing at various shear rates, 10 $s^{-1}$ was chosen to be the representative shear rate, and the viscosity of the new VES-based fluid was measured from room temperature with an increment of 10 ℉. To have a better comparison with the current VES, 20 wt% $CaCl_2$ based spent VES-based acid was used (**Figs. 5.9 and 5.10)**. The special characteristics of the new VES was that rather than just one temperature peak, there were two viscosity peaks at two different temperatures during the continuous heating. The first peak was around 185 ℉, and the viscosity of the solution was nearly 1800 cp. After that, the viscosity of the spent VES-based acid dramatically decreased,

close to the original level at room temperature. Then, the fluid viscosity started to increase and reached the second peak around 275 ℉ with the viscosity of the fluid about 900 cp.

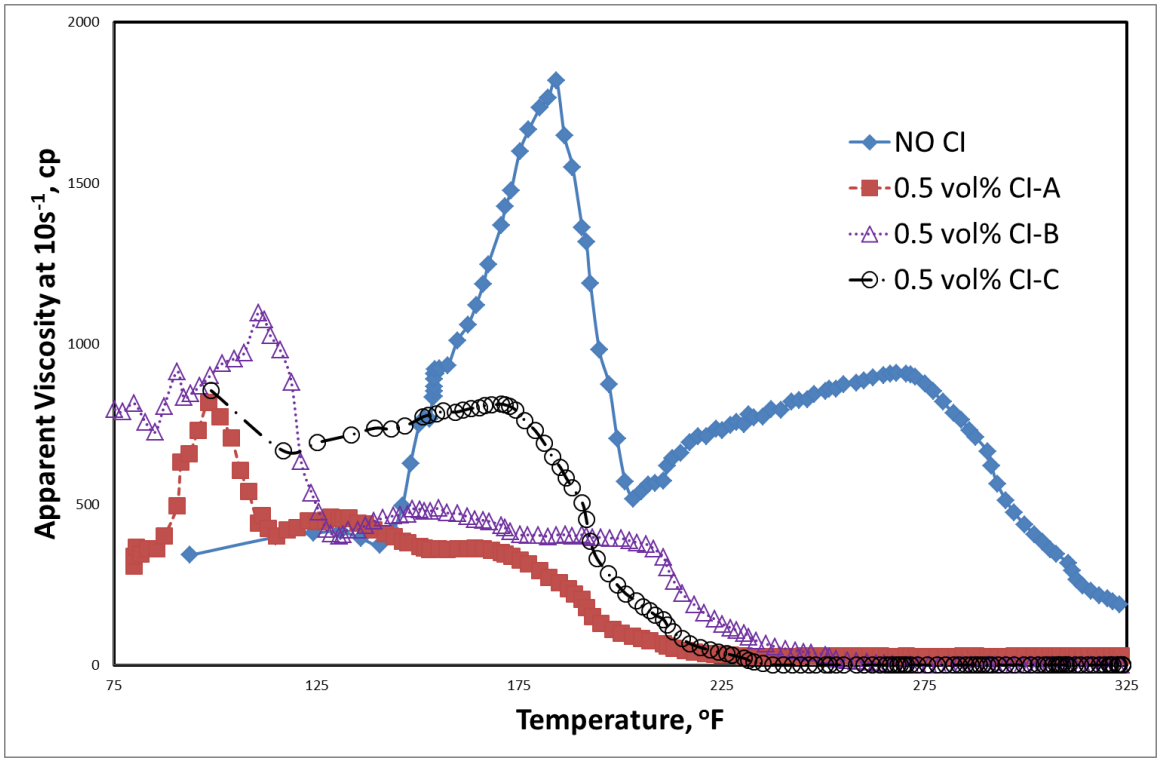


**Figure 5.9:** Effect of 0.5 vol% CI on the viscosity of 4 vol% VES-based fluid at 10 $s^{-1}$.

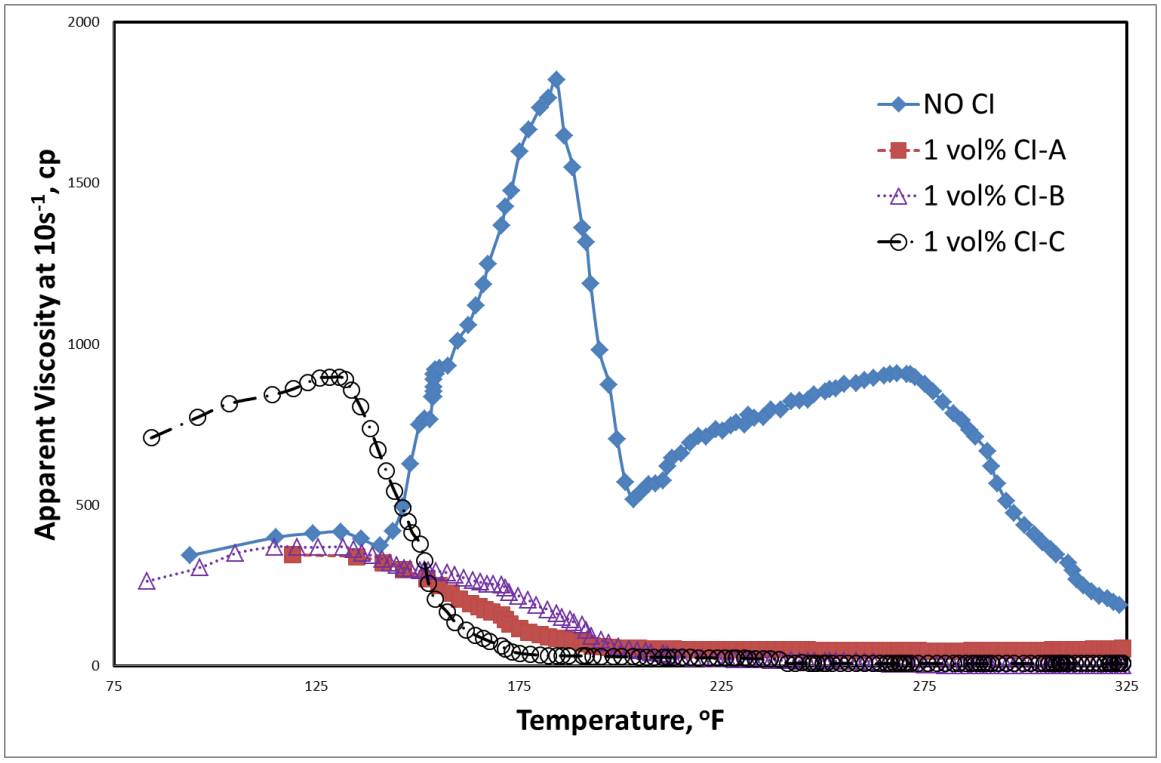


**Figure 5.10:** Effect of 1 vol% CI on the viscosity of 4 vol% VES-based fluid at 10 $s^{-1}$.

When 0.5 vol% CI were added (**Figure 5.9**), the viscosity of spent VES-based acids were reduced. Similar to the fluid without CI, two viscosity peaks were observed. However, the viscosity level and temperature were much lower. The first peaks were between 100 to 110 ℉ with the viscosity of the solution between 900 to 1000 cp. The second peaks of the three CI-based solutions were different from each other. The second peak of the CI-A based solution was around 130 ℉, and the viscosity of the fluid was around 450 cp. The second peak of CI-B based fluid was around 150 ℉, and the viscosity of the fluid was around 500 cp. The second peak of CI- C had a higher temperature and viscosity than the CI-A and B based fluid. The peak was around 175 ℉, and fluid

viscosity was nearly 800 cp. The addition of 0.5 vol% CI lowered the fluid viscosity and shifted the two peaks to lower temperatures. The addition of 1 vol% CI destroyed the new characteristics of the new VES-based fluid. Only one viscosity peak was observed around 130 ℉ for all three CI-based fluids. The viscosity of the CI-A and B based fluid was around 400 cp and the viscosity of the CI-C based fluid was much higher around 900 cp. All three solutions totally lost the fluid viscosity at nearly 200 ℉.

The conventional and the new VES were compared by temperature peak with the highest viscosity, as shown in **Figure 5.11**. The VES used by Li et al (2010) was based on amine oxide and the one used by Nasr-El-Din et al (2006b) was based on carboxybetaine. These two VES only had one viscosity peak at a relatively lower temperature. The new VES had two peaks. The first peak was around 175 ℉, and the fluid viscosity was at 1800 cp. The second peak was at a much higher temperature of 275 ℉ with a high fluid viscosity of 900 cp. There was a significant improvement between the new VES and the previous ones. A much higher viscosity was obtained at a much higher temperature, which indicated that the new VES would be very helpful in high temperature environments.

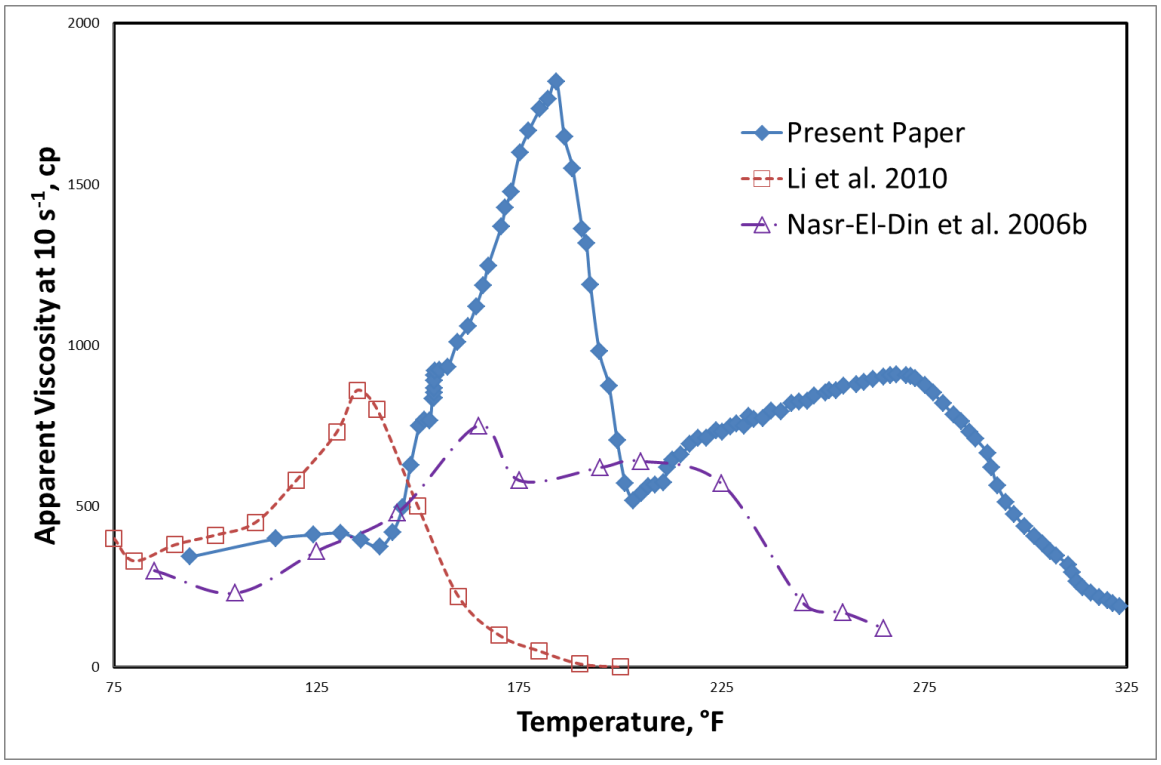


**Figure 5.11:** Viscosity of spent acids of the current VES and the new VES at 10 $s^{-1}$.

Residues of VES in the formation after acid treatment can cause unexpected formation damage, and to avoid this problem, a post-flush with mutual solvent (MS) is recommended and its effect on the new VES was evaluated. MS was believed to be able to break the wormlike micelles formed by VES, to remove the residues and provide clear wormholes. MS solutions of 5 and 10 vol% were tests together with the spent VES-based acid with a pH of 4.5.

At room temperature (**Figure 5.12)**, no significant change in viscosity was observed and both fluids exhibited a slightly higher viscosity than the one without MS. This is because the original fluid viscosity was not high; MS did not significantly reduce

the viscosity at both concentrations of MS. When the temperature was 150 ℉, both 5 and 10 vol% MS decreased the viscosity, but the difference was still within one order of magnitude (**Figure 5.13)**. MS interfered with the interaction between the calcium cations and the new VES, which caused the viscosity reduction.

When the temperature reached 250 ℉ (**Figure 5.14**), more viscosity reduction was observed in both fluids, and this time the difference was two orders of magnitude. This implied that the interaction between the MS and the new VES was more significant. Wormlike micelles were formed based on the mechanism of intolerance between oil and water. MS prohibited the formation of wormlike micelles.

When the temperature further increased to 325 ℉ (**Figure 5.15**), the VES-based fluids all had very low viscosities, and the difference between 5 and 10 vol% of MS was not significant. That is because even without any other additives, the viscosity of the original fluid was very low.

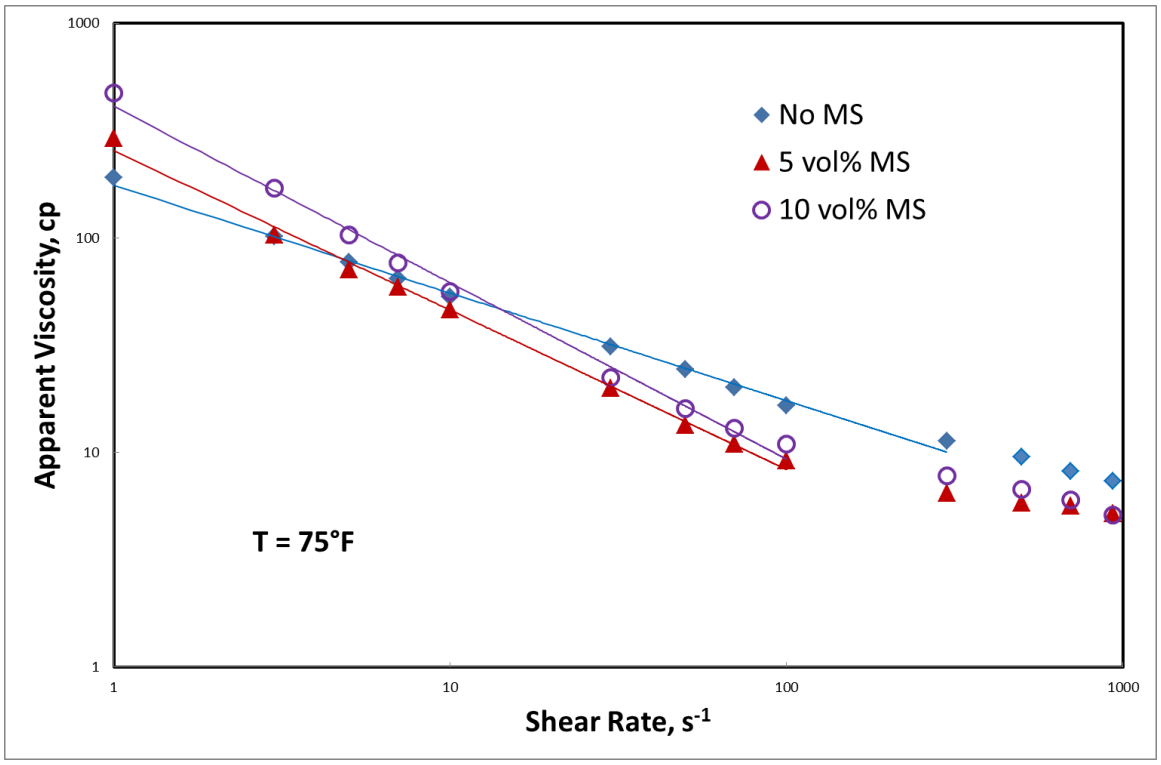


**Figure 5.12:** Effect of different concentrations of mutual solvent on the viscosity of 4 vol% VES-based fluid at 75 ℉.

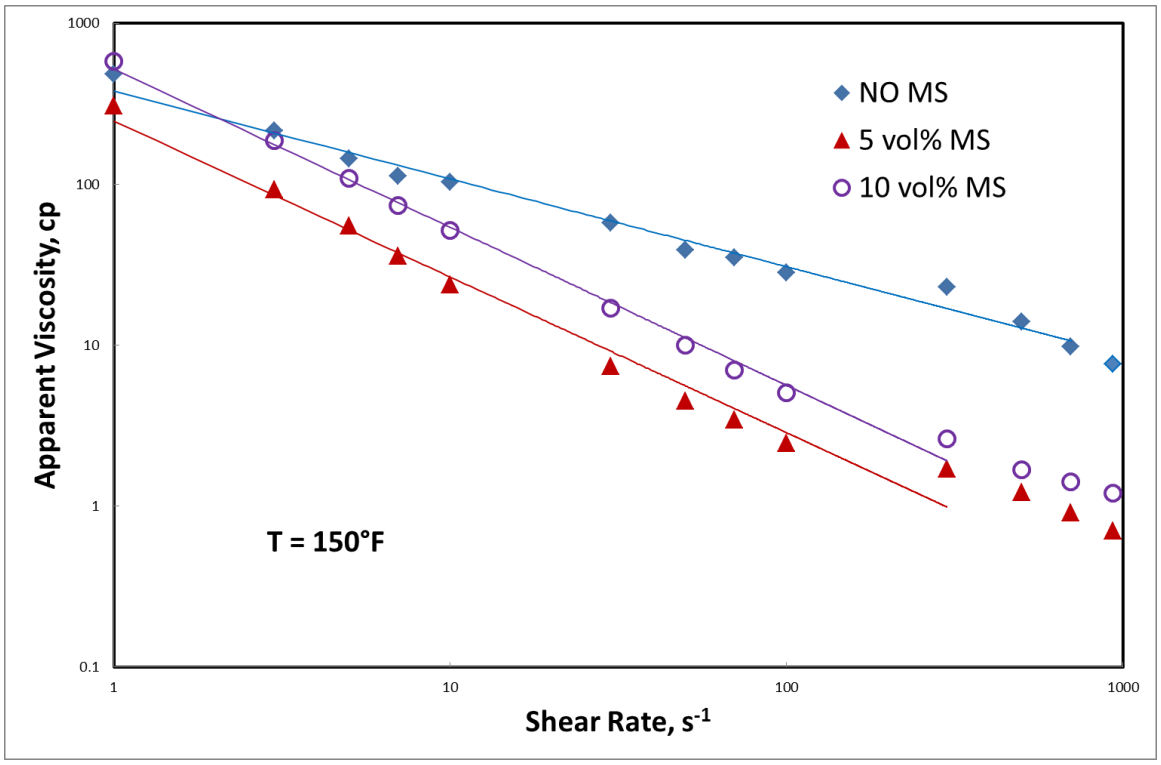


**Figure 5.13:** Effect of different concentrations of mutual solvent on the viscosity of 4 vol% VES-based fluid at 150 ℉.

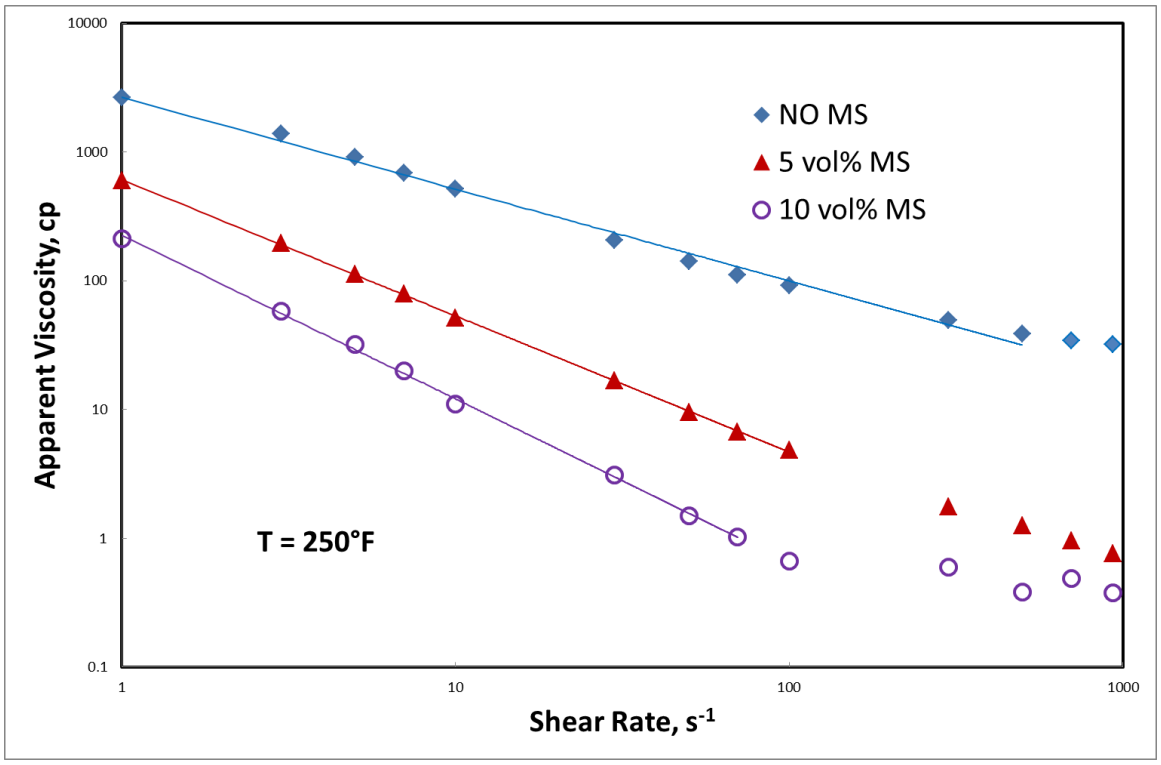


**Figure 5.14:** Effect of different concentrations of mutual solvent on the viscosity of 4 vol% VES-based fluid at 250 ℉.

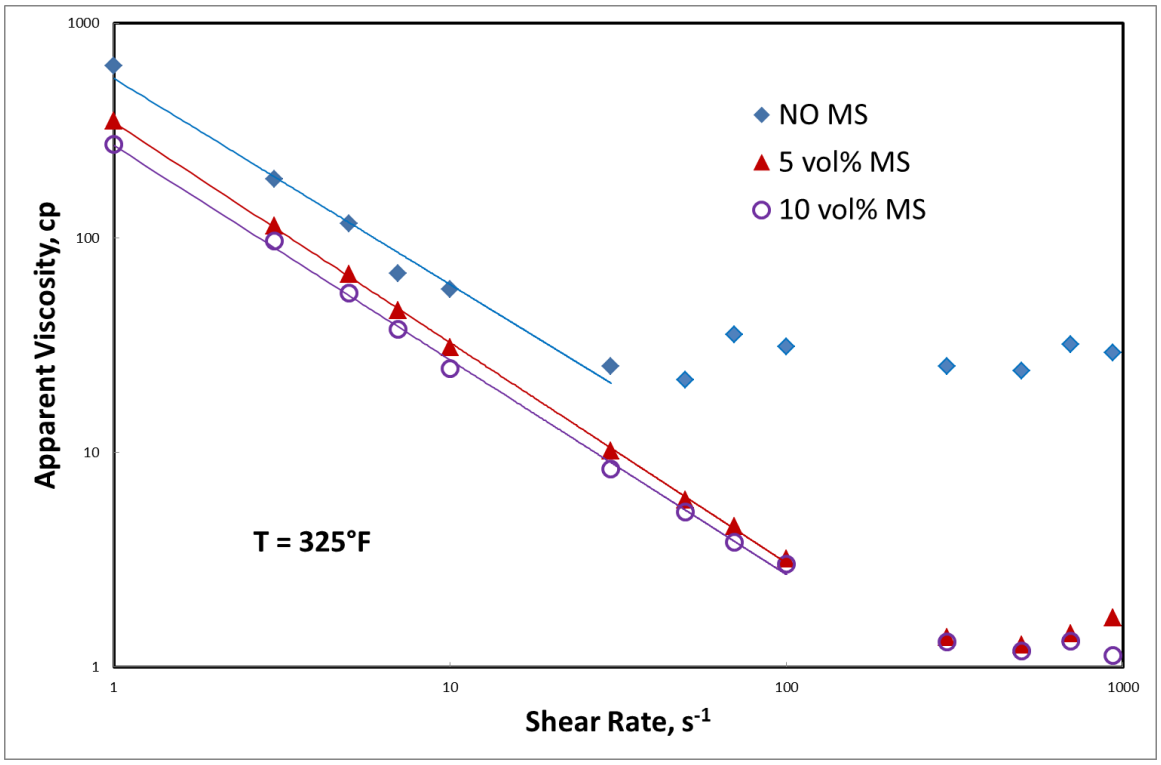


**Figure 5.15:** Effect of different concentrations of mutual solvent on the viscosity of 4 vol% VES-based fluid at 325 ℉.

### 5.5.2 Coreflood Studies

The single 20 in. coreflood was conducted at 325 ℉, a temperature at which the spent VES-based acid still can maintain high fluid viscosity. Indiana limestone with an initial permeability of 140 md was used. DI water was injected first, and when the pressure drop across the core stabilized at 325 ℉, the 4 vol% VES-based 20 wt% HCl was injected at 5 $cm^3$/min. CI-C was chosen because at 1 vol% the corresponding spent VES-based acid fluid had the highest viscosity. The injection fluid was changed back to DI water after breakthrough was achieved. The pressure drop across the core was

recorded, as shown in **Figure 5.16**. DI water was injected at the beginning, and when the pressure drop stabilized, the VES-based acid was injected. The pressure drop started to increase because the viscosity of the VES-based acid was higher than water. Then, when a wormhole was created, pressure drop started to decrease. With an increased concentration of calcium cations and pH value of the fluid, wormlike micelles started to form and significantly increase the fluid viscosity. An increase in the pressure drop was observed. Next, the acid created another wormhole and tried to pass through the entire core. Thus, we observed a decrease in pressure drop again. Similar processes were repeated until breakthrough was achieved. All fluids injected would flow through the dominant wormhole throughout the entire 20 in. long core. After taking the core out of the core holder, photos of both the inlet and outlet faces were taken (**Figure 5.17**). Multiple wormholes were noted at the inlet face of the core. However, only one dominant wormhole was observed on the outlet face of the core. The core was CAT scanned after treatment to observe the propagation of the wormhole (**Figure 5.18**). Multiple wormholes were created near the inlet, and one dominant wormhole was observed throughout the whole core. There were not only multiple wormholes, but also observed was that the dominant wormhole kept changing its direction through the core. The diameter of the wormhole decreased from the inlet to the outlet of the core.

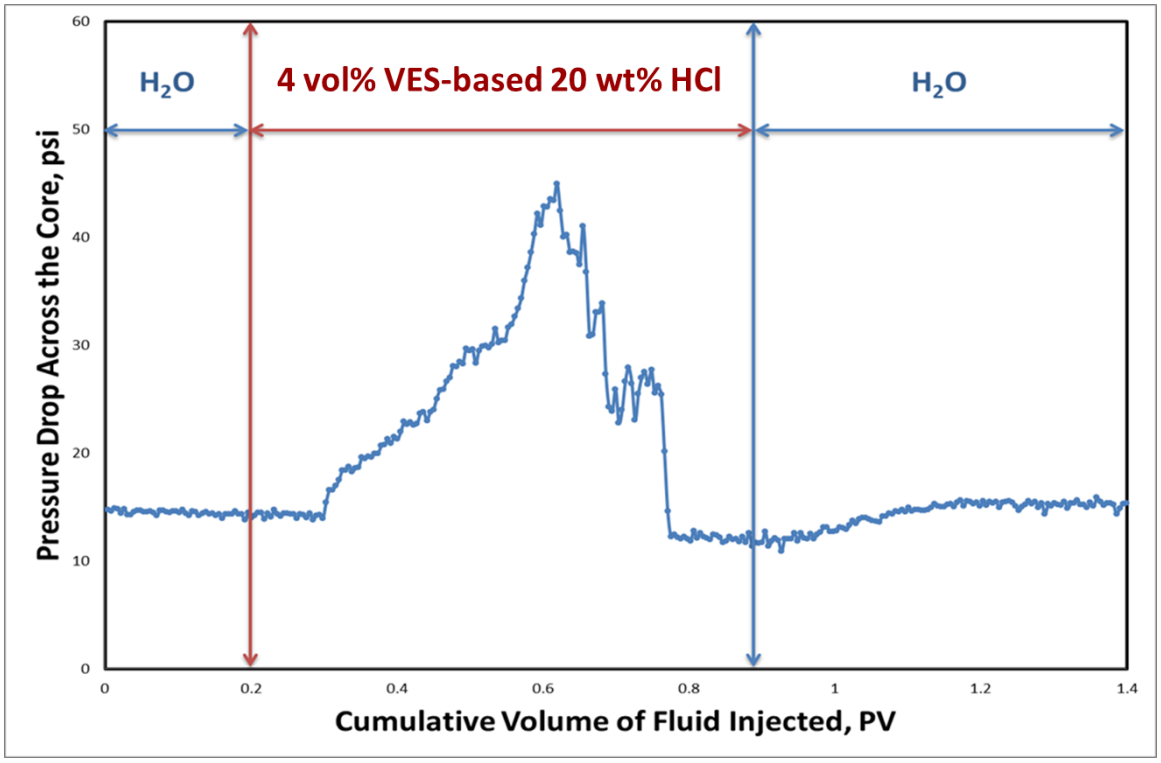


**Figure 5.16**: Pressure drop across the core during injection of 4 vol% VES-based 20 wt% HCl during single coreflood test.


**Figure 5.17**: Inlet (left) and outlet (right) faces of the 20 in. Indiana limestone core after testing with 4 vol% VES-based 20 wt% HCl.

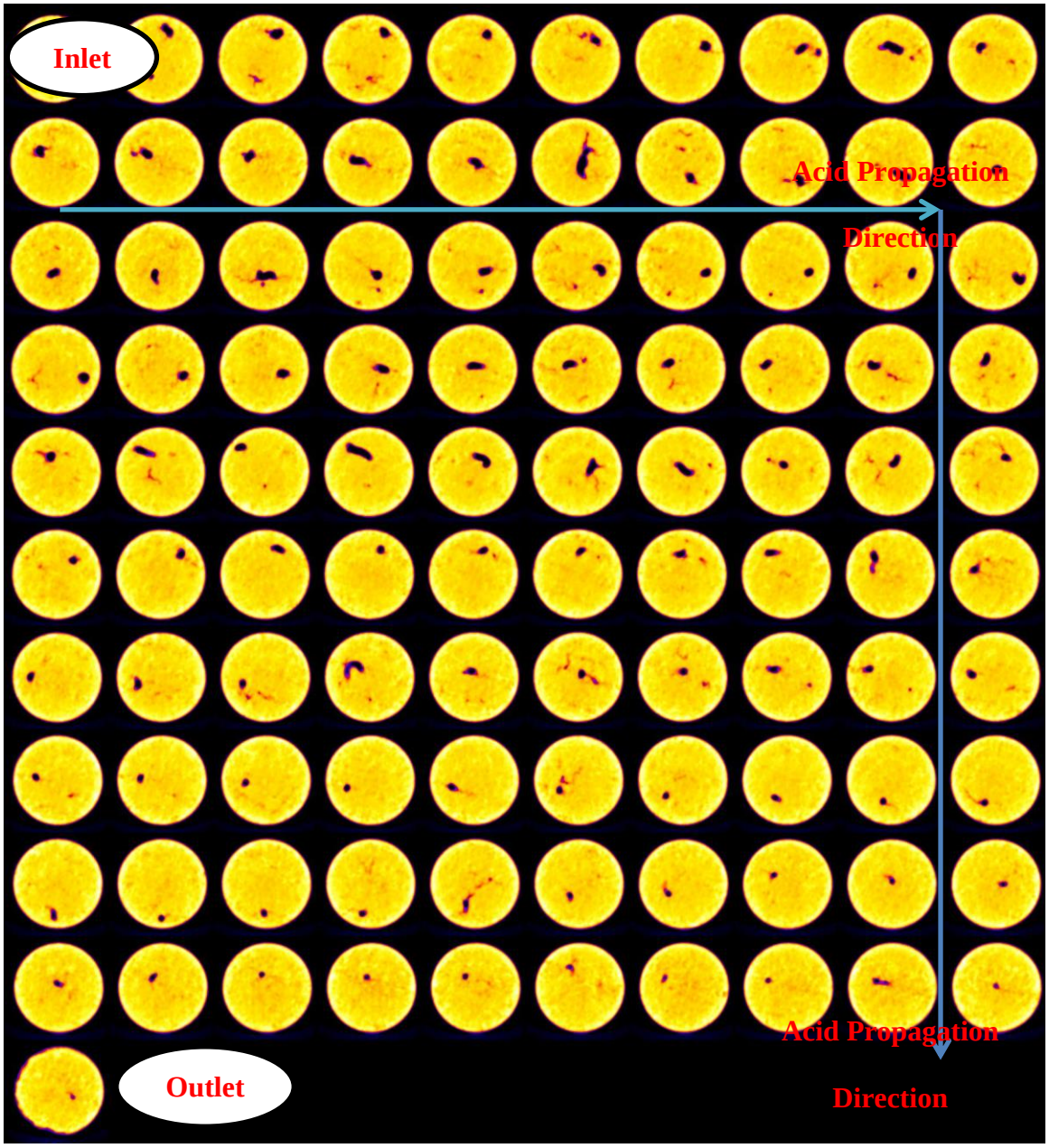


**Figure 5.18**: CAT scan images of the 20-inch Indiana limestone core after treatment with 4 vol% VES-based 20 wt% HCl in the single coreflood test.

For the first set of the parallel coreflood test conducted at 250 ℉, the initial permeability ratio of the two cores was 77. After the whole system reached equilibrium under water injection, 4 vol% VES-based 20 wt% HCl was injected at 2 $cm^3$/min until breakthrough. The DI water was injected to flush the two cores until the pressure drop across the core stabilized. During the acid injection, the pressure drop across the core increased due to the higher viscosity of the HCl solution. Then, the pressure drop quickly dropped which indicated that a wormhole was created throughout the core (**Figure 5.19**).

No acid diversion was observed. This was also confirmed according to the CAT scan after treatment (**Figure 5.20-21)**. There was a dominant wormhole inside the higher permeability core. The direction of the coreflood kept changing throughout the core. However, only the inlet face of the lower permeability core was slightly etched by the VES-based acid, which left the entire core almost untreated.

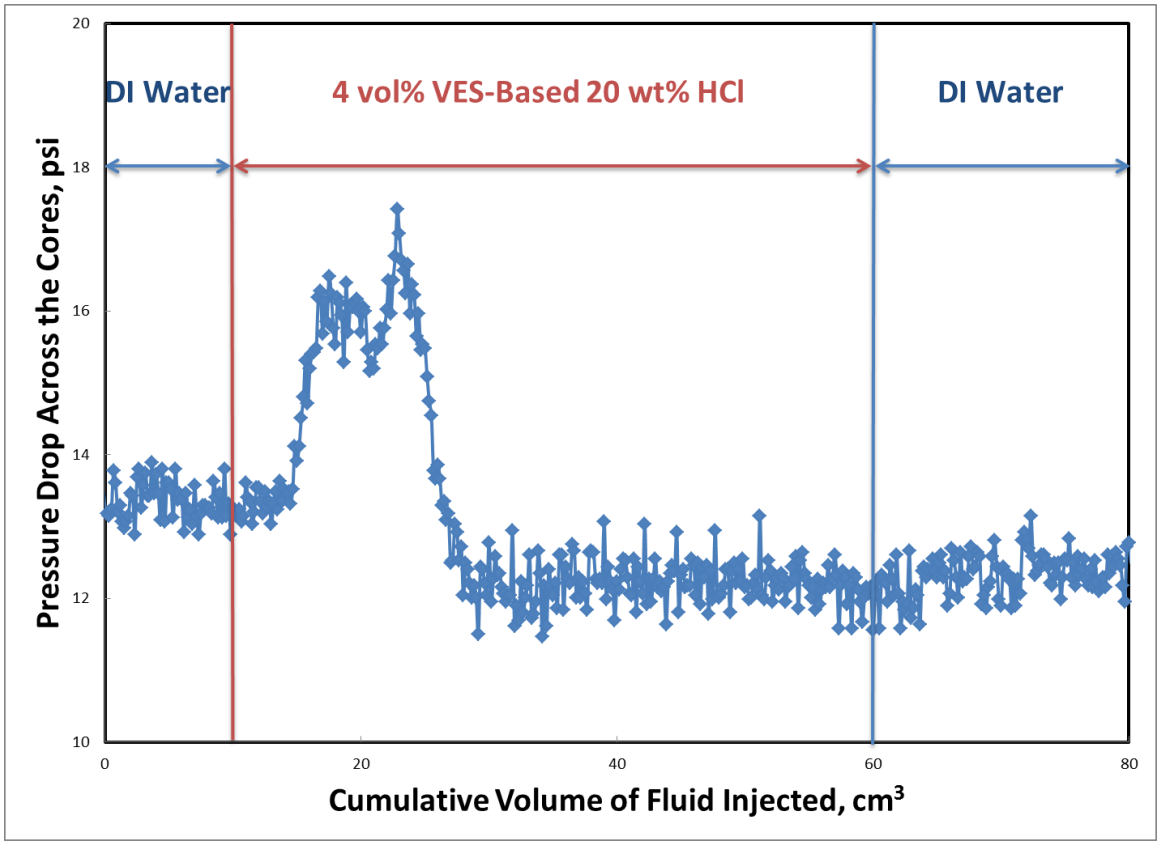


**Figure 5.19**: Pressure drop across the core during injection of 4 vol% VES-based 20 wt% HCl during the first set of parallel coreflood tests.

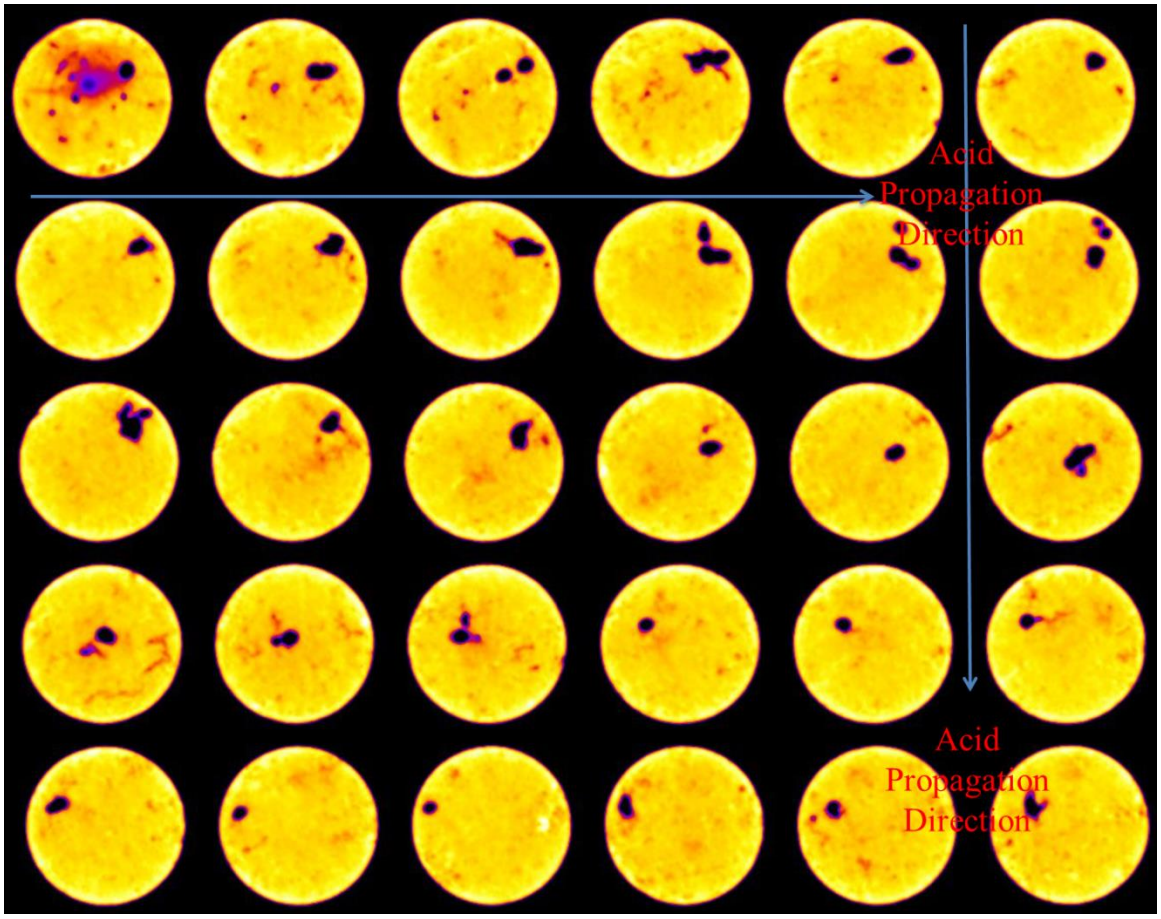


**Figure 5.20**: CAT scan images of the 6-inch Indiana limestone core ($k_{initial}$ = 128 md) after treatment with 4 vol% VES-based 20 wt% HCl in the first set of parallel coreflood tests.

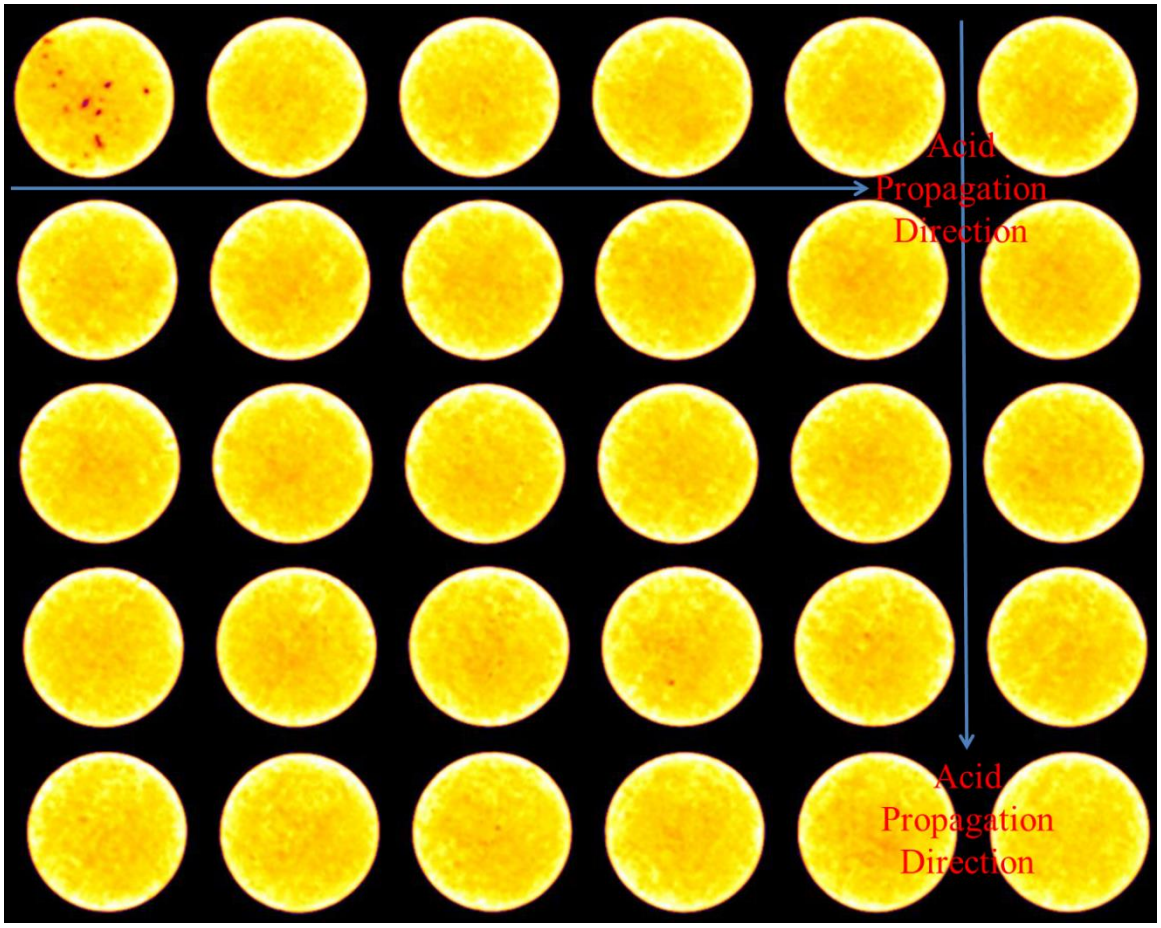


**Figure 5.21**: CAT scan images of the 6-inch Indiana limestone core ($k_{initial}$ = 1.66 md) after treatment with 4 vol% VES-based 20 wt% HCl in the first set of parallel coreflood tests.

For the second set of the parallel coreflood tests conducted at 325 ℉, with the initial permeability ratio around 2.8. DI water was injected until the whole system reached equilibrium. The same live acid was injected at 1 cc/min. During acid injection, the pressure drop across the core increased, first, due to the higher viscosity of acid (**Figure 5.22**). Then, a short wormhole was created and the pressure drop decreased.

With the neutralization of the acid solution and increase of the calcium cations, wormlike micelles were formed and the wormhole was prevented from further propagation. Thus, the VES-based acid was diverted to the relatively lower permeability core and the wormhole was created. The pressure drop across the core decreased again. A similar process occurred in the lower permeability core and the acid was diverted back to the higher permeability core. The whole process was repeated simultaneously with the increase and decrease of the pressure drop. Diversion of the acid was also supported by the CAT scan images (**Figure 5.23-24**). A dominant wormhole was created in the higher permeability core, with a constant change in propagation direction. Although the diameter of the wormhole was much smaller, the acid was still able to penetrate deeply with only less than 1 in. from the outlet untreated, which indicated that an even treatment was almost achieved. Another uncommon phenomenon was observed when DI water was injected after the acid treatment (**Figure 5.25**). DI water significantly increased the environmental pH inside the core and caused precipitation of the new VES. The precipitates temporarily plugged the wormhole and diverted DI water to the lower permeability core, in which there was much less VES gel residue. A significant amount of water was collected from the effluent of the lower permeability core.

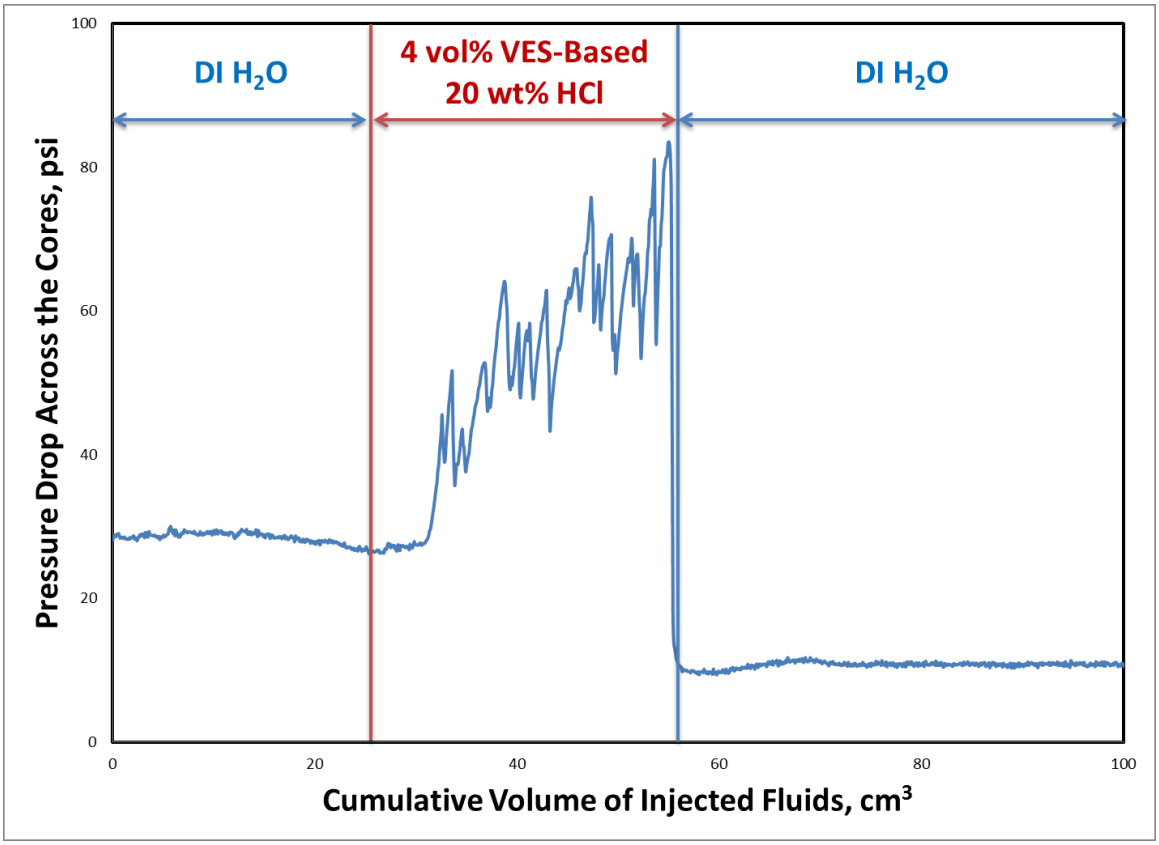


**Figure 5.22**: Pressure drop across the core during injection of 4 vol% VES-based 20 wt% HCl during the second set of parallel coreflood tests.

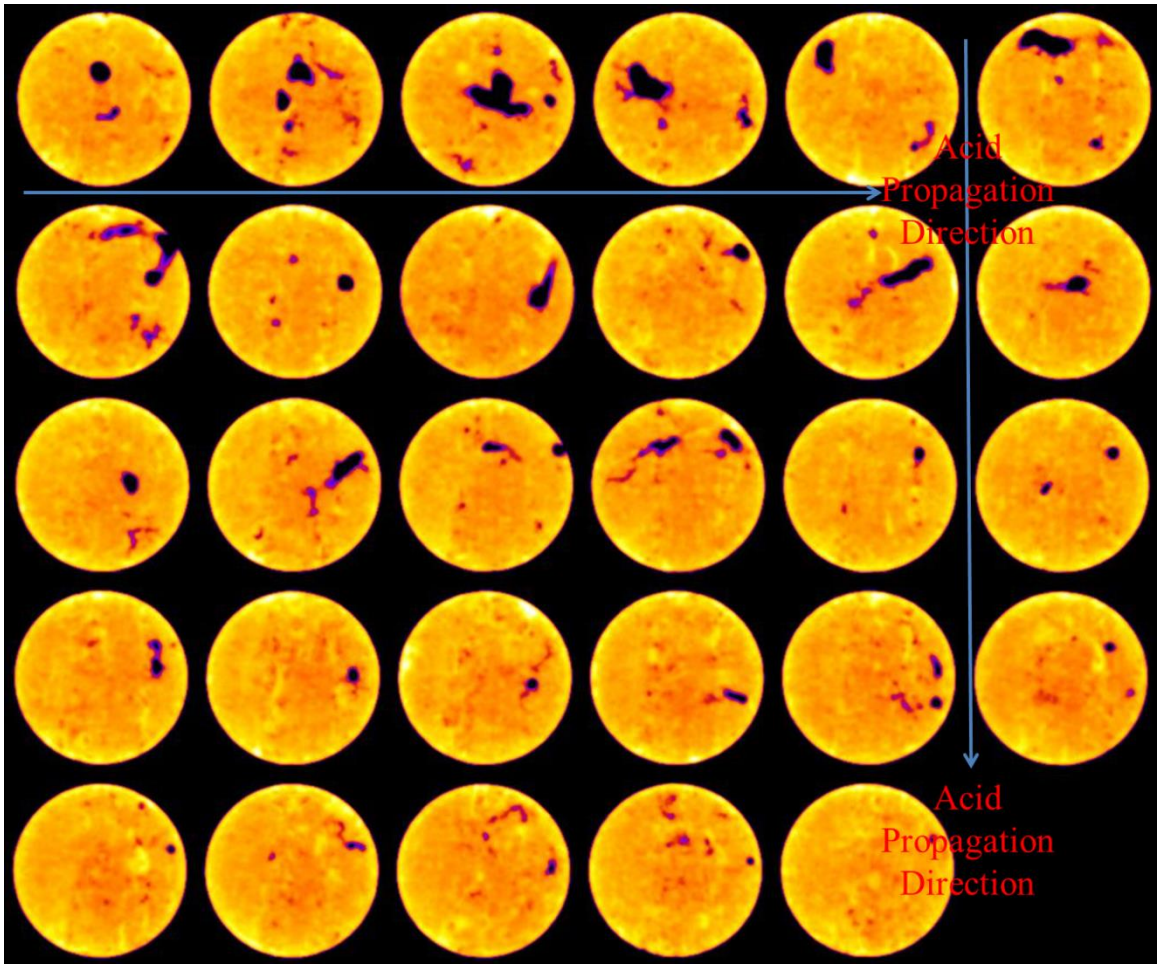


**Figure 5.23**: CAT scan images of the 6-inch Indiana limestone core ($k_{initial}$ = 7 md) after treatment with 4 vol% VES-based 20 wt% HCl in the second set of parallel coreflood tests.

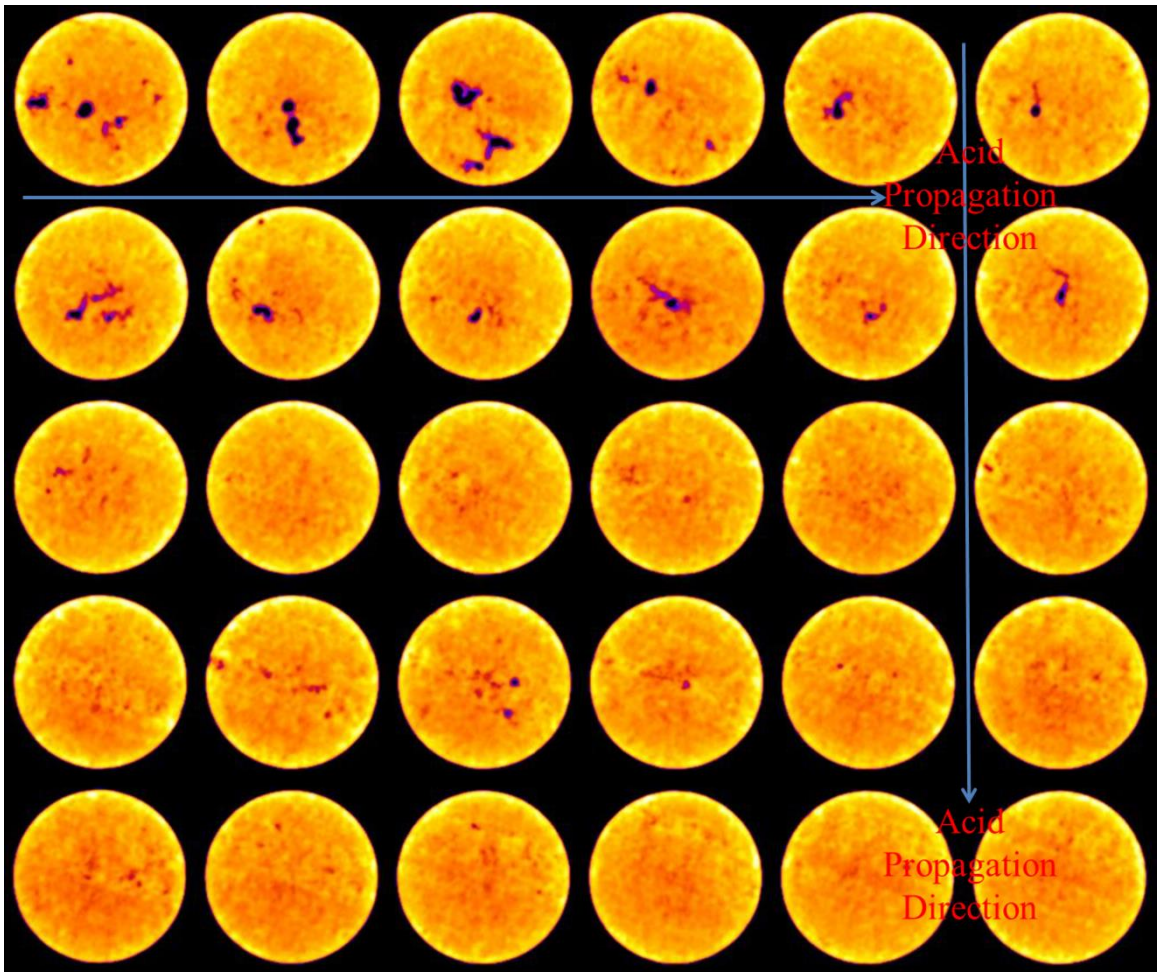


**Figure 5.24**: CAT scan images of the 6-inch Indiana limestone core ($k_{initial}$ = 2.5 md) after treatment with 4 vol% VES-based 20 wt% HCl in the second set of parallel coreflood tests.

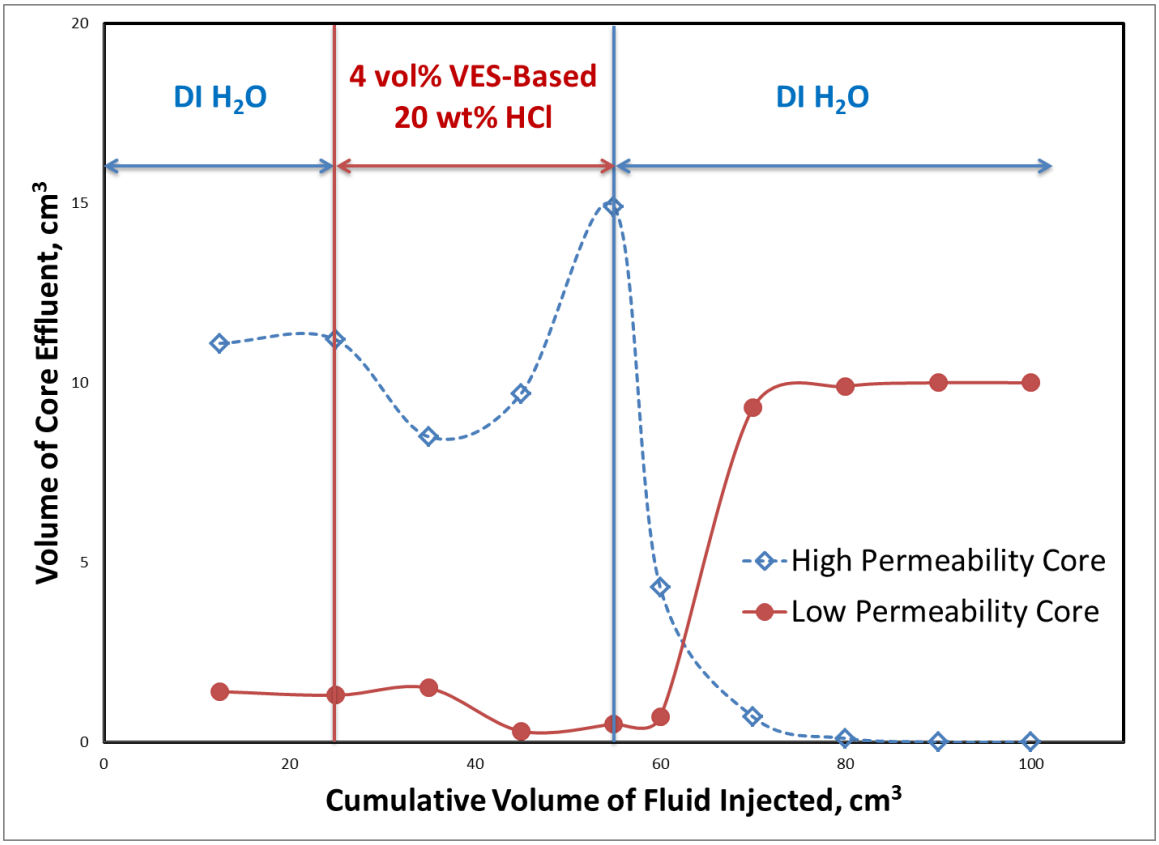


**Figure 5.25**: Volume of core effluent collected during the second set of parallel coreflood tests.

## 5.6 Conclusions

A new VES-based system was developed to extend the range of applicable temperatures. Viscosity measurements were conducted at temperatures up to 325 ℉. Three commercial corrosion inhibitors were tested at different concentrations. Coreflood studies were conducted to evaluate the performance of the new VES-based acid at reservoir conditions, observe the propagation of wormholes in carbonate core, and

achieve acid diverting in parallel cores with different initial permeabilities. Based on the results obtained, the following conclusions can be drawn:

1. The new VES-based fluid exhibited a higher viscosity at elevated temperatures than conventional VES. The peak of the old VES-1, a carboxybetaine, was at 135 ℉ with the fluid viscosity of 860 cp. The peak of the old VES-2, an amine oxide, was at 165 ℉ with the fluid viscosity of 750 cp. The new VES had two peaks. One was at 185 ℉ with a viscosity of 1800 cp, and the second one was at 270 ℉ with the apparent viscosity of the fluid at 900 cp.
2. The addition of corrosion inhibitors lowered the viscosity of the VES-based fluids. At 250 ℉, when the concentration of corrosion inhibitor was 0.5 vol%, corrosion inhibitor A had the lowest effect on the new VES viscosity; when the concentration was 1 vol%, corrosion inhibitor C had the lowest effect.
3. Mutual solvent significantly reduced the viscosity of new VES-based fluid at various temperatures with different concentrations. A post-flush with mutual solvent is recommended to break the VES gel in the formation after acid treatments.
4. The VES-based acid changed its propagation direction during the single coreflood test, and multiple wormholes were created at the inlet face of the core at 325 ℉. In parallel coreflood tests, when the contrast between the initial permeability of the two cores was too large, no diversion occurred. When the contrast was within reasonable range and the acid was injected at a moderate flow rate, acid diversion was achieved.

# 6. VISCOSIFIED GLDA WITH VES AND POLYMER

## 6.1 Background

GLDA has been very well studied and proven to be effective in matrix acidizing. However, when GLDA was pumped into formations with heterogeneous permeabilities, the treatment of the lower permeability region could not meet the expectation. Thus, viscosifying agents could be introduced to GLDA as they are used in HCl. The treatment fluid viscosity could be increased during acidizing and the preference to higher permeability zones will be reduced. Thus, homogeneous distribution of the treatment fluid could be achieved.

## 6.2 Materials and Equipment

GLDA was the same one used in session 4. In total, three VES and two polymers were evaluated. One VES is the amine oxide evaluated in session 2 and 3. One VES is the new VES aiming for high temperature application used in session 5. The other VES used is a carboxybetaine VES as mentioned in the introduction session. The polymers are xanthan gum and guar gum. KOH and $H_4$EDTA solids were also used in this study. Viscosity measurements were the key evaluation and the HP/HT rheometer was used.

## 6.3 Fluid Preparation and Experimental Procedure

The final solution had a concentration of 20 wt% of GLDA. Thus, to prepare a 100 g of the treatment fluid, 50 g of GLDA was stored first in a beaker. Then, a mixer

was placed on top of the beaker with the mixing speed at 400 rpm to prevent bubble generation. Then, corresponding amounts of other chemicals were added into the solution. In the end, DI water was added to set the overall weight of the fluid to 100 g. The viscosity measurements were conducted with the HP/HT rheometer. A shear rate of 100 $s^{-1}$ was used to mix the fluid before it reached the target temperature. Once the fluid was heated to the designed temperature, the viscosity measurements were conducted from 0.1 to 1,000 $s^{-1}$. A fresh sample was used in each test.

## 6.4 Results and Discussion

At the very beginning, since GLDA was designed to replace HCl for high temperature applications, the HT VES was investigated first. However, the poor solubility of the VES at low salinity or acidity environment caused the precipitation of the VES (**Figure 6.1**). Flakes formed by the HT VES were observed, and the fluid was not qualified for acidizing treatment since it was not homogeneous. Thus, the other two VES and the two polymers were the main viscosifying agents that were well studied.

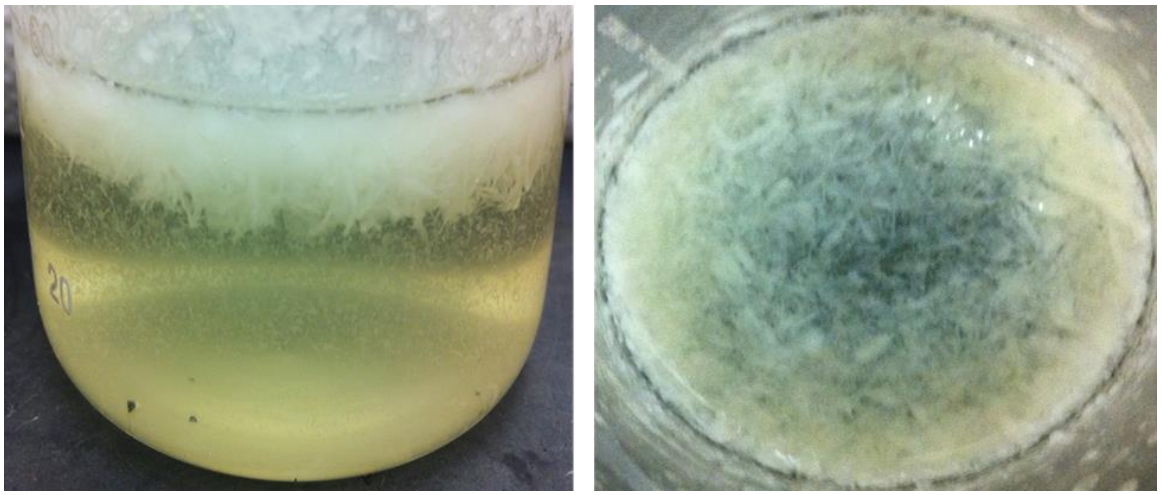

**Figure 6.1**: Flakes and phase separation when preparing HT VES-based GLDA.

When no additives were added, the GLDA solution itself was a non-Newtonian fluid showing shear thinning properties (**Figure 6.2**). When the amine oxide VES (referred as VES-A) was used, the addition of the VES significantly increased the fluid viscosity. On the other hand, the addition of GLDA in the VES-based solution also increased the fluid viscosity (**Figure 6.3**). Generally, additional VES further viscosifies the fluid. However, in the GLDA additional VES adversely reduced the fluid viscosity. A similar behavior was noticed when the carboxybetaine VES (VES-B) was used. VES-B did viscosify the GLDA solutions. Additional VES-B adversely lowered the fluid viscosity (**Figure 6.4**).

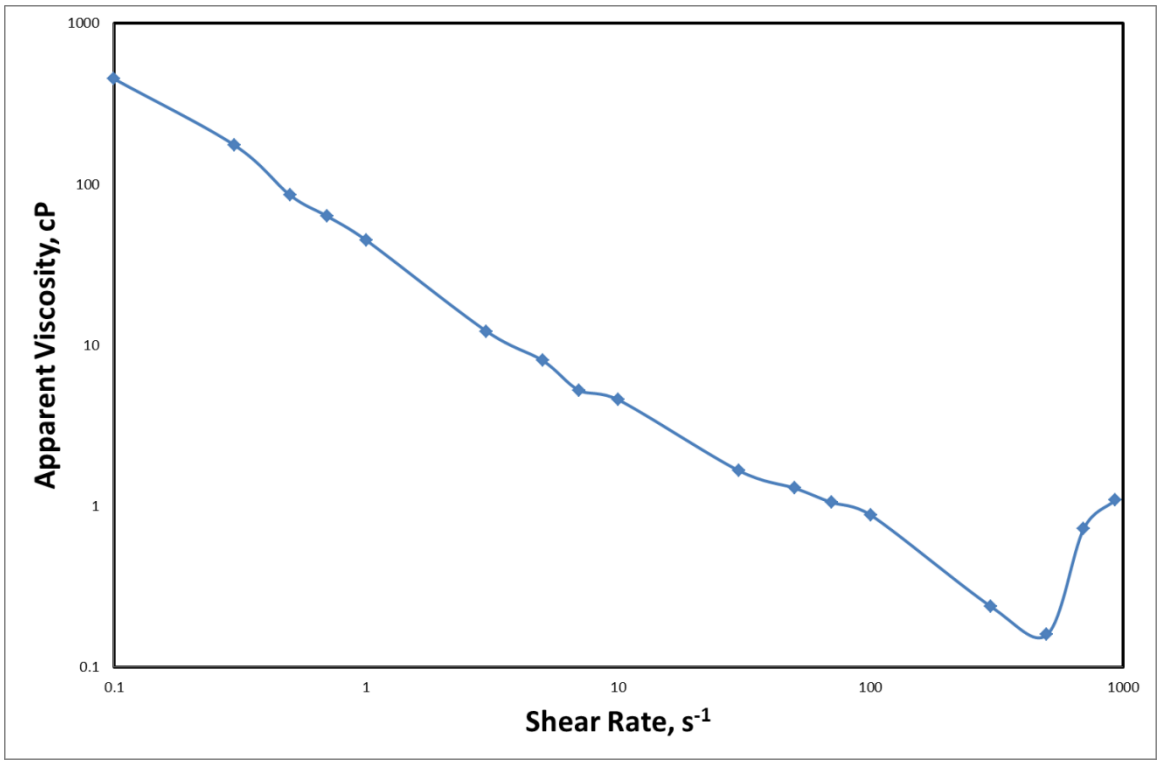


**Figure 6.2**: Viscosity of 20 wt% GLDA at various shear rates at 200 ℉.

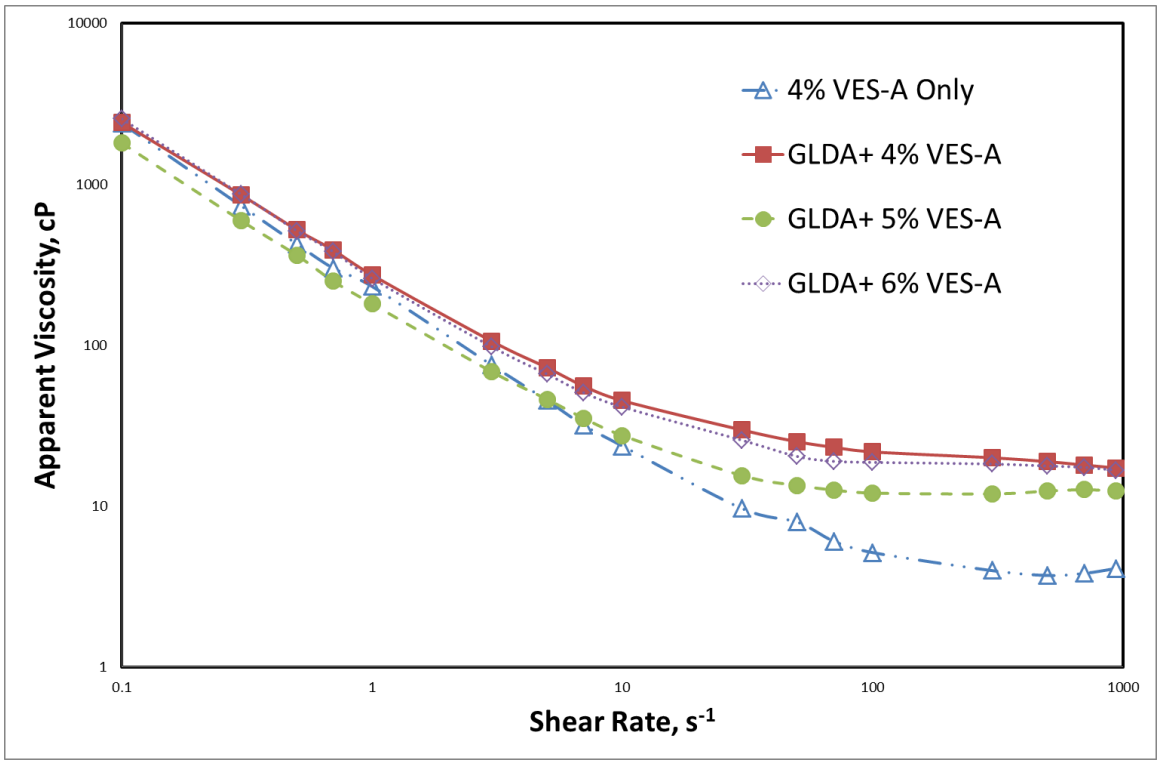


**Figure 6.3**: Viscosity of GLDA solutions at various VES-A concentrations at 200 ℉.

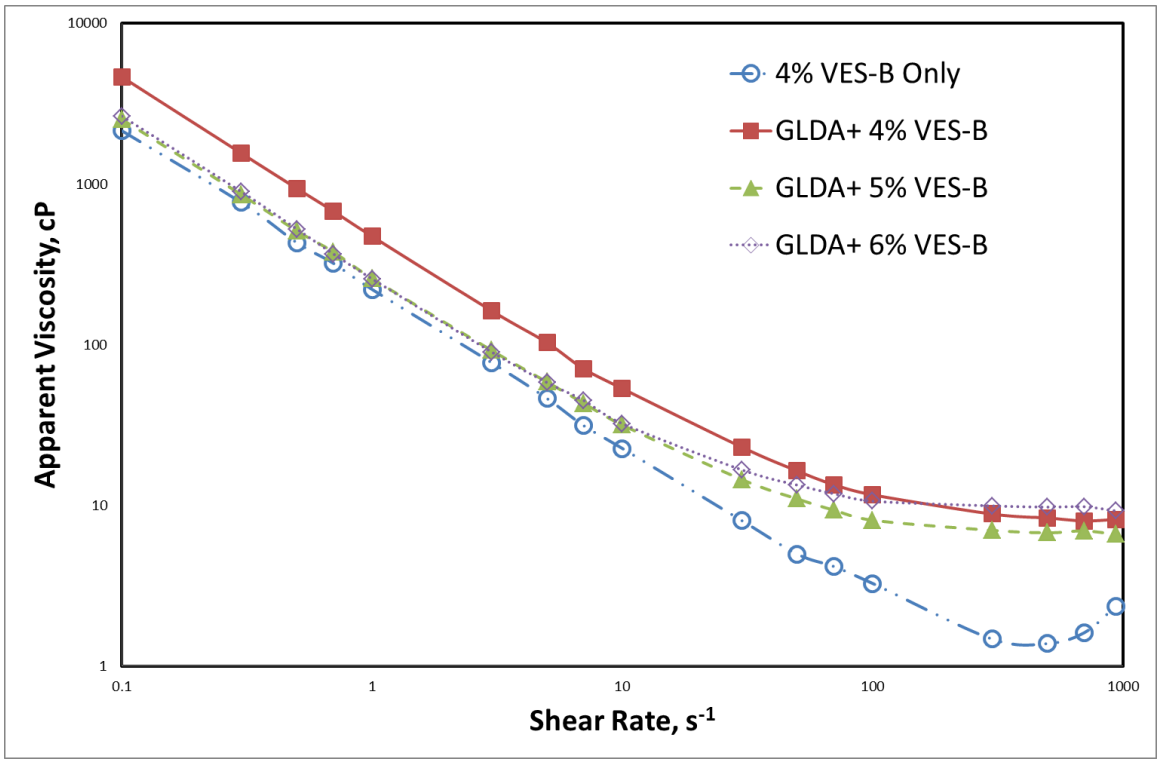


**Figure 6.4**: Viscosity of GLDA solutions at various VES-B concentrations at 200 ℉.

Similarly, xanthan gum and guar gum were used at a concentration of 0.2 wt% to viscosify the GLDA solutions. The effect of temperature on the fluid viscosity was investigated (**Figure 6.5**). The addition of GLDA into xanthan gum reduced the polymer-based fluid. Heating the viscosified GLDA solution could help to increase the fluid viscosity when the fluid temperature rose from 75 to 200 ℉. However, if the fluid was over heated to 300 ℉, the fluid viscosity started to decrease. This could be explained as the initial heating process to 200 ℉ enhances the solubility of the polymers, and the viscosity increases with better polymer interaction. However, overheating caused polymer degradation and the fluid viscosity was reduced. Similarly, when guar gum was

used, the GLDA reduced the fluid viscosity of 0.2 wt% guar solution. Overheating of the guar based GLDA solutions can reduce the fluid viscosity (**Figure 6.6**).

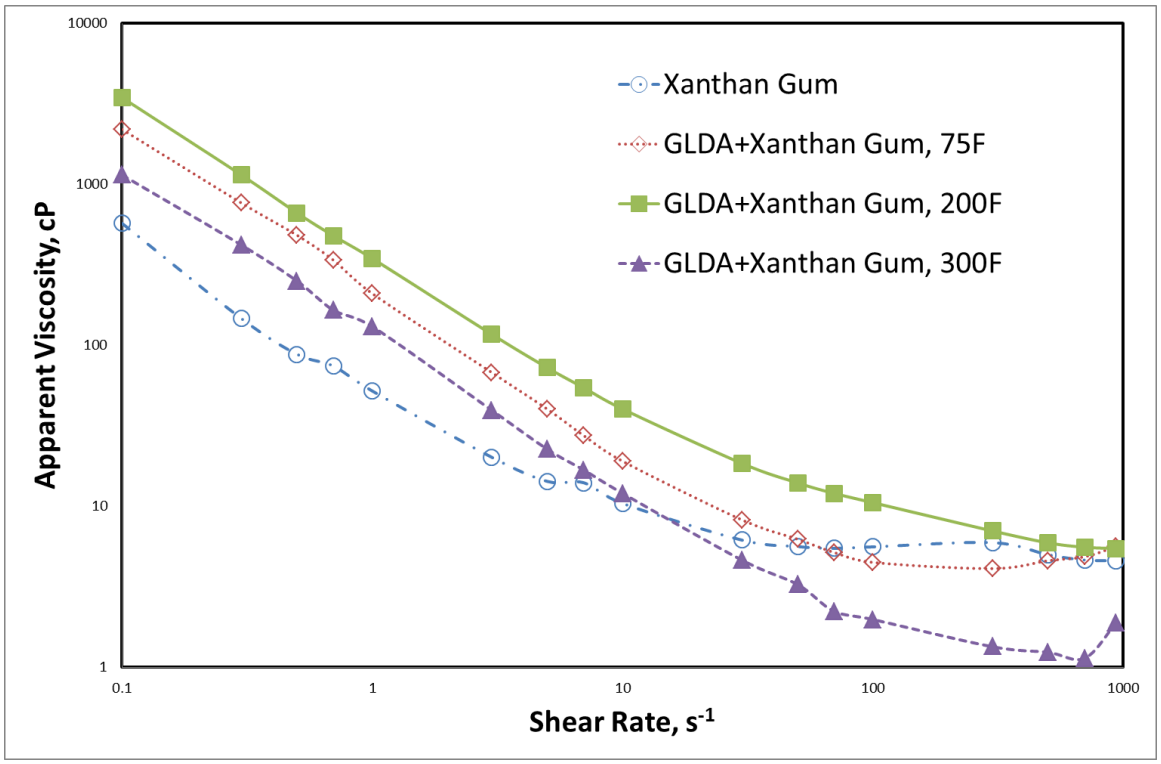


**Figure 6.5**: Viscosity of 0.2 wt% xanthan gum-based GLDA solutions at various temperatures.

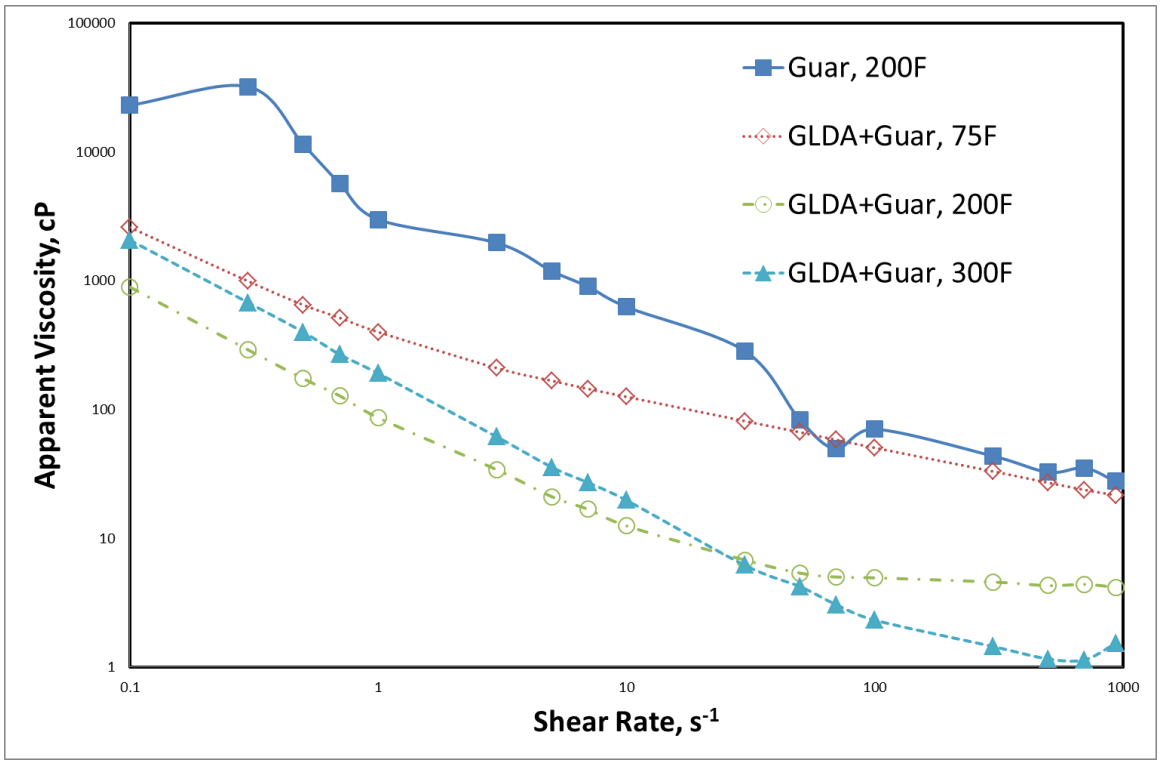


**Figure 6.6**: Viscosity of 0.2 wt% guar-based GLDA solutions at various temperatures.

EDTA was also a widely used chelating agent in the oil and gas industry and it was the first one introduced to substitute HCl to stimulate carbonate formations. Thus, EDTA based gelled stimulation fluids were prepared with the same method as the GLDA solutions. Unfortunately, EDTA was not soluble enough to have all solids dissolved in an acidic environment. However, the solubility of EDTA can be significantly increased at high temperatures. Thus, all tests were conducted at 200 ℉. Without interfering with the fluid pH, the EDTA solutions had higher viscosity than that of the GLDA solutions (**Figure 6.7-6.10**). This was because excess amounts of EDTA together with other additives formed an over saturated solution during the tests. Thus,

the interactions between various molecules were enhanced. Meanwhile, when the fluid pH was adjusted to around 5.0, the GLDA based solution had a higher viscosity than that of the EDTA-based fluid (**Figure 6.10**). The dissociated EDTA can no longer affect the interaction between the viscosifying agent and the GLDA-based solution had a higher viscosity since it is much more soluble than EDTA without adjustments of the pH.

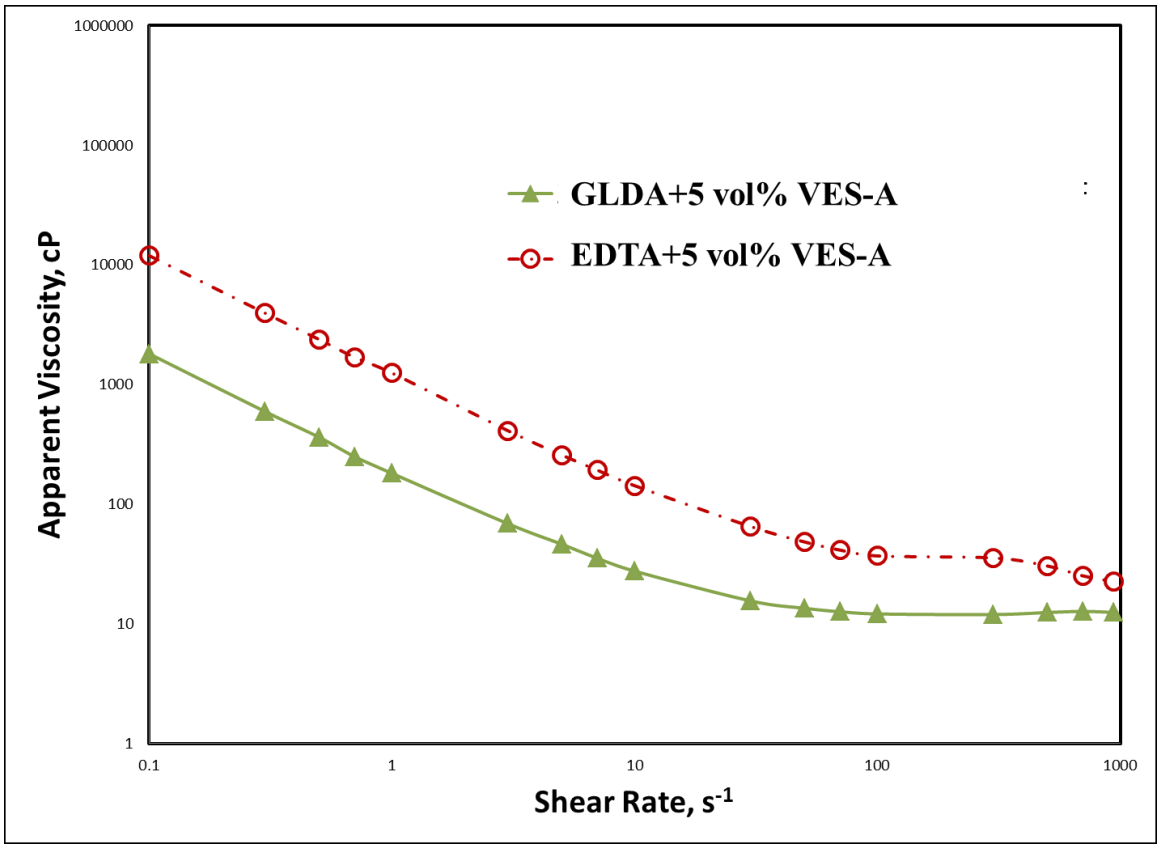


**Figure 6.7**: Viscosity of 5 vol% VES-A based GLDA and EDTA solutions at 200 ℉.

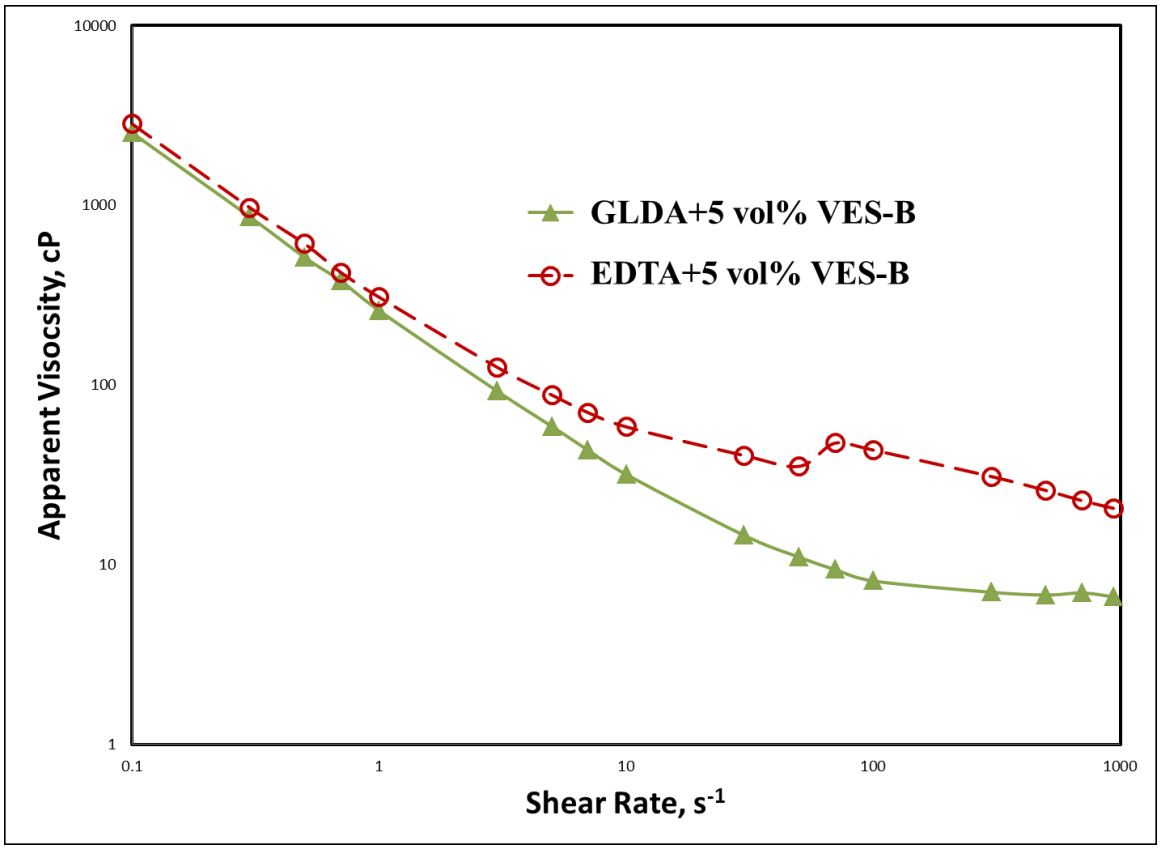


**Figure 6.8**: Viscosity of 5 vol% VES-B based GLDA and EDTA solutions at 200 ℉.

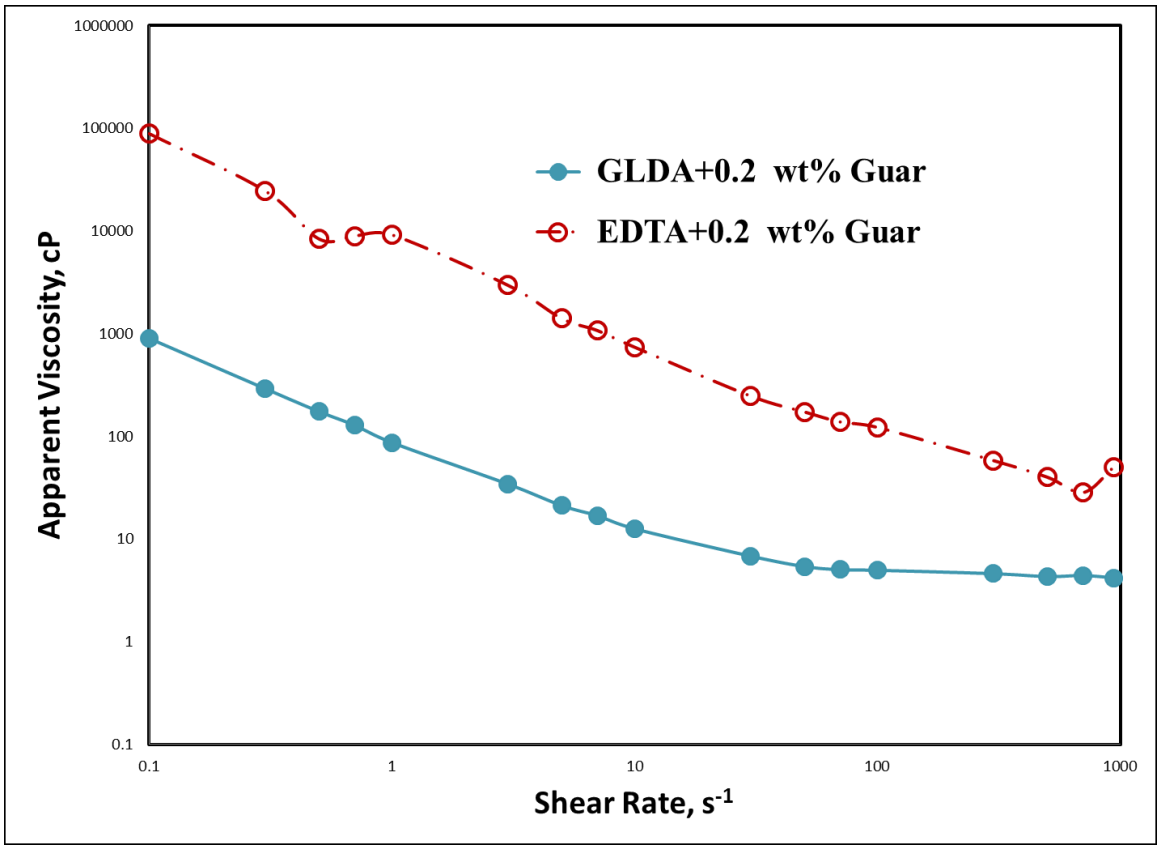


**Figure 6.9**: Viscosity of 0.2 wt% guar-based GLDA and EDTA solutions at 200 ℉.

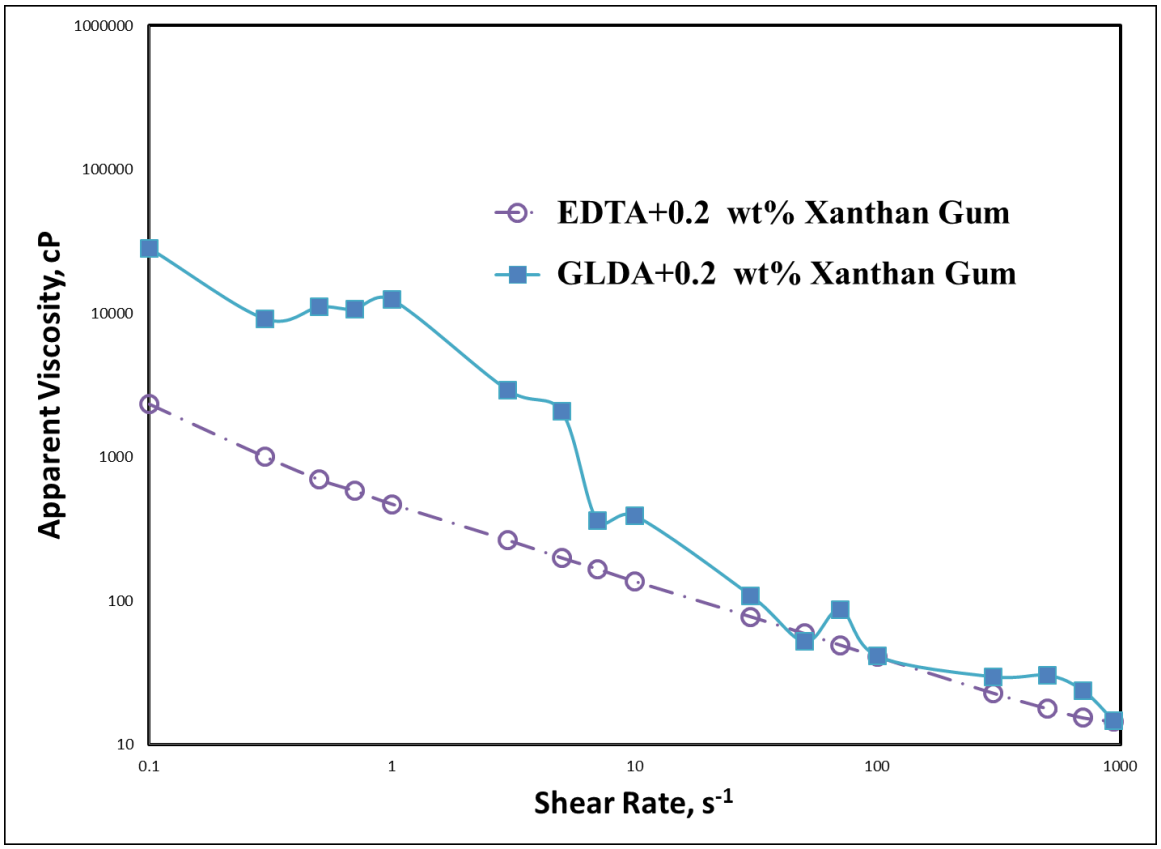


**Figure 6.10**: Viscosity of 0.2 wt% xanthan gum-based GLDA and EDTA solutions at 200 ℉.

## 6.5 Conclusions

Gelled GLDA fluids were analyzed with HP/HT rheometer for their potential well stimulation applications. The following conclusions can be draw:

1. The solubility of VES should be considered before using as viscosifying agents. A higher concentration of VES does not guarantee a higher fluid viscosity. It could adversely reduce the fluid viscosity.

2. Polymer based viscosifying agents had a range of effective temperature. Both low temperature fluid and overheating fluid cannot meet the criteria to achieve an even distribution of the treatment fluid. A proper temperature should be determined for each special formula.
3. When the pH was lower than 4, GLDA based fluids had lower viscosity than that of the EDTA based fluids. However, by adjusting the fluid pH to a level higher than 5, GLDA based fluids had a higher viscosity of the EDTA based fluids.

# 7. CONCLUSIONS

Heterogeneous high temperature carbonate reservoirs have drawn significant attention as large amount of hydrocarbons are still trapped in the formation. Conventional techniques cannot efficiently develop these reservoirs. Thus, various additives and acid systems were investigated and evaluated.

After a series of measurements of rheological properties of the amine oxide VES-based acids and coreflood tests with the VES-based acids injection into two different carbonate rocks at various injection rates, the following conclusion can be drawn:

1. At ambient conditions, the viscosity of the live VES-based acid was higher than that of the partially neutralized (pH 4.5). At temperatures greater than 140 ℉, the viscosity of partially neutralized acid was higher than the live acid.
2. G' of the live VES-based acid was dominant at ambient temperature, while when the temperature increased to 85°F, G" became the dominant characteristic of the live VES acid.
3. At room temperature, the 5 wt% HCl VES-based acid had the highest viscosity among various concentrations of HCl.
4. VES-based acid was only able to build up the pressure drop across the core at injection rates less than 1 $cm^3$/min when it was injected to 80 md permeability cores. However, at injection rates of 1 $cm^3$/min and higher, VES was not able to build up any pressure drop across the core when it was injected inside 4 md cores.

5. Acid pore volume to breakthrough and the amount of VES retained in the core were reduced when low permeability cores were used.
6. Calcium propagated faster than the HCl, while the surfactant propagated with the same rate as HCl. In addition, the pore volume needed to detect the calcium and the maximum calcium concentrations were not dependent on the acid injection rate.
7. CT scans confirmed that wormhole branches were observed in the second half of the core.

According to the coreflood tests conducted and the analysis of the core effluent samples, the following conclusions can be draw:

1. VES acid was not able to build up a pressure drop across the core when it was injected inside 70 md permeability cores at various acid concentrations and injection rates when only one fourth of the pore volume was injected.
2. At high concentrations of HCl, the calcium ions and the VES propagated with the same velocity. When a low concentration of HCl was employed, calcium ions propagated faster.
3. Surfactant retention is higher when the acid concentration and the injection rates were lower. This number could be up to 100%.
4. CT scans confirmed only small and short wormhole branches at the area near the inlet, and one wormhole dominated until the end with a decreasing diameter.

According to the coreflood tests and the CT scan images, the following conclusions can be drawn:

1. Both cationic surfactant and corrosion inhibitor can lower the reaction kinetics between GLDA and the carbonate rock formation. While the treatment with the presence of corrosion inhibitor only provided the lowest stimulation outcome.
2. A Combination of the cationic surfactant and the corrosion inhibitor can significantly increase the stimulation outcome. However, more treatment fluid was required to create the same length of the wormholes.

A new VES-based system was developed to extend the range of applicable temperatures. Viscosity measurements were conducted at temperatures up to 325 ℉. Three commercial corrosion inhibitors were tested at different concentrations. Coreflood studies were conducted to evaluate the performance of the new VES-based acid at reservoir conditions, observe the propagation of wormholes in carbonate core, and achieve acid diverting in parallel cores with different initial permeabilities. Based on the results obtained, the following conclusions can be drawn:

1. The new VES-based fluid exhibited a higher viscosity at elevated temperatures than conventional VES. The peak of the old VES-1, a carboxybetaine, was at 135 ℉ with the fluid viscosity of 860 cp. The peak of the old VES-2, an amine oxide, was at 165 ℉ with the fluid viscosity of 750 cp. The new VES had two peaks. One was at 185 ℉ with a viscosity of 1800 cp, and the second one was at 270 ℉ with the apparent viscosity of the fluid at 900 cp.
2. The addition of corrosion inhibitors lowered the viscosity of the VES-based fluids. At 250 ℉, when the concentration of corrosion inhibitor was 0.5 vol%,

corrosion inhibitor A had the lowest effect on the new VES viscosity; when the concentration was 1 vol%, corrosion inhibitor C had the lowest effect.

3. Mutual solvent significantly reduced the viscosity of the new VES-based fluid at various temperatures with different concentrations. A post-flush with mutual solvent is recommended to break the VES gel in the formation after acid treatments.
4. The VES-based acid changed its propagation direction during the single coreflood test, and multiple wormholes were created at the inlet face of the core at 325 ℉. In parallel coreflood tests, when the contrast between the initial permeability of the two cores was too large, no diversion occurred. When the contrast was within reasonable range and the acid was injected at a moderate flow rate, acid diversion was achieved.

Gelled GLDA fluids were analyzed with a HP/HT rheometer for their potential well stimulation applications. The following conclusions were draw;

1. The solubility of VES should be considered before using as viscosifying agents. A higher concentration of VES does not guarantee higher fluid viscosity. It could adversely reduce the fluid viscosity.
2. Polymer based viscosifying agents had a range of effective temperatures. Both low temperature fluid and overheating fluid cannot meet the criteria to achieve even distribution of the treatment fluid. A proper temperature should be determined for each special formula.

3. When the pH was lower than 4, GLDA based fluids had a lower viscosity than that of the EDTA based fluids. However, by adjusting the fluid pH to a level higher than 5, GLDA based fluids had a higher viscosity than the EDTA based fluids.

## REFERENCES


Al-Ghamdi, A., Nasr-El-Din, M.A., Hill, A.D. et al. 2009. Diversion and Propagation of Viscoelastic Surfactant Based Acid in Carbonate Cores. Paper presented at the SPE International Symposium on Oilfield Chemistry, The Woodlands. Texas, 20-22 April. SPE-121713.

Al-Ghamdi, A.H., Mahmoud, M.A., Hill, A.D., and Nasr-El-Din, H.A. 2010. When Do Surfactant-Based Acids Work as Diverting Agents? Paper presented at International Symposium and Exhibition on Formation Damage Control, Lafayette, Louisiana, 10-12 February. SPE-128074.

Bazin, B., Roque, C., Chauveteau, G.A., and Boute, M.J. 1999. Acid Filtration Under Dynamic Conditions To Evaluate Gelled Acid Efficiency in Acid Fracturing. *SPE Journal* **4** (4): 360-367.

Brode, P.F., III. 1988. Adsorption of Ultra-Long-Chain Zwitterionic Surfactants on a Polar Solid. *Langmuir* **4** (1): 176-180.

Brown, J.E., King, L.R., Nelson, E.B. et al. 1996. Use of a Viscoelastic Carrier Fluid in Frac-Pack Applications. Paper presented at the SPE Formation Damage Control Symposium, Lafayette, Louisiana, 14-15 February. SPE-31114.

Candau, S.J. and Oda, R. 2001. Linear Viscoelasticity of Salt-Free Wormlike Micellar Solutions. *Colloids and Surfaces A: Physicochemical and Engineering Aspects* **183–185**: 5–14.

Cates, M.E. and Candau, S.J. 1990. Statics and Dynamics of Worm-like Surfactant Micelles. *J. Phys.: Condens. Matter* **2**: 6869-6892.

Chang, F.F., Acock, A.M., Geoghagan, A. et al. 2001b. Experience in Acid Diversion in High Permeability Deep Water Formations Using Visco-Elastic-Surfactant. Paper presented at the SPE European Formation Damage Conference, The Hague, Netherlands, 21-22 May. SPE-68919.

Chang, F.F., Love, T.G., Affeld, C.J. et al. 2000. New Material and Technique for Matrix Stimulation in High-Water-Cut Oil Wells. *SPE Drilling & Completion* **15** (2): 126-131.

Chang, F.F., Qiu, X., and Nasr-El-Din, H.A. 2007. Chemical Diversion Techniques Used for Carbonate Matrix Acidizing: An Overview and Case Histories. Paper presented at the International Symposium on Oilfield Chemistry, Houston, Texas, U.S.A., 28 February–2 March. SPE-106444.

Chang, F., Qu, Q., and Frenier, W. 2001a. A Novel Self- Diverting-Acid Developed for Matrix Stimulation. Paper presented at the SPE Oilfield Chemistry Symposium, Houston, Texas, 13- 16 February. SPE-65033.

Chase, B., Chmilowski, W., and Dang, Y. 1997. Clear Fracturing Fluids for Increase Well Productivity. *Oilfield Review*; *Autumn*: **20**, 33.

Chu, Z., Dreiss, C.A., and Feng, Y. 2013. Smart Wormlike Micelles. *Chem. Soc. Rev.* **42:** 7174-7203.

Chu, Z. and Feng, Y. 2009. A Facile Route towards the Preparation of Ultra-Long-Chain Amidosulfobetaine Surfactants. *Synlett* **16**: 2655–2658.

Chu, Z. and Feng, Y. 2012. Empirical Correlations between Krafft Temperature and Tail Length for Amidosulfobetaine Surfactants in the Presence of Inorganic Salt. *Langmuir* **28** (2): 1175−1181.

Chu, Z., Feng, Y., Su, X., and Han, Y. 2010. Wormlike Micelles and Solution Properties of a C22-Tailed Amidosulfobetaine Surfactant. *Langmuir* **26** (11): 7783–7791.

Crews, J.B., Huang, T., and Wood, W.R. 2008. New Technology Improves Performance of Viscoelastic Surfactant Fluids. *SPE Drilling & Completion* **23** (1): 41-47.

Crews, J.B. and Huang, T. 2007. Internal Breakers for Viscoelastic-Surfactant Fracturing Fluids. Paper presented at the International Symposium on Oilfield Chemistry, Houston, Texas, 28 February-2 March. SPE-106216.

Dahayanake, M.S., Yang, J., and Niu, J. et al. 2001. Viscoelastic Surfactant Fluids and Related Methods of Use. US 6,258,859.

Daniel, S., Morris, L., Chen, Y. et al. 2002. New Visco-Elastic Surfactant Formulations Extend Simultaneous Gravel-Packing and Cake-Cleanup Technique to Higher-Pressure and Higher-Temperature Horizontal Open-Hole Completions: Laboratory Development and a Field Case History from the North Sea. Paper presented at the International Symposium and Exhibition on Formation Damage Control, Lafayette, Louisiana, 20-21 February. SPE-73770.

Davies, T.S., Ketner, A.M., and Raghavan, S.R. 2006. Self-Assembly of Surfactant Vesicles that Transform into Viscoelastic Wormlike Micelles upon Heating. *J. Am. Chem. Soc.* **128** (20): 6669-6675.

Deysarkar, A.K., Dawson, J.C., Sedillo, L.P., and Knoll-Davis, S. 1984. Crosslinked Acid Gel. J. *Canadian Petroleum Technology* **23** (1): 26-32.

Dreiss, C.A. 2007. Wormlike Micelles: Where Do We Stand? Recent Developments, Linear Rheology and Scattering Techniques. *Soft Matter* **3**: 956–970.

Fredd, C.N. and Fogler, H.S. 1997. Chelating Agents as Effective Matrix Stimulation Fluids for Carbonate Formations. Paper presented at the International Symposium on Oilfield Chemistry, Houston, Texas, 18-21 February. SPE-37212.

Fredd, C.N. and Fogler, H.S. 1998. Alternative Stimulation Fluids and Their Impact on Carbonate Acidizing. *SPE Journal* **3** (1): 34-41.

Frenier, W.W. 2001. Novel Scale Removers Are Developed for Dissolving Alkaline Earth Deposits. Paper presented at the SPE International Symposium on Oilfield Chemistry, Houston, Texas, 13-16 February. SPE-65027.

Frenier, W.W., Fredd, C.N., and Chang, F. 2001. Hydroxyaminocarboxylic Acids Produce Superior Formulations for Matrix Stimulation of Carbonates at High Temperatures. Paper presented at the SPE Annual Technical Conference and Exhibition, New Orleans, Louisiana, 30 September-3 October. SPE-71696.

Frenier, W.W., Wilson, D., Crump, D. et al. 2000. Use of Highly Acid-Soluble Chelating Agents in Well Stimulation Services. Paper presented at the SPE Annual Technical Conference and Exhibition, Dallas, Texas, 1-4 October. SPE-63242.

Greenhill-Hooper, M.J., O'Sullivan, T.P., and Wheeler, P.A. 1988. The Aggregation Behavior of Octadecylphenylalkoxysulfonates. I. Temperature Dependence of the Solution Behavior. *Journal of Colloid and Interface Science* **124** (1):77-87.

Hill, A.D., and Rossen, W.R. 1994. Fluid Placement Diversion in Matrix Acidizing. Paper presented at the Centennial Petroleum Engineering Symposium, Tulsa, Oklahoma, 29–31 August. SPE-27982.

Hoffmann, H. 1994. Viscoelastic Surfactant Solutions. *ACS Symposium Series* **578**: 2-31.

Hoffmann, H., and Ebert, G. 1988. Surfactants, Micelles and Fascinating Phenomena. *Angew. Chem. Int. Ed. Engl.* **27**: 902-912.

Hoffmann, H., Rauscher, A., Gradzielski, M., and Schulzt, S.F. 1992. Influence of Ionic Surfactants on the Viscoelastic Properties of Zwitterionic Surfactant Solutions *Langmuir* **8** (9): 2140-2146.

Hu, Y.T., Boltenhagen, P., and Pine, D.J. 1998. Shear Thickening in Low-Concentration Solutions of Wormlike Micelles. I. Direct Visualization of Transient Behavior and Phase Transitions. *J. Rheol.* **42**: 1185-1208.

Iwasaki, T., Ogawa, M., Esumi, K., and Meguro, K. 1991. Interactions between Betaine-Type Zwitterionic and Anionic Surfactants in Mixed Micelles. *Langmuir* **7** (1): 30-35.

Israelachvili, J.N., Mitchell, D.J., and Ninham, B.W. 1976. Theory of Self-Assembly of Hydrocarbon Amphiphiles into Micelles and Bilayers. *J. Chem. Soc., Faraday Trans.* **2** (72): 1525-1568.

Koehler, R.D., Raghavan, S.R., and Kaler, E.W. 2000. Microstructure and Dynamics of Wormlike Micellar Solutions Formed by Mixing Cationic and Anionic Surfactants. *J. Phys. Chem. B* **104** (47): 11035-11044.

Kubala, G. 1986. Aqueous Gelling and/or Foaming Agents for Aqueous Acids and Methods of Using the Same. US patent 4,591,447.

Kumar, R., Kalur, G.C., Ziserman, L. et al. 2007. Wormlike Micelles of a C22-Tailed Zwitterionic Betaine Surfactant: From Viscoelastic Solutions to Elastic Gels. *Langmuir* **23** (20): 12849-12856.

Lepage, J., Wolf, C.D., Bemelaar, J. et al. 2011. An Environmentally Friendly Stimulation Fluid for High-Temperature Applications. *SPE Journal* **16** (1): 104-110.

Li, L., Nasr-El-Din, H.A., and Cawiezel, K.E. 2010. Rheological Properties of a New Class of Viscoelastic Surfactant. *SPE Production & Operations* **25** (3): 355-366.

Li, L., Nasr-El-Din, H.A., Crews, J.B. et al. 2011. Impact of Organic Acids/Chelating Agents on the Rheological Properties of an Amidoamine-Oxide Surfactant. *SPE Production & Operations* **26** (1): 30-40.

Lin, Z., Cai, J.J., Scriven, L.E. et al. 1994. Spherical-to-Wormlike Micelle Transition in CTAB Solutions. *The Journal of Physical Chemistry* **98** (23): 5984-5993.

Lin, Z., Chou, L., Lu, B. et al. 2000. Experimental Studies on Drag Reduction and Rheology of Mixed Cationic Surfactants with Different Alkyl Chain Lengths. *Rheologica. Acta.* **39** (4): 354-359.

Lungwitz, B., Brady, M., and Daniel, S. et al. 2002. Viscoelastic Surfactant Fluids Stable at High Brine Concentrations. US 20020033260.

Lungwitz, B., Fredd, C., Brady, M., Miller, M., Ali, S., and Hughes, K. 2006. Diversion and Cleanup of Viscoelastic Surfactant-Based Self-Diverting Acid. *SPEPO* **22** (1): 127-121.

McCarthy, S.M., Qu, Q., and Vollmer, D. 2002. The Successful Use of Polymer-Free Diverting Agents for Acid Treatments in the Gulf of Mexico. Paper presented at the International Symposium and Exhibition on Formation Damage Control, Lafayette, Louisiana, 20-21 February. SPE-73704.

Metcalf, S., Lopez, H., Hoff, C., and Woo, G. 2000. Gas Production from Low Permeability Carbonates Enhanced Through Usage of a New Acid Polymer System. Paper presented at the SPE/CERI Gas Technology Symposium, Calgary, 3-5 April. SPE-59756.

Mahmoud, M.A., Nasr-El-Din, H.A., Wolf, C.D. et al. 2010a. An Effective Stimulation Fluid for Deep Carbonate Reservoirs: A Core Flood Study. Paper presented at the International Oil and Gas Conference and Exhibition in China, Beijing, China, 8-10 June. SPE-131626.

Mahmoud, M.A., Nasr-El-Din, H.A., Wolf, C.D. et al. 2010b. Stimulation of Carbonate Reservoirs Using GLDA (Chelating Agent) Solutions. Paper presented at the Trinidad and Tobago Energy Resources Conference, Port of Spain, Trinidad, 27-30 June. SPE-132286.

Mahmoud, M.A., Nasr-El-Din, H.A., Wolf, C.D. et al. 2011a. Effect of Lithology on the Flow of Chelating Agents in Porous Media during Matrix Acid Treatments. Paper presented at the SPE Production and Operations Symposium, Oklahoma City, Oklahoma, 27-29 March. SPE-140149.

Mahmoud, M.A., Nasr-El-Din, H.A., Dewolf, C. et al. 2011b. Effect of Reservoir Fluid Type on the Stimulation of Carbonate Cores Using Chelating Agents. Paper presented at the Brazil Offshore, Maca, Brazil, 14-17 June. SPE-143086.

Mahmoud, M.A., Mohamed, I.M., Nasr-El-Din, H.A. et al. 2011c. When Should We Use Chelating Agents in Carbonate Stimulation? Paper presented at the SPE/DGS Saudi Arabia Section Technical Symposium and Exhibition, Al-Khobar, Saudi Arabia, 15-18 May. SPE-149127.

Mahmoud, M.A., Nasr-El-Din, H.A., Wolf, C.D. et al. 2011d. Evaluation of a New Environmentally Friendly Chelating Agent for High-Temperature Applications. *SPE Journal* **16** (3): 559-574.

Mahmoud, M.A., Nasr-El-Din, H.A., Wolf, C.D. et al. 2011e. Optimum Injection Rate of a New Chelate That Can Be Used to Stimulate Carbonate Reservoirs. *SPE Journal* **16** (4): 968-980.

Nasr-El-Din, H.A., Al-Ghamdi, A.H., Al-Qahtani, A.A. et al. 2008. Impact of Acid Additives on the Rheological Properties of a Viscoelastic Surfactant and Their Influence on Field Application. *SPE Journal* **13** (1): 35-47.

Nasr-El-Din, H.A., Al-Habib, N.S., Al-Mumen, A.A., Jemmali, M., and Samuel, M. 2006c. A New Effective Stimulation Treatment for Long Horizontal Wells Drilled in Carbonate Reservoirs. *SPEPO* **21** (3): 330–338.

Nasr-El-Din, H.A., Chesson, J.B., Cawiezel, K.E., Devine, C.D. 2006a. Lessons Learned and Guidelines for Matrix Acidizing and Diversion Techniques in Carbonate Formations. Paper presented at the SPE Annual Technical Conference & Exhibition, San Antonio, Texas, 24-27 September. SPE-102468.

Nasr-El-Din, H.A., Chesson, J.B., Cawiezel, K.E., Devine, C.S., 2006b. Field Success in Carbonate Acid Diversion, Utilizing Laboratory Data Generated by Parallel Flow Testing. Paper presented at the SPE Annual Technical Conference & Exhibition, San Antonio, Texas, 24-27 September. SPE-102828.

Nasr-El-Din, H.A. and Samuel, M. 2007. Lessons Learned from Using Viscoelastic Surfactants in Well Stimulation. *SPEPO* **22** (1): 112-120.

Nasr-El-Din, H.A., Samuel, E. and Samuel, M., 2003. Application of a New Class of Surfactants in Stimulation Treatment. Paper presented at the SPE International Improved Oil Recovery Conference, Kuala Lumpur, Malaysia, 20-21 October. SPE-84898.

Nasr-El-Din, H.A., Al-Mohammed, A.M., Al-Aamri, A.D. et al. 2009. Quantitative Analysis of Reaction-Rate Retardation in Surfactant-Based Acids. *SPE Production & Operations* **24** (1): 107-116.

Nehmer, W.L. 1988. Viscoelastic Gravel-Pack Carrier Fluid. Paper presented at the SPE Formation Damage Control Symposium, Bakersfield, California, 8-9 February. SPE-17168.

Nelson, E.B., Lungwitz, B., and Dismuke K. et al. 2003. Viscosity Reduction of Viscoelastic Surfactant Based Fluids. US 6,881,709.

Pabley, A.S., Ewing, B.C., and Callaway, R.E. 1982. Performance of Crosslinked Hydrochloric Acid in the Rocky Mountain Region. Paper presented at the SPE Rocky Mountain Regional Meeting, Billings, Montana, 19-21 May. SPE-10877.

Parlar, M., Nelson, E.B., Walton, I.C. et al. 1995. An Experimental Study on Fluid-Loss Behavior of Fracturing Fluids and Formation Damage in High-Permeability Porous Media. Paper presented at the SPE Annual Technical Conference and Exhibition, Dallas, Texas, 22-25 October. SPE-30458.

Qi, Y., and Zakin, J.L. 2002. Chemical and Rheological Characterization of Drag-Reducing Cationic Surfactant Systems. *Ind. Eng. Chem. Res.* **41** (25): 6326-6336.

Rabie, A., Mahmoud, M.A., and Nasr-El-Din, H.A. 2011. Reaction of GLDA with Calcite: Reaction Kinetics and Transport Study. Paper presented at the SPE International Symposium on Oilfield Chemistry, The Woodlands, Texas, 11-13 April. SPE-139861.

Raghavan, S.R. and Kaler, E.W. 2001. Highly Viscoelastic Wormlike Micellar Solutions Formed by Cationic Surfactants with Long Unsaturated Tails. *Langmuir* **17** (2): 300-306.

Rehage, H. and Hoffmann, H. 1988. Rheological Properties of Viscoelastic Surfactant Systems. J. Phys. Chem. **92** (16): 4712-4719.

Rose, G.D. and Foster, K.L. 1988. Drag Reduction and Rheological Properties of Cationic Viscoelastic Surfactant Formulations. *Journal of Non-Newtonian Fluid Mechanics* **31**: 59-85.

Samuel, M.M., Card, R.J., Nelson, E.B. et al. 1999. Polymer-Free Fluid for Fracturing Applications. *SPE Drilling & Completion* **14** (4): 240-246.

Samuel, M., Card, R.J., Nelson, E.B., Brown, J.E., Vinod, P.S., Temple, H.L, Qu, Q., and Fu, D.K. 1997. Polymer-free Fluid for Fracturing. Paper presented at the SPE Annual Conference and Exhibition, San Antonio, TX, 5-8 October. SPE 38622.

Stewart, B.R., Mullen, M.E., Howard, W.J. et al. 1995. Use of a Solids-Free Viscous Carrying Fluid in Fracturing Applications: An Economic and Productivity Comparison in Shallow Completions. Paper presented at the SPE European Formation Damage Conference, The Hague, Netherlands, 15-16 May. SPE-30114.

Wang, Y., Zhang, Y., and Liu, X. et al. 2013. Effect of a Hydrophilic Head Group on Krafft Temperature, Surface Activities and Rheological Behaviors of Erucyl Amidobetaines. *J. Surfact. Deterg.* **16**.

Williams, B.B., Gidley, J.L., and Schechter, R.S., 1979. Acidizing Fundamentals. *Monograph Series* **1**: 1-11.

Yang, J. 2002. Viscoelastic Wormlike Micelles and Their Applications. *Current Opinion in Colloid and Interface Science* **7**: 276-281.

Yeager, V. and Shuchart, C. 1997. In Situ Gels Improve Formation Acidizing. *Oil & Gas J.* **95** (3): 70-72.

Yu, M. and Nasr-El-Din, H.A. 2009. Quantitative Analysis of Viscoelastic Surfactants. Paper presented at the SPE International Symposium on Oilfield Chemistry, The Woodlands. Texas, 20-22 April. SPE-121715.

Yu, M., Mahmoud, M.A., Nasr-El-Din, H.A. 2011. Propagation and retention of Viscoelastic Surfactants Following Matrix-Acidizing Treatments in Carbonate Cores. *SPE Journal* **16** (4): 993-1001.